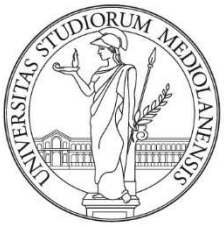

UNIVERSITÀ DEGLI STUDI DI MILANO

FACOLTÀ DI SCIENZE DEL FARMACO

CORSO DI DOTTORATO IN SCIENZE FARMACEUTICHE

XXXIV CICLO

TESI DI DOTTORATO DI RICERCA

IMMUNO-AFFINITY CAPTURE AND RELEASE OF EXTRACELLULAR VESICLES AND THEIR CHARACTERIZATION AS NOVEL DIAGNOSTIC TOOLS

DARIO BRAMBILLA

Matricola R12242

Tutor: Dr. Marcella Chiari

Co-Tutor: Prof. Marina Carini

ANNO ACCADEMICO 2020/2021

“A dream is a creation of the intelligence,

the creator being present

but not knowing how it will end.”

C. Pavese

To Diego:

Follow your dreams,

I will always be there to make them come true.

TABLE OF CONTENTS

LIST OF ABBREVIATIONS

AF4	Asymmetric Flow Field Flow Fractionation
AFM	Atomic Force Microscopy
AIBN	2,2'-Azobis(2-methylpropionitrile)
ATP	Adenosine Triphosphate
AUC	Area Under Curve
B&W	Binding and Washing
BBB	Blood Brain Barrier
BK	Bradykinin
BP	Linear Bradykinin Peptide
BPb	Branched Bradykinin Peptide
BPn	Negative Bradykinin Peptide
BPt	Tandem Bradykinin Peptide
BSA	Bovine Serum Albumin
CD	Cluster of Differentiation
cDNA	Complementary DNA
CE-LIF	Capillary Electrophoresis coupled with Laser-Induced Fluorescence
CFDA-SE	5(6)-Carboxyfluorescein diacetate N-succinimidyl ester
cfDNA	Cell Free DNA
CFSE	Abbreviation for CFDA-SE
CI	Confidence Interval
CIC	Conventional Immuno-Capturing
CMOS	Complementary Metal-Oxide Semiconductor

CPDA	Citrate Phosphate Dextrose Adenine anticoagulant
Cryo-EM	Cryogenic Electron Microscopy
CTC	Circulating Tumor Cell
ctDNA	Circulating Tumor DNA
CuAAC	Copper-Catalyzed Azide-Alkyne Cycloaddition
Cy3	Cyanine 3
Cy5	Cyanine 5
DAC	DNA-Antibody Conjugate
DBCO	Dibenzocyclooctine
DDI	DNA-Directed Immobilization
DI	De-Ionized
DLD	Deterministic Lateral Displacement
DLS	Dynamic Light Scattering
DMA	*N,N*-dymethilacrylamide
DMEM	Dulbecco's Modified Eagle's Medium
DMSO	Dimethyl Sulfoxide
DNA	Deoxyribonucleic Acid
DNA-PAINT	DNA Points Accumulation for Imaging in Nanoscale Topography
dsDNA	Double Stranded DNA
EDTA	Ethylenediaminetetraacetic Acid
EGFR	Epithelial Growth Factor Receptor
ELISA	Enzyme-Linked Immunosorbent Assay
EpCAM	Epithelial Cell Adhesion Molecule
ESCRT	Endosomal Sorting Complexes Required for Transport
EV	Extracellular Vesicle

Fab	Antigen Binding Fragment
FB	Fluidized Bed
FC	Flow Cytometry
FCS	Fetal Calf Serum
GPC-1	Glypican 1
HDL	High Density Lipoprotein
HEK	Human Embryonic Kidney
HFD	Hydrostatic Filtration Dialysis
HSP90	Heat Shock Protein 90
IgG	Immunoglobulin G
IL-6	Interleukin 6
IP	Immuno-Precipitation
IRIS	Interferometric Reflectance Imaging Sensor
ISEV	International Society for Extracellular Vesicles
LDL	Low Density Lipoproteins
LED	Light-Emitting Diode
MAPS	3-(trimethoxysilyl) propyl methacrylate
MB	Molecular Beacon
MCCV	Monte-Carlo Cross Validation
mRNA	Messenger RNA
MS	Mass Spectrometry
MV	Microvesicle
MVB	Multi Vesicular Body
MWCO	Molecular Weight Cut-Off
NanoFCM	Nanoscale Flow Cytometry

NAS	*N*-acryloyloxysuccinimide
NBI	Nickel-Based Isolation
NGS	Next Generation Sequencing
NHS	N-hydroxysuccinimide
NMR	Nuclear Magnetic Resonance
NSCLC	Non-Small Cells Lung Cancer
NTA	Nanoparticle Tracking Analysis
PBS	Phosphate Buffer Saline
PBS-M	Phosphate Buffer Saline added with Magnesium Chloride
PCR	Polymerase Chain Reaction
PE	Phycoerythrin
PEG	Polyethylene Glycol
PLS	Partial Least Squared regression
PMT	Photomultiplier Tubes
POC	Point of Care
PTM	Post-Translational Modification
RI	Refractive Index
RNA	Ribonucleic Acid
ROC	Receiver Operating Curve
RT-IRIS	Real Time Interferometric Reflectance Imaging Sensor
RT-qPCR	Real Time Quantitative Polymerase Chain Reaction
SDS	Sodium Dodecyl Sulphate
SDS-PAGE	Sodium Dodecyl Sulphate Polyacrylamide Gel Electrophoresis
SEC	Size-Exclusion Chromatography
SEM	Scanning Electron Microscopy

SPAAC	Strain-Promoted Azide-Alkyne Cycloaddition
SPCM	Single-Photon Counting Modules
SP-IRIS	Single Particle Interferometric Reflectance Imaging Sensor
SSC	Side Scattering
ssDNA	Single Stranded DNA
SVM	Support Vector Machines
TEM	Transmission Electron Microscopy
TFF	Tangential Flow Filtration
THF	Tetrahydrofuran
Tris	2-Amino-2-(hydroxymethyl)propane-1,3-diol
TRPS	Tunable Resistive Pulse Sensing
TSG101	Tumor Susceptibility Gene 101 protein
TSPAN8	Tetraspanin 8
T-TBS	Tris Buffered Saline added with Tween 20
UC	Ultracentrifugation
UF	Ultrafiltration
VEGF	Vascular Endothelium Growth Factor
VLDL	Very Low Density Lipoproteins
WB	Western Blot

AIM OF THE THESIS

Extracellular vesicles (EVs) are membrane vesicles secreted by cells into bodily fluids. Different subpopulations of EVs can be distinguished based on their size and release mechanism: i) exosomes (smaller than 150 nm in diameter), ii) microvesicles (100 nm - 1 μm in diameter, directly budded from the cell membrane), and iii) apoptotic bodies (released by dying cells during apoptosis or necrosis).

Since their specific cargo (metabolites, nucleic acids, and proteins) and membrane proteins are a kind of signature that reflects the composition of the cell of origin, EVs have gained increasing attention as biomarkers for many diseases, including cancer and neurodegenerative diseases. Their analysis can be potentially exploited in liquid biopsy approaches.

Unfortunately, many problems still have to be overcome to exploit the potential of EVs in diagnostics. First, there is a lack of efficient technologies for high purity separation of EVs, since it is difficult to distinguish between different subpopulations and to avoid contamination from lipoproteins and protein aggregates.

To date, five groups of EVs isolation techniques have been developed. They are differential ultracentrifugation-based techniques, size-based techniques, immuno-affinity capture-based techniques, precipitation, and microfluidics-based techniques. Since all these methods have drawbacks, there is a pressing need for improvement. In addition, EVs detection, quantification and characterization are problematic due to their small size and low refractive index. For this reason, there is demand for new high-throughput analytical methods. The current state-of-the-art regarding EVs separation and characterization is described in **Chapter 1**.

This Ph.D. project's main goal is the development of reversible immuno-affinity techniques to achieve the separation of EVs from complex bodily fluids. Using this strategy, EVs are captured by specific antibodies immobilized on solid surfaces. Immuno-affinity precipitation offers unmatched results in terms of purity and selectivity, giving the possibility to isolate specific EVs subpopulations.

Many kits for antibody-mediated separation of EVs are commercially available but unfortunately suffer from drawbacks limiting their use. The major limitation of the kits mentioned above is the problematic release of an EV from the antibody: the interaction

between the antibody and its biological target is difficult to revert and usually requires harsh conditions such as low pH or high ionic strength buffers, often in combination with detergents. Unfortunately, these conditions lead to damage or breaking of EVs, impairing characterization methods that rely on imaging techniques (e.g., Nanoparticle Tracking Analysis, Transmission Electron Microscopy and Nanoscale Flow Cytometry), and require the presence of intact vesicles.

A new perspective is provided within this thesis: immuno-affinity separation approaches usually require solid surfaces where antibodies are immobilized and are able to capture their antigen. Instead of releasing the antigen by breaking the interaction with the antibody, we propose novel strategies of reversible immobilization of antibodies. In this way, EVs can be released by detaching the antibody from the surface under mild conditions, thus preserving their intact vesicular structure and allowing their characterization by imaging techniques.

Two different separation strategies have been developed:

- **Chapter 2, 3, and 4** describe the so-called DNA-directed immobilization (DDI) of antibodies, an approach where antibodies are immobilized on the surface through a double stranded DNA-linker. The antibody is tagged with a single stranded DNA while the complementary strand of DNA is immobilized on the surface. Exploiting the annealing of complementary strands, the antibody is then immobilized on the support. The presence of the DNA-linker enables the release of the antibody from the surface through the enzymatic cleavage of DNA catalyzed by DNase I. This approach allows the release of intact EVs under mild conditions (iso-osmotic buffer and 37°C).

  The synthesis of DNA-antibody conjugates and experimental protocol to perform DDI were developed on a microarray platform and proved to be effective in increasing the binding capacity of antiCD63 antibody, as described in **Chapter 2**. This peculiar advantage was exploited, and DDI was used to fabricate multiplexed antibody microarrays for the analysis of EVs, as described in **Chapter 3**.

  This approach was then transferred to magnetic beads, providing the effective separation of EVs from human blood plasma. EVs separated using this strategy were analyzed with different imaging techniques including Nanoparticle Tracking Analysis, Transmission Electron Microscopy, Nanoscale Flow Cytometry, and SP-IRIS (a label free technique that allow digital counting, sizing and phenotyping of individual nanoparticles captured on a silicon microarray chip by analyzing the reflectivity of a LED light along the surface of the sensor). Separation of EVs using DDI in combination with DNase I is reported in **Chapter 4**.

- **Chapter 5, 6, and 7** describe the second strategy developed within this Ph.D. project, which is based on using a streptavidin-binding aptamer called StrepApt5. The surface-immobilized aptamer can bind streptavidin, which in turn allows the immobilization of biotinylated antibodies. After interaction with EVs has occurred, the streptavidin-antibody complex can be released from the surface upon incubation with the sequence of DNA complementary to StrepApt5 (cDNA). In fact, in the presence of cDNA, the aptamer forms a double helix losing its 3D structure and thus the affinity toward streptavidin.

  The strategy was first developed and optimized on a microarray platform as described in **Chapter 5**. The use of StrepApt5 demonstrated to provide effective immobilization of streptavidin and biotinylated antibodies in a reversible fashion. Additionally, aptamer-mediated immobilization of antiCD9 provided remarkable improvements compared with conventional immobilization strategies.

  The strategy was then transferred to beads. Since the immobilization of the aptamer on commercial beads did not provide satisfactory results, a custom resin based on polymer-coated silica beads was developed as depicted in **Chapter 6**. In particular, silica beads were coated using a DMA-based copolymer. After coating characterization, the solid matrix was used to immobilize different biological probes to determine their binding capacity.

  Chapter 7 describes the immobilization of StrepApt5 on coated silica beads and its use in the separation of EVs from complex biological media.

Chapter 8 describes the INDEX Project. The goal of this project is the development of an integrated platform for the in-line separation and characterization of EVs, with potential application in liquid biopsy. The platform is composed by two distinct module, one for the separation and the second for the detection of EVs. Their integration is strictly dependent on the EVs' reversible capture strategy chosen.

Within the project, the DNA-directed immobilization of antibodies, coupled with enzymatic released mediated by DNase I, was selected to provide reversible immuno-affinity capture of EVs. The technical validation demonstrated that system integration can be successfully achieved. Clinical validation for the use of the platform in liquid biopsy of lung cancer was carried out showing ground-breaking results.

CHAPTER 1

EXTRACELLULAR VESICLES SEPARATION, CHARACTERIZATION AND IMPLICATIONS IN LIQUID BIOPSY

1. Biology and applications of extracellular vesicles

Extracellular vesicles (EVs) are a heterogeneous population of particles ranging from 30 nm to 5 μm in diameter[1] delimited by a lipid bilayer membrane. Naturally released from cells (including bacteria, plants and animals[2]) into extracellular space, EVs cannot replicate, since they do not contain a functional nucleus[3]. They were first observed in plasma by Wolf in 1967, who called them "platelet dust"[4]. Initially disregarded as means of removing toxic or non-necessary molecules from the cells, EVs are now constantly gaining attention since their role in cell-to-cell communication has been disclosed.

Both, lipid membrane and cargo composition of EVs, including nucleic acids, proteins, lipids, carbohydrates, glycans, and metabolites[5], mirror the status of the parent cell. EVs can target recipient cells through specific interaction of proteins exposed on their membrane and receptors expressed on recipient cells. Once docked on the recipient cell membrane through receptor binding, EVs may either cause functional responses by transferring their cargo or be internalized inside the cell. Upon internalization, EVs can:

- Exchange transmembrane proteins and lipids.
- Activate/inactivate metabolic pathways (eventually changing recipient cell phenotype).
- Be directed to lysosomes and act as a source of metabolites for recipient cells[2].

In mammalians, EVs are produced by all cell types, under both physiological and pathological conditions. They are contained in a variety of biological fluids including blood, urine, cerebrospinal fluid, bronchoalveolar fluid, and feces[5].

EVs are currently classified into three main groups, i.e., exosomes, microvesicles, and apoptotic bodies. Exosomes are nanovesicles ranging 30-150 nm in diameter formed through endosomal pathway[6]. They originate from the inward budding of the membrane of early endosomes, which mature into multivesicular bodies (MVBs) during this process. MVBs are directly involved in sorting, storage, recycling, and release of cellular components.

In particular, MVBs can be directed to lysosomes for degradation or fuse with the cell membrane causing exosomes to be secreted into extracellular matrix[7]. ESCRT proteins regulate exosome formation and MVBs transportation; exosomes are particularly enriched in these proteins (together with ESCRT associated proteins like Alix, TSG101 and HSP90). Membrane organizer proteins like tetraspanins (especially CD9, CD63 and CD81) are commonly found on the membrane of exosomes. In general, exosomal proteins show a higher degree of glycosylation compared to cell lysate[1]. Exosomes can produce a plethora of biological effects, including cell maintenance, immune response stimulation (acting as antigen presenting vesicles). Still, they are also involved in pathological pathways which lead to disease progession[8].

MVs are formed through direct outward budding or pinching of the cell's plasma membrane and are generally 100 nm – 1 μm in size. Compared to cell lysate, MVs are enriched in tetraspanins, heat shock proteins, integrins, and cytoskeletal proteins[2]. All these proteins generally present more post-translation modifications (PTMs), especially glycosylation and phosphorylation, than cell lysate and exosomes. In fact, the degree of PTMs could potentially be used to distinguish between exosomes and MVs[9]. Microvesicles are directly involved in cell-to-cell communication also in cancer cells, where they are called oncosomes, and their size may be larger (up to 10 μm for large oncosomes)[10].

Apoptotic bodies are generally 50 nm – 5 μm in size and originate from dying cells. During apoptosis, cells contract increasing hydrostatic pressure and causing the separation of plasma membrane from the cytoskeleton. Then, upon blebbing and fragmentation of the plasma membrane, apoptotic bodies are formed[5]. In contrast with exosomes and MVs, apoptotic bodies' composition is quite similar to cell lysates (only a low degree of protein glycosylation is found). They also contain intact organelles and chromatin[1].

Since EVs are heterogeneous in size, physical properties, and composition. Considering the lack of consensus on specific markers of EV subtypes, distinguishing and separating an EV subpopulation from the others is a challenging task. For this reason, the International Society of Extracellular Vesicles (ISEV) suggests to avoid terms like exosomes or microvesicles to describe EVs, unless a particular biogenesis pathway is unquestionably assigned. The general recommendation, also considering the state-of-the-art regarding EV separation and analysis, is to divide EVs subtypes based on a) their physical properties (e.g., size or density), b) biochemical composition (for example, CD63+ EVs), or c) description of condition or cell of origin (e.g., podocyte EVs, hypoxic EVs)[3].

In recent years EVs, in particular exosomes and MVs, have generated an extraordinary interest due to their potential applications in clinics and diagnostics. First of all, EVs are carriers of biomarkers that relates to physiological and pathological states in the human body. Their abundance in biological fluids makes their analysis compatible with liquid biopsy. In this diagnostic approach the detection of specific biomarkers in easily accessible bodily fluids (e.g. blood) could potentially led to replacement of the conventional tissue biopsy.
Another potential application of EVs is their use as vaccines. As already mentioned, EVs can act as antigen-presenting vesicles, and this feature could be exploited using engineered EVs. They are also ideal for the development of drug delivery systems since they can simultaneously transport nucleic acids and proteins inside the lipid bilayer, thus preventing their degradation until the site of release is reached[1].
Unfortunately, the state-of-the-art techniques for EVs separation and analysis are still inadequate to meet regulatory agencies' needs in order to approve their use in diagnostic and clinical fields. For this reason, further improvement is mandatory.

2. Extracellular vesicles in liquid biopsy of cancer

Earlier detection is key to reducing cancer deaths. Most localized cancers do not need systemic treatment and can be removed only by surgery. When distant metastasis develop, even systemic treatments are rarely effective[11]. For this reason, early detection of cancer is of utmost importance; up to date, a systematic screening of the population for the development of cancer cannot be performed due to current sampling methods that mainly involve tissue biopsy.
Tissue biopsy is a surgical procedure to remove a portion of tumoral tissue to provide its phenotyping, thus elucidating the prognosis and deciding the most appropriate treatment option. Unfortunately, traditional biopsies are invasive, unrepeatable, imply potential complications, and cannot be performed if the patient's conditions are critical or if the tumor is inaccessible[12].
Over the last decades, the concept of precision medicine has dramatically changed perspectives in medical oncology, as patient-tailored therapies have significantly improved patients' outcomes. Precision medicine requires tumor characterization and evolution monitoring over time. It appears that tissue biopsy cannot meet these requirements; this is why, during the last few years, the concept of *liquid biopsy* has gained ground.

Liquid biopsy is a revolutionary technique that implies the detection of tumoral components into biological fluids (that can be obtained from patients through minimally invasive methods, e.g., a blood draw). The limited invasiveness and costs, as well as the ease of repeatability of this technique make it suitable not only for cancer prognosis or the choice of the best treatment strategy, but also to provide an early diagnosis, to evaluate the effectiveness of the therapy (and eventually the development of drug resistance phenomena), to monitor the clonal evolution of cancer, and to follow the patient during remission. All these features, on the whole, improve patient outcome[12,13].

Unfortunately, liquid biopsy is still far from being applied by clinicians, but many achievements have been accomplished during the last few years. Up to date, three tumoral markers are analyzed to gather cancer information: circulating tumor cells (CTCs), circulating tumor DNA (ctDNA), and EVs[12].

CTCs, first described in 1869, are released by both primary and secondary tumor sites and, after entering the bloodstream, are responsible for forming distant metastasis. CTCs can be analyzed for their concentration (that directly relates to prognosis) and the presence of tumoral biomarkers, but also to study RNA expression and DNA abnormalities. Unfortunately, CTCs are extremely rare, causing sensitivity issues and limiting their application for the early diagnosis of cancer[13].

In blood stream, there is cell-free DNA (cfDNA) which probably originates from apoptotic or necrotic cells. The subpopulation of cfDNA, which comes from tumoral cells, is called circulating tumor DNA (ctDNA). ctDNA can be transferred to recipient cells, where it generates the genetic instability that leads to a metastatic transformation. Unfortunately, ctDNA is susceptible to degradation in the bloodstream due to enzymes and presents a rapid clearance in the liver and kidneys. Moreover, purification protocols may affect levels of ctDNA[12,13].

More recently tumor-derived extracellular vesicles started to be considered eligible liquid biopsy biomarkers. In fact, EVs present numerous advantages since they are abundant in most biological fluids and their composition is a signature of the cell of origin. Additionally, nucleic acids contained inside EVs are protected from degradation mediated by ribonucleases, and DNases by the lipid bilayer membrane[14].

EVs are used by cancer cells to promote their proliferation and play many different roles in tumorigenicity. They can exert a cargo-dependent oncogenic response in recipient cells, for example, enabling the propagation of aggressive/oncogenic phenotype in different subpopulations of cancer cells transferring oncogenes into recipient cells[15]. They can also

modulate the microenvironment mediating either pro- and anti-inflammatory effects, as well as the immune response[16]. EVs also promote the horizontal transmission of drug resistance using different mechanisms: transfer of drug resistance-conferring molecules or nucleic acids or sequestering the drug before it reaches the tumor, thus creating a sublethal concentration of the drug (as already demonstrated for Trastuzumab)[17].

Moreover, EVs can promote angiogenesis or tumor invasiveness by transferring mediators like IL-6, VEGF, and metalloproteinases, thus creating a pre-metastatic niche for tumor[5].

EVs could be potentially analyzed at different levels in order to diagnose cancer at an early stage. Several evidences show increased levels of EVs in the plasma of cancer patients[18], suggesting that concentration of EVs could be analyzed for diagnosis but also prognosis of cancer since it has been demonstrated that malignant tumors produce higher levels of extracellular vesicles[19,20].

Besides measuring levels of EVs in bodily fluids, also EV-related biomolecules could be analyzed and are important biomarkers with potential clinical application in cancer diagnosis[21]. For example, recent findings show that differences in lipid composition (i.e., phosphatidylserine and lactosylceramide levels) allow discriminating prostate cancer and healthy patients with high sensitivity and specificity[22]. Nucleic acids also represent an essential class of biomarkers. Different studies have highlighted the importance of RNAs as molecular signatures for cancer diagnosis and indicators of cancer metastasis[23], while the presence of DNA inside EVs is still debated.

Tumor-derived EVs also contain proteins from their origin cells, making them an attractive biomarker in cancer diagnosis. Several evidences support the diagnostic potential of EV-associated proteins. CD151 and tetraspanin 8 (Tspan8) have been associated with lung cancer[24], while TRIM3, a protein that plays a role as a tumor inhibitor, is downregulated in EVs from gastric cancer patient[25]. Also, post-translational modifications (PTMs) of proteins reflect the cell of origin, and may be analyzed to find a cancer-related fingerprint (for example, the degree of phosphorylation of EGFR can be used as a biomarker to monitor the effectiveness of antitumoral treatment)[26].

A peculiar advantage of EV-analysis in liquid biopsy approaches is the innate ability of extracellular vesicles to cross the blood-brain barrier (BBB). Due to this phenomenon, EVs released from brain tumors that are usually inaccessible to conventional tissue biopsy can be found in the bloodstream, separated, and analyzed with minimally invasive procedures[5].

However, the implementation of EVs in clinical settings for cancer diagnosis and monitoring is still limited. Indeed there is an urgent need for improvement in EVs separation and

analysis techniques, as the presence of contaminants may alter downstream analyses. In addition, tumor-derived EVs often represent only a tiny fraction of total EVs, and the presence of vesicles released from normal cells hampers the analysis, increasing background signals and thus lowering the sensitivity of methods.
In this context, a further improvement in immuno-affinity enrichment techniques would be dramatically helpful in specifically separating EVs released from cancer cells. In this way, background signals from healthy cell-derived EVs would be lowered, enhancing both sensitivity and specificity of cancer diagnosis[21].

3. Separation techniques for extracellular vesicles

Extracellular vesicles are characterized by high heterogeneity; in fact, different EV subclasses, in addition to presenting similar composition in biomolecules, share the same size and density. Viruses and other plasma components (e.g. lipoproteins) overlap with EVs in terms of size and density as shown in Figure 1.1[27]. For this reason, choosing an appropriate method for EVs separation from biological fluids is challenging, and the best choice is often a combination of different enrichment strategies, as recommended by ISEV[3]. Depending on the intended use (i.e. a specific application or analysis technique), one can choose different methods based on the required yield, structural integrity, and purity[28].
Separation methodologies have been improved significantly during the last decade. The most widely used methods exploit: EVs physical properties (e.g. size or density), polymer-induced precipitation or aggregation, and chemical interaction with some components of the outer membrane (affinity capture or charge-based methods). In recent years, microfluidic systems have been developed in order to reduce sample volumes and separation time.

3.1 Density-based techniques

Historically, *ultracentrifugation* (UC) is the most applied separation method for EVs[27]. It provides EVs enrichment based on buoyant density. *Differential ultracentrifugation* is generally exploited and consists of different centrifugation steps with increasing centrifugal forces. Larger contaminants are removed using low-speed centrifugations (500-16,000 x g), while EVs are pelleted and thus separated with high-speed centrifugation (usually 100,000-200,000 x g)[29].

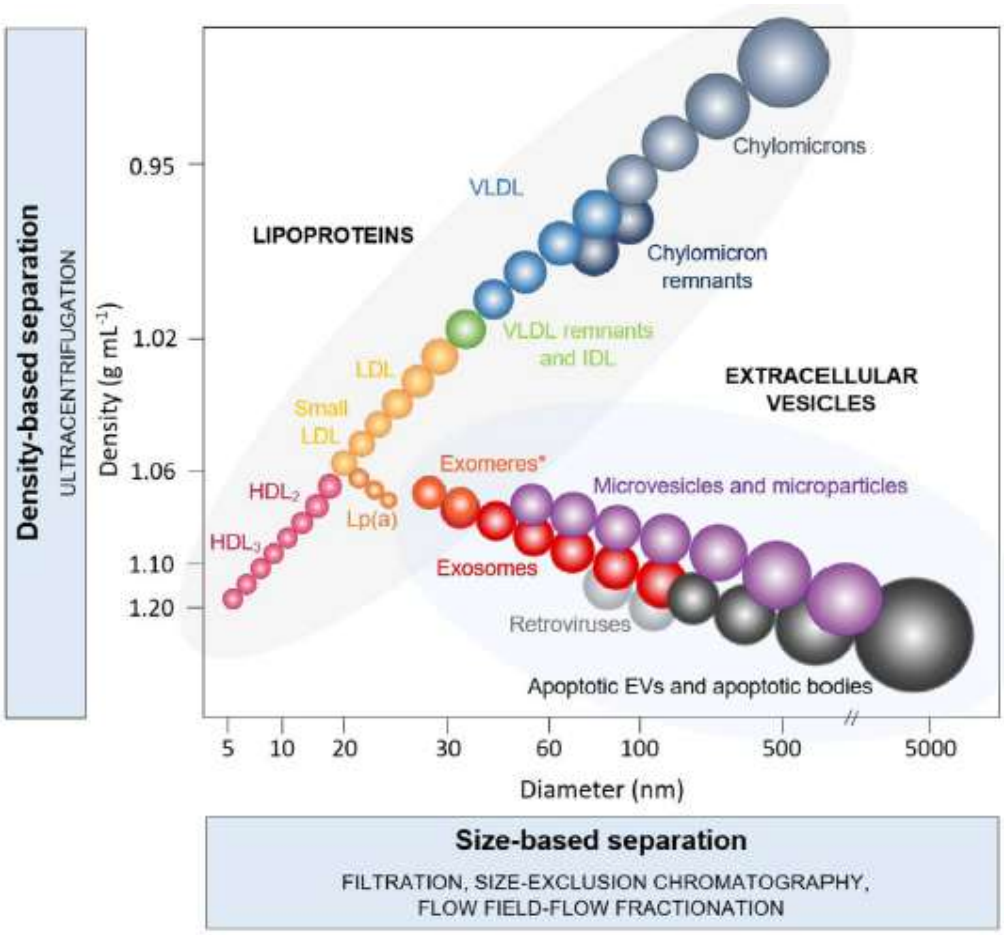

Figure 1.1 *Classification of different nano- and micro-sized particles commonly found in biological samples on the basis of their size and density*[27].

Ultracentrifugation allows processing large sample volumes using a small set of reagents and consumables. Even though these features made ultracentrifugation the most widely applied method for EVs separation, it is far from ideal since it suffers from many limitations. The main disadvantages of ultracentrifugation are that it is time-consuming, requires expensive instrumentation, and the separation outcome strongly depends on acceleration, rotor type, and sample viscosity (it is thus hard to produce a standardized protocol). In addition, high forces may damage EVs, and contamination with particles that share similar density (e.g. viruses, lipoproteins, protein aggregates, and cellular debris) can be observed[28,29].

The presence of contaminants can be limited using *density gradient ultracentrifugation*. EV-containing samples are loaded on a density gradient matrix (the gradient is obtained using sucrose or preferably iodixanol that being iso-osmotic with EVs, induces less damage). When a centrifugal force is applied, particles with different densities can be recovered in different regions of the gradient. Although density gradient ultracentrifugation is one of the

best method for EVs separation, it provides samples contaminated with high-density lipoproteins (HDLs) since they share similar density with EVs[28,29].

3.2 Size-based techniques

Size-based separation methods represent an important class of approaches to enrich EVs from a biological source. One of the most commonly used techniques is *ultrafiltration* (UF). Biological samples are forced to pass through a membrane filter with specific cutoff pores. Usually, different steps with decreasing pore size are applied to separate subclasses of EVs based on their diameter. A significant advantage of ultrafiltration is that it does not require expensive instrumentation and is a considerably faster, simpler, and less laborious than ultracentrifugation[29]. Unfortunately, this method suffers from protein contamination and EV damage or breakage caused by high shear stresses induced by pressure or vacuum. Additionally, EVs can be trapped on the pores of the membrane, causing clogging issues that reduce recovery yield[30].

Clogs can be reduced using *tangential flow filtration* (TFF), an approach where the stream of EV-containing sample is tangential to the membrane filter instead of passing directly through it. TFF has been successfully applied to concentrate EVs starting from diluted solutions as urine and cell culture supernatants[27]. Another separation technique is the *hydrostatic filtration dialysis* (HFD): a diluted EV-containing solution is in contact with a 1000 kDa MWCO (Molecular Weight CutOff) dialysis filter. Fluids and particles smaller than 1000 kDa pass through the filter due to the hydrodynamic pressure of the sample. During the process, contaminants are removed, and volume decreased, showing less EV losses on the membrane when compared to UF[31].

An important size-based separation technique with continuously growing application is *size exclusion chromatography* (SEC). SEC separates particles based on their size or hydrodynamic diameter and generally uses chromatographic columns loaded with porous stationary phases with a specific exclusion limit. Particles smaller than the exclusion limit are retained in the stationary phase while larger particles are eluted at different times based on their size (EVs are eluted before protein/protein aggregates)[27].

Remarkably, EVs separated via SEC preserve their integrity and biological activity better than vesicles enriched by UC. In addition, a lower degree of contamination from protein, protein aggregates and high density lipoproteins is observed. The technique is adapted for complex matrices as plasma and easily scalable[32]. Major disadvantages are: the cost of chromatographic sorbents, low yield, sample dilution (a downstream concentration step

might be required based on the application), contamination with lipoproteins (chylomicrons, VLDL, VLDL remnants, and LDL), and the preferential selection of smaller EVs compared to UC[33].

3.3 Preferential precipitation-based techniques

Another option to enrich EVs from complex solutions is to reduce their solubility and/or induce their aggregation so that the vesicles can be easily recovered by low-speed centrifugation. The first example is the *precipitation with hydrophilic polymers*, especially polyethylene glycol (PEG). PEG acts as water excluding polymer and "seizes" water molecules causing the precipitation of EVs[1]. A significant advantage is the simplicity, as well as the independence from pH and salt concentration. On the other side, PEG-mediated precipitation is non-selective, and separated EVs are contaminated by nucleoproteins, protein aggregates, lipoproteins, and viral particles, together with PEG itself[34].

Alternatively, *precipitation with protamine* can be used to separate EVs. Protamine is a positively charged protein that can cause aggregation of EVs through electrostatic interaction with negatively charged vesicles outer membrane. The application of this strategy is limited by several drawbacks: the procedure is rather long, suspending protamine in aqueous media might be cumbersome. In addition, removal of protamine requires gel filtration[35].

A further approach is represented by *precipitation with sodium acetate*. The salt is supposed to neutralize EVs surface negative charges and promote EVs aggregation through hydrophobic interactions. This method is compatible with large sample volumes, does not require expensive reagents that need to be removed at the end of the purification. Notably, this approach suffers from co-precipitation of non-EV contaminants[36].

3.4 Charge-based techniques

Instead of neutralizing negative charges on the surface of EVs, one can exploit the charges in charge-based separation techniques. Among them, noteworthy are: *Electrophoresis* (which separates EVs based on their electrophoretic mobility), and *Ion Exchange Chromatography*. Contamination from negatively charged biomolecules or particles is the common drawback of these techniques[27]. N*ickel-based isolation* of EVs (NBI) shares a similar mechanism. Nickel-functionalized agarose beads are used to isolate EVs from plasma. Interestingly, EVs are released from the resin not by changing the ionic strength of

the buffer but using metal chelators (EDTA and citric acid), thus preserving EVs stability and integrity[37].

3.5 Affinity-based techniques

A different option to enrich EVs is to exploit their surface chemical composition instead of their physical properties using *affinity interaction approaches*. Proteins, lipids, and polysaccharides are exposed on the surface of EVs and may act as ligands for manifold molecules[28]. EVs can be selectively separated from complex biological fluids through specific interaction between an affinity agent and its ligand.

The most widespread enrichment method uses antibodies as affinity agents in the so-called *immuno-precipitation technique* (IP). Antibodies are bound to solid surfaces (e.g. magnetic beads, resins, plates) and capture EVs with high selectivity through interaction with their targets, obtaining EVs samples with the highest purity. EVs separated using this technique generally show a higher degree of EV-related proteins. In addition, the use of antibodies allows the separation of EVs from a particular cell or tissue and to harvest specific EV fractions. Unfortunately, antibodies are expensive, there is a lack of specific EV markers and detaching an extracellular vesicle from a bound antibody is challenging (especially if intact EVs are needed for downstream applications or analysis). For these reasons the use of antibodies is still limited, and density or size-based techniques are usually preferred[29].

To reduce the process costs, antibodies can be replaced by *aptamers*. Aptamers are single stranded oligonucleotides that once folded into a 3D structure can bind targets with high selectivity and specificity[38]. Zhang et al.[39] developed an affinity capture system based on a DNA aptamer targeting CD63 that combines the purity of affinity interaction methods with the non-destructive release enabled by aptamers. Upon incubation with the complementary sequence of DNA, the aptamer loses its tertiary structure to form the double helix, releasing EVs from the surface of magnetic beads. Unfortunately, the low number of aptamers directed against specific targets limits their application. As an alternative, *peptides* can also be exploited as affinity agents. A good example is Venceremin, a class of peptides that recognizes heat shock proteins[40].

Not only proteins can be addressed for affinity interaction-based separation, but also lipids and polysaccharides. For example, phosphatidylserine can be recognized by Tim4 protein in the presence of calcium ions, while specific saccharides can bound different lectin's families. Finally heparin can bind the surface of EVs and has been exploited to separate vesicles. The exact affinity mechanism is still unclear[27].

All affinity-based approaches share the same advantages: simple instrumentation (they are also suitable for automatization) and, most importantly, superior specificity. On the other hand, affinity agents might be expensive; The experimental parameters need to be precisely optimized, and the elution, especially from beads, is often troublesome[27].

3.6 Microfluidic-based techniques

Since 2010, miniaturized *microfluidic devices* have emerged as potential tools for EVs separation with important advantages: reduced time, costs, and sample volume, and possibility to combine separation and analysis on the same device (Lab-on-a-chip). These developments will facilitate the introduction of EVs in point-of-care diagnostics (POCs).

Microfluidic devices based on immune-precipitation have been developed to combine extraction and characterization of EVs with minimal manipulation steps. Mixing of antibody-coated beads in a microfluidic device improves the interaction with EVs, thus reducing processing time if compared with standard protocols[29]. It also allows integrating different miniaturized characterization techniques (e.g. miniaturized NMR, fluorescently-labeled antibodies, electrochemical detection and flow cytometry[41–44]).

Recently, *size-based microfluidic separation techniques* have emerged, with the advantage of being label-free. Good examples of these innovative techniques are asymmetric-flow field-flow fractionation (AF4)[45], deterministic lateral displacement (DLD)[46] and acoustophoresis[47].

Despite in the recent decade much efforts have been placed into developing new separation strategies for EVs, there is a need for further improvement. Due to the drastic overlap in physicochemical and biochemical properties between EV-subclasses, there is no a single strategy able to isolate a specific EV-subpopulation. After a separation step, a complex mixture of EVs and other components is often obtained. So far, the combination of different separation techniques represents the best solution to enrich EVs from biological samples[1]. In this scenario, developing new strategies for EV separation is mandatory.

4. Characterization techniques for extracellular vesicles

Once EVs are adequately separated from contaminants, they need to be characterized at physical or functional level. The analysis may alternatively focus on morphological properties or biochemical composition.

4.1 Physical characterization

To gain information about morphology and physical properties, it is mandatory to choose a separation technique that allows the recovery of intact EVs. Current methodologies for the direct analysis of EVs from a physical point of view include the estimation of vesicles size distribution and concentration and the direct imaging of EVs[48].

Size distribution and concentration of EVs are essential parameters to consider since they are influenced by the cell's state (both physiological and pathological)[49]. Both parameters can be analyzed by *Dynamic Light Scattering* (DLS), a technique where a monochromatic and coherent laser beam passes through a particle suspension. When the laser encounters a particle, the light is scattered. The intensity of the scattered light is plotted as a function of time and its fluctuations are correlated with the Brownian motion of particles, which, in turn, correlate with their size. The significant advantage of this technique is that DLS can size particles in a 1 nm – 6 μm range, which is optimal for EVs. Unfortunately, an important limitation when working with EVs is that when DLS analyzes polydisperse suspensions, the size distribution is strongly influenced by larger particles, since they scatter more light, while smaller particles are underestimated[50].

Nanoparticle Tracking Analysis (NTA) is a more sensitive technique for the analysis of polydisperse suspensions. For this reason, NTA has become one of the most widely applied methods for the characterization of EV samples. In this technique, the light of a laser beam that passes through a sample and is scattered by the particles. The light passes through a microscope and is recorded by a high-resolution CMOS camera. In this way Brownian motions of particles can be recorded, and the size determined using the Stokes-Einstein equation. NTA can also measure the concentration of EVs. The advantages of this technique are: i) detection range between 30 nm and 1000 nm, ii) sample recovery after the measurement, and iii) phenotyping through fluorescence detection of labeled EVs. The major limitation are: i) the high volume of sample needed, ii) the strong influence of experimental parameters on results, and iii) the limited concentration range (10^6-10^9 particles/mL)[48,50].

The size distribution and concentration of EVs can also be measured by *Tunable Resistive Pulse Sensing* (TRPS). In this technique, particles are forced to pass through a nanopore. When a particle is within the nanopore, a change in resistivity that correlates with particle size is measured. Moreover, by counting the number of events, it is possible to assess particle concentration in the sample. TRPS can also measure the Zeta-Potential of EVs, but it still has some limitation in detecting nano-sized vesicles[48].

Flow Cytometry (FC) has been widely applied to the analysis of cells. Single particles are forced into single file lines and pass through a laser beam. Light is scattered and measured to count and size particles. In addition, FC possesses a fluorescence readout, which detect the fluorescence produced by decorating particles with fluorescent labels. One major limitation of conventional FC is the detection limit of 200 nm, which is quite high to analyze an EV population. For this reason, different approaches have been introduced to enable EVs detection. For example, flow cytometry that analyzes EVs immuno-captured on beads [48,50]. Recently NanoFCM has introduced the NanoAnalyzer, a high-resolution flow cytometer that can analyze nanovesicles down to 40 nm in diameter. The excellent resolution of this instrument is obtained combining side scattering (SSC) and fluorescence readout[51].

Another option to investigate the morphology of EVs is their direct imaging by electron microscopy, i.e., *Transmission Electron Microscopy* (TEM) and *Scanning Electron Microscopy* (SEM). Both techniques use a beam of electrons, but while TEM produces images using electrons transmitted through the sample, SEM analyzes electrons scattered from the sample. Generally, TEM is used to investigate the internal structure of EVs, while SEC is preferred to evaluate their surface morphology. The major limitation of these techniques is their requirement for sample treatment. EV samples need to be fixed on grids, dehydrated and stained, and all these operations might alter or damage their morphology. To avoid such issues, *Cryo-EM* can be chosen as the analytical technique: samples are placed in vitreous ice and kept at the temperature of liquid nitrogen, thus reducing the damage caused by the electron beam. Unfortunately, electron microscopy techniques are generally expensive, low throughput, and time consuming[21,48,50].

Atomic Force Microscopy (AFM) is another option to give insights into EVs morphology. AFM exploits a cantilever that can deform while interacting with an EV sample deposited on mica surfaces. The cantilever deformation is sensed by laser reflection and turned into a 3D image of the surface. A possible limitation is that EVs, lacking in structural elements such as the cytoskeleton, tend to deform during sample preparation and imaging[48]. However, it is possible to exploit the deformation of EVs to measure their stiffness using AFM, thus introducing a different parameter with potential implications in diagnostics[52,53].

A novel detection method for EVs has been developed and commercialized during the last few years: the *Single Particle Interferometric Reflectance Imaging Sensor* (SP-IRIS). The technique, developed by the group of Professor Selim Unlu at Boston University is commercialized by Nanoview Biosciences. ExoView R100, is an instrument that provides label-free interferometric digital counting, sizing, and phenotyping of sEVs (ranging from 50

to 200 nm in diameter). The instrument uses microarray chips made of silicon layered with silicon dioxide. EV-specific antibodies are bound to the surface of the chip and capture extracellular vesicles based on their surface composition. The instrument shines light from a LED source onto the chip. The interference of light reflected from the surface is modified by the presence of nanovesicles producing a distinct signal (an increase in image contrast) that directly correlates with vesicle size[54].

4.2 Biochemical characterization

In parallel to a physical characterization of EVs, the analysis of their biochemical composition is essential to fully exploit their diagnostic potential. In fact, under pathological conditions EVs' surface and cargo composition is altered compared to vesicles released by "healthy" cells, thus offering different targets to be analyzed including proteins, nucleic acids, lipids and glycans[21].

EV-related proteins are mainly detected using *Western Blot* (WB) analysis or *Enzyme-Linked Immunosorbent Assay* (ELISA), and both methods exploit the affinity interaction between antibodies and proteins of interest, which ensures high selectivity and specificity.

WB is also known as immunoblotting and requires an initial separation of proteins based on their molecular weight using SDS-PAGE electrophoresis, followed by an affinity recognition of target proteins using primary and secondary antibodies labeled to allow chemiluminescence or fluorescence detection.

ELISA is a commonly used method to provide qualitative and quantitative protein detection based on specific antigen binding. ELISA is faster, easier to handle, and prone to high-throughput analyses, but it suffers from variability. During the last few years, antibodies have been accompanied by aptamers as recognition elements. In fact, antigen binding capability of aptamer can be coupled with mature nucleic acids technology, making their use a promising alternative to antibodies[21].

Unfortunately, since the EV-field is rapidly growing and novel markers are constantly discovered and proposed, antibodies or aptamers are not always available for the desired markers. This limitation can be circumvented by proteomics analysis using *Mass Spectrometry* (MS) that does not require labeling of biomarkers. MS, providing complete information about protein content in EVs, is more likely to find new disease-specific biomarkers, as demonstrated by the identification of GPC-1 as a marker for pancreatic cancer-derived EVs[55]. Despite their high potential, MS techniques are limited in their application by the requirement of ultra-pure samples (the presence of soluble proteins as

contaminants may alter MS analysis) and low repeatability, which make this technique unsuitable for clinical purposes[21].

Other essential components of EV cargo are nucleic acids. The principal representative is RNA that plays a key role and has an enormous potential in clinical diagnosis and therapy. Different types of RNA can be found inside EVs, including mRNAs and micro-RNAs. RNA is usually analyzed using *Next Generation Sequencing* (NGS) techniques that require different steps: separation of EVs, extraction of RNA, transcription to cDNA, and real-time quantitative Polymerase Chain Reaction (RT-qPCR). NGS can be either exploited to quantify known RNA sequences or to identify new ones[21].

PCR-free methods for the qualitative and quantitative analysis of RNA have also been developed, represented by microarrays and molecular beacons (MB). Microarray assays are based on the selective interaction between RNAs and complementary probes immobilized on the surface of a chip. Using this technique, up to 1000 different sequences can be analyzed simultaneously, but the quantification ability is limited in comparison with NGS, and there is no possibility to discover new sequences of interest[56].

Molecular beacons are oligonucleotide sequences with a hairpin structure. A fluorophore and a quencher are placed at the opposite sides of their sequence, so that fluorescence is quenched until the hairpin structure is maintained. Upon annealing with complementary RNA, MBs lose the hairpin structure, and a strong fluorescence is emitted. Recently MBs have been successfully used to identify mRNAs and micro-RNAs from cancer-derived EVs, in some cases without needing for previous EVs separation or RNA extraction[57].

EV-related lipids can also be analyzed, mainly by MS techniques, while EV-derived glycans can be detected using lectins or antibodies that bind to specific glycan motifs[21].

CHAPTER 2

DNA-DIRECTED IMMOBILIZATION OF ANTIBODIES

1. DNA-directed immobilization (DDI) approach

The *DNA-directed immobilization of antibodies* (DDI) is an approach that was originally developed in 1994 by Niemeyer et al.[58] to translate the success of DNA microarrays into protein microarrays.

Using DDI proteins are tagged with single stranded DNA (ssDNA) while microarray surfaces are functionalized with complementary ssDNAs. Upon the interaction between complementary strands, proteins are immobilized on microarray chip's surface through a double stranded DNA (dsDNA) linker[59] (see Figure 2.1). This method represents a smart strategy to translate easy-to-generate DNA microarrays into protein microarrays, thus extending technological robustness from DNA to protein microarrays production.

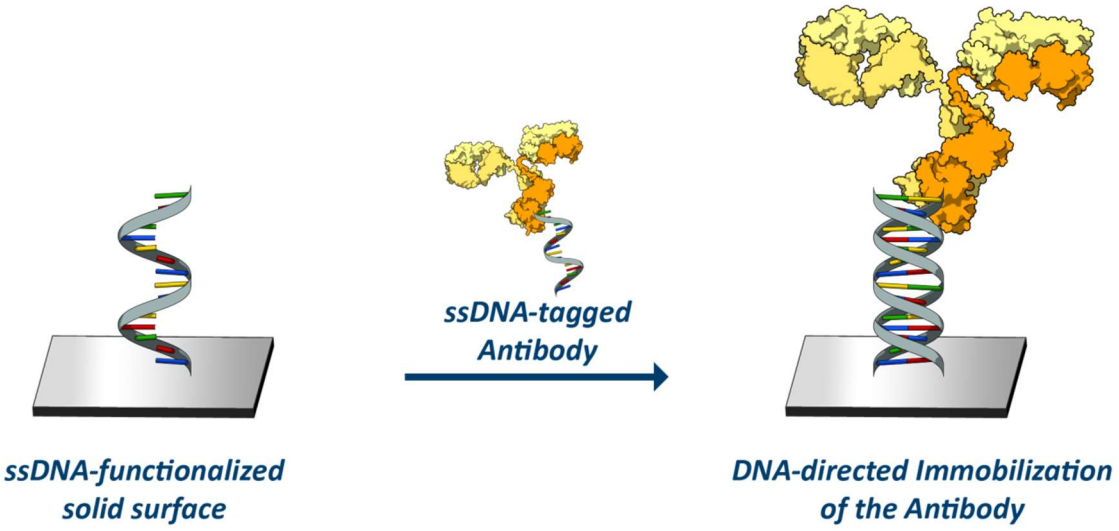

***Figure 2.1**. General scheme representing DNA-directed immobilization of antibodies.*

Double stranded DNA has been demonstrated to be an excellent linker for antibodies on solid surfaces since it enhances the availability of antibody binding sites for biological nanoparticles capture by decreasing the steric hindrance surrounding the protein[60]. This

characteristic has already been confirmed in work by Seymour et al.[61] where DDI of antibodies was used to capture viruses on microarray substrates.
Based on these preliminary evidences we developed a protocol that allows the easy and reproducible synthesis of DNA-antibody conjugates, and we evaluated the possibility to exploit antibodies immobilized via DDI in immuno-capturing of EVs.

2. Development of an immuno-capture platform for extracellular vesicles using DDI

The first prerequisite to perform the DDI of antibodies is the synthesis of DACs. To pursue this goal we chose a two-step reaction that is summarized in Figure 2.2. Briefly, antibodies were reacted with a bifunctional linker that presents an active ester (N-hydroxysuccinimide, NHS) at one end and a dibenzocyclooctine (DBCO) moiety on the opposite end. The NHS group reacts with the ε-amino groups of lysine side chains, thus introducing DBCO groups on the surface of the antibody. After removing unreacted linkers, DBCO-modified antibodies reacted with ssDNA sequences modified with an azido group on 5' end. The strain-promoted azide-alkyne cycloaddition (SPAAC) reaction led to the synthesis of DAC[62].

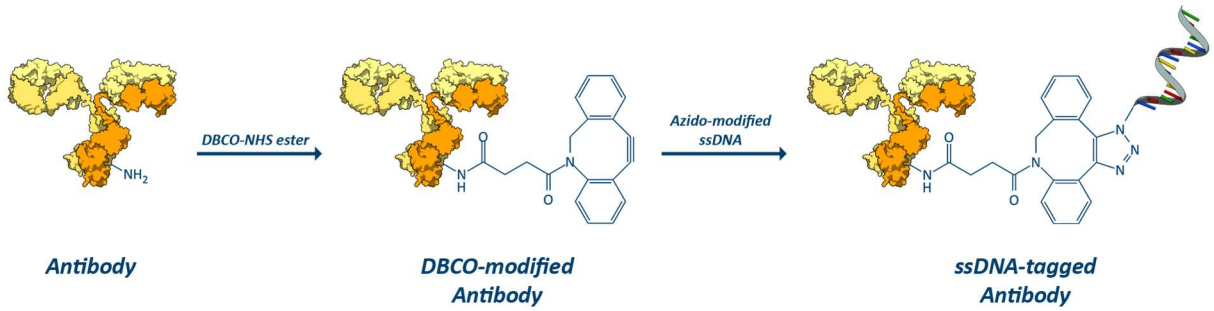

Figure 2.2. Schematic representation of synthetic pathway for DNA-antibody conjugates preparation.

After protocol optimization we synthesized a conjugate of antiCD63 antibody with DNA-tag1 (antiCD63-tag1). CD63 is a transmembrane protein, a member of the tetraspanin family, and is a common constituent of EVs' membrane[1]. Thus, antibodies that bind CD63 can be used to capture and separate EVs on solid surfaces.
Next, we compared the immobilization efficiency of the DNA-tagged antiCD63 on its complementary DNA sequence (i.e., DNA-capture1) with the covalent immobilization of the

same antibody. Additionally, we checked the antibody ability to capture EVs upon DNA conjugation, always comparing its efficiency with that if the same antibody covalently immobilized on sensor's surface.

A set of microarray experiments were designed and are described in the next Sections.

We performed all microarray tests on silicon chips layered with silicon dioxide (the layer's thickness was carefully chosen based on of the detection technique). Silicon chips were coated using MCP-2, a ter-copolymer of *N,N*-dymethilacrylamide (DMA) (97% in moles), *N*-acryloyloxysuccinimide (NAS) (2% in moles) and 3-(trimethoxysilyl) propyl methacrylate (MAPS) (1% in moles). MCP-2 forms a 3-D layer for the immobilization of probes with retained capture efficiency and suppression of non-specific binding, extensively used for biosensing (see copolymer structure in Figure 2.3)[63,64]. NAS is the reactive unit inside the copolymer responsible for immobilizing amino groups of biological probes through an acylation reaction.

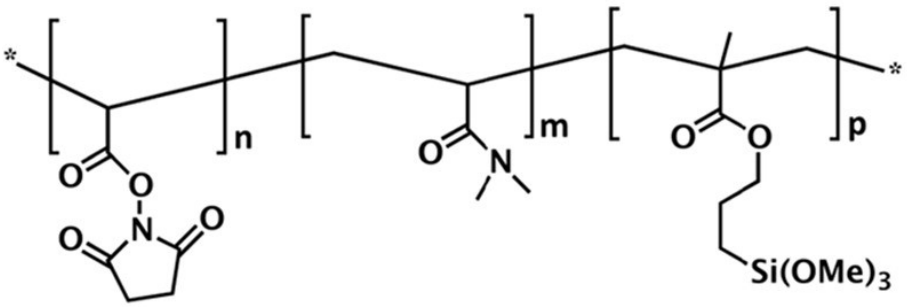

***Figure 2.3**. Chemical structure of MCP-2 ter-copolymer: m=97, n=2, p=1.*

The efficiency of the DNA-directed immobilization of antibodies was tested by a *real-time Interferometric Reflectance Imaging Sensor* (RT-IRIS) device, using a low-magnification IRIS setup designed to perform in-liquid measurements. The biomass that accumulates on different spots as an analyte-containing solution flows into a microfluidic chamber is detected in real-time. The instrument is fully described in [65,66]. Briefly, the technology takes advantage of common path interference to enhance the visibility of the biomass accumulated on the surface. Common path interference is achieved by illuminating a silicon/silicon oxide layered chip (Si/SiO_2) from the top with a combination of four-color LEDs. The thickness of the silicon oxide layer of the chip, 110 nm, is optimized to obtain constructive interference so that the shift of the reflectance curve due to biomass accumulation on the chip correlates with the thickness of the transparent layer. The images were acquired through Micro-Manager software and analyzed in ImageJ to provide reflectance values. A custom-made MATLAB

software converts the raw signal data to mass density. The analysis is illustrated in detail in [67].

Counting of EVs on single spots was performed with ExoView R100, an instrument commercialized by Nanoview Biosciences that employs a technique called *Single Particle Interferometric Reflectance Imaging Sensor* (SP-IRIS). This technique takes advantage of an optical configuration similar to the classic IRIS one. In this case, however, the resolution is much higher due to the presence of a high-magnification objective. The application is different: the SP-IRIS provides digital sizing and counting of individual nanoparticles bound to the surface, ranging from 50 nm to 200 nm in diameter[68]. A single wavelength LED, carefully chosen based on the oxide layer thickness, is used to make single nanoparticles visible. In this work, silicon chips layered with 55 nm of silicon dioxide were used in combination with a near-UV wavelength LED source. Scans of the surface along the focal direction – that is, the direction parallel to the objective - were performed, and changes in the contrast of a single nanoparticle at distinct focal planes could be directly correlated to its size.

2.1 Materials

Ammonium sulphate ((NH4)2SO4), dibenzocyclooctyne-N-hydroxysuccinimidyl ester (DBCO-NHS ester), phosphate buffer saline tablets (PBS), Trizma base, 37% chloric acid (HCl), sodium azide (NaN_3), boric acid, ethylenediaminetetraacetic acid (EDTA), sucrose, xylene cyanol, SYBR green, acrylamide, bisacrylamide, Coomassie brilliant blue, sodium phosphate (Na_3PO_4), sucrose monolaurate, sodium chloride (NaCl), Tween 20, glycerol, sodium dodecyl sulfate (SDS), bromophenol blue, polyclonal rabbit IgG, ethanolamine, trehalose dihydrate and Amicon Ultra centrifugal filters (MWCO 100K) were purchased from Sigma Aldrich (St. Louis, MO, USA). All solvents were used as received. Sodium azide-free mouse anti-human CD63 (clone MEM-259) was provided by HansaBioMed Life Sciences Ltd (Tallinn, Estonia). Oligonucleotides were synthesized by MWG-Biotech AG (Ebevsberg, Germany): see Section 2.1.1 for DNA sequences. ssDNA-tag1 were modified with a C3-azido linker at the 5' end, while ssDNA-capture1 and COCU8 were modified with a C6-amino linker at 5’ end. Oligonucleotides were freeze-dried and resuspended in DI water at a final concentration of 100 μM before use. Centrifugation was carried out using Eppendorf MiniSpin (Eppendorf, Hamburg, Germany). Negative controls were used in each experiment. In antibody DNA-directed immobilization experiments, COCU8 was used as a negative control to demonstrate that the ssDNA modified antibody is specifically captured

only by the oligonucleotide sequence complementary to DNA-tag1. In experiments involving EVs, polyclonal rabbit IgG was used as the negative control. Untreated silicon chips with 110 nm thermal grown oxide (12.5 x 25 mm) were supplied by SVM, Silicon Valley Microelectronics Inc. (Santa Clara, CA, USA). NV10B silicon chips for SP-IRIS measurements were supplied by NanoView Biosciences (Boston, MA, USA). Both chips were pretreated using a HARRICK Plasma Cleaner, PDC-002 (Ithaca, NY, USA), connected to an oxygen line. Spotting was performed using SciFLEXARRAYER S12 (Scienion, Berlin, Germany). Nanoparticle Tracking Analysis was performed with NanoSight NS300 using 3.2 Dev Build 3.2.16 software (Malvern Instruments Ltd, Malvern, United Kingdom).

2.1.1 Oligonucleotide sequences

- *DNA-tag1*: 5'-AAAAAGCCTACGAATGAACAGACTG-3'
- *DNA-capture1*: 5'-ATATGTACCCACCGCATTCTCAGTCTGTTCATTCGTAGGC-3'
- *COCU8*: 5'-GCCCACCTATAAGGTAAAAGTGA-3'

2.1.2 Optimized synthesis of DACs

To a polyclonal rabbit IgG solution in PBS (100 µL, 1 mg/mL) 2.46 µL of DBCO-NHS ester 4 mM (15 equivalents) were added and the mixture was allowed to react 30 min at room temperature. The reaction was quenched in 5 min at room temperature by adding 10 µL of 1 M Tris/HCl pH 8.0. Unreacted DBCO-NHS ester was removed through centrifugation on Amicon Ultra 100 MWCO filters (3 × 5 min at 12.000×*g*). After centrifugation, the volume was adjusted to 100 µL with PBS. DNA-antibody conjugation was performed by adding 6.67 µL (1 equivalent) of azido modified DNA-tag1 from a 100 µM stock solution to 100 µL of DBCO-modified antibody (1 mg/mL). The reaction mixture was incubated overnight at 37 ◦C. Unreacted DNA-tags were removed through centrifugation on Amicon Ultra 100 MWCO filters (3 × 5 min at 12.000×*g*). After centrifugation, the volume was adjusted to 99 µL with PBS. Finally, 1 µL of 2% w/v sodium azide solution was added as a preservative (up to a final azide concentration of 0.02%). Using this protocol polyclonal rabbit IgG was conjugated with DNA-tag1.

2.1.3 Optimization of DNA-antibody conjugation

2.1.3.1 Gel electrophoresis analysis. To 10 µL of a 1 mg/mL solution of unmodified antibody or DAC, 1 µL of 100 µM complementary DNA (i.e. DNA-capture1) was added, and the resulting solution was diluted to 20 µL with sample buffer 2X (90 mM Tris, 90 mM boric acid,

2 mM EDTA, 1 mM sucrose, 0.08% xylene cyanol added with SYBR green 20X obtained diluting a 10.000X stock solution). The obtained samples were loaded on a 7% acrylamide-bisacrylamide gel. After electrophoresis, double-strand DNA bands were revealed using a UV lamp while protein bands with Coomassie brilliant blue.

2.1.3.2 SPAAC reaction temperature optimization. The following protocol was repeated on three aliquots, each time changing SPAAC reaction temperature. To a polyclonal rabbit IgG solution in PBS (100 µL, 1 mg/mL) 2.46 µL of DBCO-NHS ester 4 mM (15 equivalents) were added and the mixture was allowed to react 30 min at room temperature. The reaction was quenched by adding 10 µL of 1M Tris/HCl, pH 8, and left 5 min at room temperature. Unreacted DBCO-NHS ester was removed through centrifugation on Amicon Ultra 10 MWCO filters (3x5 min at 12.000 x g). After centrifugation, the volume was adjusted to 100 µL with PBS. To perform DNA-conjugation, 6.67 µL of azido-modified DNA-tag1 100 µM (1 equivalent) were added to the three aliquots and each of them was incubated overnight at different temperatures (4, 25 and 37°C). Unreacted DNA-tag1 was removed through centrifugation on Amicon Ultra 30 MWCO filters (3x5 min at 12.000 x g). After centrifugation, the volume was adjusted to 99 µL with PBS. Finally, 1 µL of 2% w/v sodium azide solution was added as a preservative (final azide concentration 0.02%). An additional aliquot, was treated as described above without performing the first purification step (for this aliquot SPAAC was carried out at 4°C).

2.1.3.3 Purification step optimization. To a sodium azide free antibody solution in PBS (100 µL, 1 mg/mL) 2.46 µL of DBCO-NHS ester, 4 mM (15 equivalents), were added and the mixture was allowed to react 30 min at room temperature. The reaction was quenched by adding 10 µL of 1M Tris/HCl pH 8 and left 5 min at room temperature. Unreacted DBCO-NHS ester was removed through centrifugation on Amicon Ultra MWCO filters (3x5 min at 12.000 x g). After centrifugation, the volume was adjusted to 100 µL with PBS. To perform DNA-conjugation, 6.67 µL of azido-modified DNA-tag1 100 µM (1 equivalent) were added, and the mixture was incubated overnight at 37°C. Unreacted DNA-tag1 was removed through centrifugation on Amicon Ultra filters (3x5 min at 12.000 x g). After centrifugation, the volume was adjusted to 99 µL with PBS. Finally, 1 µL of 2% w/v sodium azide solution was added as a preservative (final azide concentration 0.02%). The following protocol was repeated twice on aliquots “A” and “B”. For the aliquot “A”, a 10 MWCO centrifugal filter was used for the first purification, while a 30 MWCO filter was used for the second purification.

For the aliquot “B”, two filters with the same cutoff (100 MWCO) were used in both purification steps.

2.1.4 Synthesis of MCP-2

MCP-2 is the commercial name for copoly(DMA-NAS-MAPS). The polymer was synthesized by free radical polymerization, as reported elsewhere[69]. The total concentration of the monomer feed in the solvent was 20% w/v. Briefly, after degassing anhydrous THF with argon, DMA, NAS, and MAPS were added to the reaction flask so that the total monomer feed was 20% w/v. The reaction mixture was heated to 65 °C for two hours in the presence of AIBN. The crude material was cooled to room temperature and diluted 1:1 with dry THF; the solution was then precipitated in petroleum ether (10 times the volume of the reaction mixture) to eliminate unreacted monomers. The polymer was collected by filtration as a white powder and dried under vacuum at room temperature.

2.1.5 Synthesis of antiCD63-tag1

AntiCD63-tag1 was synthesized starting from azide free mouse antiCD63 IgG and azido-modified DNAtag1. To a mouse antiCD63 IgG solution in PBS (100 µL, 1 mg/mL) 2.46 µL of DBCO-NHS ester 4 mM (15 equivalents) were added and the mixture was allowed to react 30 min at room temperature. The reaction was quenched in 5 min at room temperature by adding 10 µL of 1 M Tris/HCl pH 8.0. Unreacted DBCO-NHS ester was removed through centrifugation on Amicon Ultra 100 MWCO filters (3 × 5 min at 12.000×*g*). After centrifugation, the volume was adjusted to 100 µL with PBS. DNA-antibody conjugation was performed by adding 6.67 µL (1 equivalent) of azido modified DNA-tag1 from a 100 µM stock solution to 100 µL of DBCO-modified antibody (1 mg/mL). The reaction mixture was incubated overnight at 37 ◦C. Unreacted DNA-tags were removed through centrifugation on Amicon Ultra 100 MWCO filters (3 × 5 min at 12.000×*g*). After centrifugation, the volume was adjusted to 99 µL with PBS. Finally, 1 µL of 2% w/v sodium azide solution was added as a preservative (up to a final azide concentration of 0.02%).

2.1.6 Microarray chips functionalization

Proteins were dissolved at 2 mg/mL in 50 mM trehalose in PBS, while DNAcapture1 was dissolved in 150 mM sodium phosphate buffer containing 0.01% sucrose monolaurate at pH 8.5. Depending on the detection technique used, the different probes were spotted onto the surface of different silicon/silicon oxide chips. All chips were coated with MCP-2 and spotted

using a noncontact microarray spotter (sciFLEXARRAYER S12, Scienion, Berlin) equipped with an 80 µm nozzle. 400 pL of solution were spotted at room temperature and 65% humidity. Immediately after spotting, the chips were stored overnight in a sealed chamber filled at the bottom with sodium chloride saturated water (40 g/100 mL H_2O). After incubation, they were treated with a blocking solution of ethanolamine (50 mM in 0.1M Tris/HCl buffer pH 9) at room temperature for 1 h. Then chips were rinsed with bidistilled water and dried under a nitrogen stream.

2.1.7 Evaluation of DNA-Directed Immobilization efficiency with RT-IRIS measurements

Different concentrations of DNAcapture1 (0.5, 5, 10, and 25 µM), antiCD63 and a 10 µM solution of COCU8 (a sequence of DNA used as the negative control since it does not bind the DNA-antibody conjugate) were deposited on a silicon chip as described in section 2.1.6. Once ready, the chip was assembled with an adhesive spacer, and an AR-coated glass slide to form a chamber for in-flow measurements [65]. The cartridge thus obtained was loaded into the RT-IRIS instrument and PBS was flowed for 15 min to stabilize the probes. A solution of antiCD63-DNAtag1 was then injected at three increasing concentrations (namely 0.5, 5, and 10 µg/mL) into the system and recirculated for 20 min at an average flow rate of 200 µL/min. The chip was washed after the injection of each antibody concentration with PBS.
Interferometric images were acquired during the whole process with a blue LED light (465 nm). Four-color images, used to generate a look-up table for the conversion to mass density, were acquired at the beginning and at the end of each step[67].

2.1.8 Capture of extracellular vesicles on microarray chip

5 µM DNAcapture1, antiCD63, and polyclonal rabbit IgG (as negative control) were spotted on nine SP-IRIS chips as described in Section 2.1.6. Chips were incubated with a 5 µg/mL solution of antiCD63-DNAtag1 for 1 h at room temperature to perform DDI. Chips were washed 10 min in PBS, rinsed with bidistilled water, and dried. Pre-scan images of the chips were acquired. Chips were divided into groups of three and incubated with three different concentrations (10^8, 10^9, and 10^{10} particles/mL in PBS) of EVs isolated from HEK-293 cell culture media as described in 2.2.9 (isolated sample was diluted in PBS to reach the desired concentration). The incubation was carried out at room temperature in a humid chamber for 2.5 h. The chips were then washed for 10 min in PBS, rinsed with bidistilled water, and dried. Finally, they were analyzed using the SP-IRIS technique on ExoView R100.

2.1.9 Separation of EVs from HEK-293 cell culture medium by ultracentrifugation

HEK-293 cells were seeded on 150 mm dishes in DMEM culture medium supplemented with 10% EV-depleted FCS (obtained by recovering the supernatant after ultracentrifugation of the FCS at 150.000 x g for 17 h), 2 mM L-Glutamine, 100 U/mL penicillin, and 100 µg/mL streptomycin-sulfate. After 72 h incubation, the culture medium was collected and centrifuged at 450 x g for 25 min to remove cell debris. The obtained supernatant was filtered through 0.22 µm filter and then ultracentrifuged at 150.000 x g for 2 hours at 4°C (Beckman Coulter). The EV-containing pellet was finally resuspended in PBS.

2.1.10 Characterization of EVs isolated from HEK-293 cell culture supernatants by ultracentrifugation

2.1.10.1 Nanoparticle Tracking Analysis. All samples were analyzed using Nanosight NS300 (Malvern Panalytical, Malvern, UK) configured with a 532 nm laser. Videos were analyzed by the in-build NanoSight Software NTA 3.2 Dev Build 3.2.16. The Camera type, Camera level, and Detect Threshold were sCMOS, 14 and 4, respectively. A syringe pump with constant flow injection was used. The number of completed tracks in NTA measurements was 5 (a 60 seconds movie was registered for each measurement). The sample was diluted in PBS to a final volume of 1 mL. The ideal concentration was assessed by pre-testing the optimal particle per frame value (20-100 particles per frame).

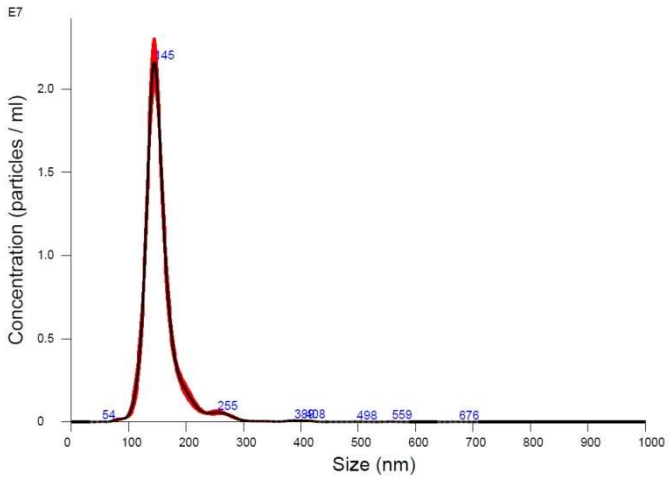

***Figure 2.4**. Nanoparticle Tracking Analysis of EVs isolated from HEK-293 cell culture media by ultracentrifugation.*

2.1.10.2 Western Blot Analysis. Protein content was determined using a protein assay kit (BioRad, CA, USA). Bovine serum albumin (BSA) was used as standard. For tetraspanin detection, the sample was lysed in a non reducing sample buffer (62.5 mM Tris–HCl pH 6.8, 10% glycerol, 2% SDS, and 0.04% bromophenol blue) and boiled for 5 min at 95°C. Then, 15 µg of proteins were loaded on 12% SDS-PAGE gel. For the detection of other proteins, the sample was lysed in reducing sample buffer (62.5 mM Tris–HCl pH 6.8, 10% glycerol, 2% SDS, 1.25% 2-mercaptoethanol and 0.01% bromophenol blue) and boiled for 5 min at 95°C. Then, 24 µg of proteins were loaded on 12% SDS-PAGE gel. After protein separation, gels were electro-transferred onto a nitrocellulose membrane. Nonspecific binding sites were blocked with 5% (w/v) skimmed milk in T-TBS (150mM NaCl, 20mM Tris-HCl pH 7.4, and 0.5% Tween 20). Membranes were incubated overnight at 4°C with the following antibodies: anti-CD63 (1:1000, #556019, BD Pharmingen, CA, USA), anti-CD81 (1:5000, #555675; BD Pharmingen), anti-Alix (1:500, #sc-271975, Santa Cruz, CA, USA) and anti-Calnexin (1:1000, #C7617, Sigma-Aldrich, MO, USA). After several washes in T-TBS, membranes were incubated with goat anti-mouse IgG conjugated to horse-radish peroxidase (1:5000, #170-6516, BioRad Laboratories Inc., CA, USA) for 45 min. Positive immunoreactive bands were detected by the enhanced chemiluminescence method (Immobilon^{TM} HRP substrate, #WBKLS0500, Millipore Corp., MA, USA).

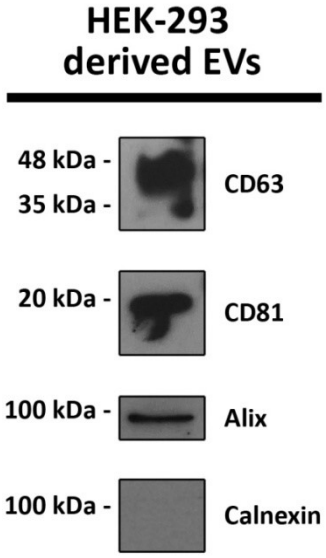

***Figure 2.5**. Western Blot analysis of EVs isolated from HEK-293 cell culture media by ultracentrifugation.*

2.1.10.3 TEM Microscopy. Transmission electron microscopy (TEM) was performed on isolated EVs resuspended in PBS to analyze their ultrastructural morphology. According to

proper dilution, the sample was adsorbed to 300 mesh carbon-coated copper grids (Electron Microscopy Sciences, Hatfield, PA, USA) for 5 min in a humidified chamber at room temperature. EVs on grids were then fixed in 2% glutaraldehyde (Electron Microscopy Sciences, Hatfield, PA, USA) in PBS for 10 min and then briefly rinsed in bidistilled water. Grids with adhered EVs were examined with a Philips CM 100 transmission electron microscope TEM at 80kV, after negative staining with 2% phosphotungstic acid, brought to pH 7.0 with NaOH. The images were captured by a Kodak digital camera.

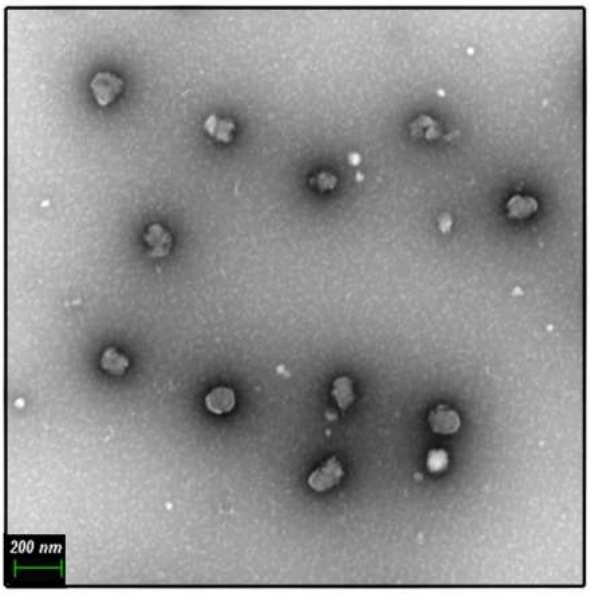

***Figure 2.6**. TEM microscopy image of EVs isolated from HEK-293 cell culture media by ultracentrifugation. Scale bar indicates 200 nm.*

3. Results & Discussion

To synthesize DACs, DBCO-NHS ester was chosen as the bifunctional linker to address lysine residues on antibodies and provide a DBCO-modified antibody. Lysine residues were modified because they are usually abundant in proteins' primary sequence and are generally well exposed and easily accessible in their 3D structure. This feature was critical to develop a synthesis protocol that aimed to be easily adaptable to different antibodies and proteins. Moreover, lysine modification has already been exploited to synthesize clinically relevant antibody-drug conjugates (e.g., Kadcyla® and Zevalin®)[70].

In the second step, the DBCO-modified antibody was reacted with a DNA sequence modified with an azido group. The antibody and the ssDNA were reacted overnight at 37°C, to promote the SPAAC reaction that leads to the formation of a stable triazole, thus obtaining the DAC.

The protocol described in Section 2.1.2 results from an optimization work designed to improve the robustness and reproducibility of the synthesis. In particular, two variables that are most likely to impact on the overall yield of the synthesis were considered i) the purification steps and ii) the temperature of the reaction between the DBCO-modified antibody and the azido-modified DNA.

A polyclonal rabbit IgG was used to optimize experimental conditions. At first, we investigated the effect of temperature on SPAAC conjugation reaction. Three aliquots of polyclonal rabbit IgG were modified as described in 2.1.3.2. The obtained DACs, and native antibody were loaded on a 7% acrylamide-bisacrylamide gel together with their complementary DNA strand (DNA-capture1) and SYBR green for dsDNA UV detection. Another gel, prepared in the same way, was stained using Coomassie brilliant blue, and (Figure 2.7).

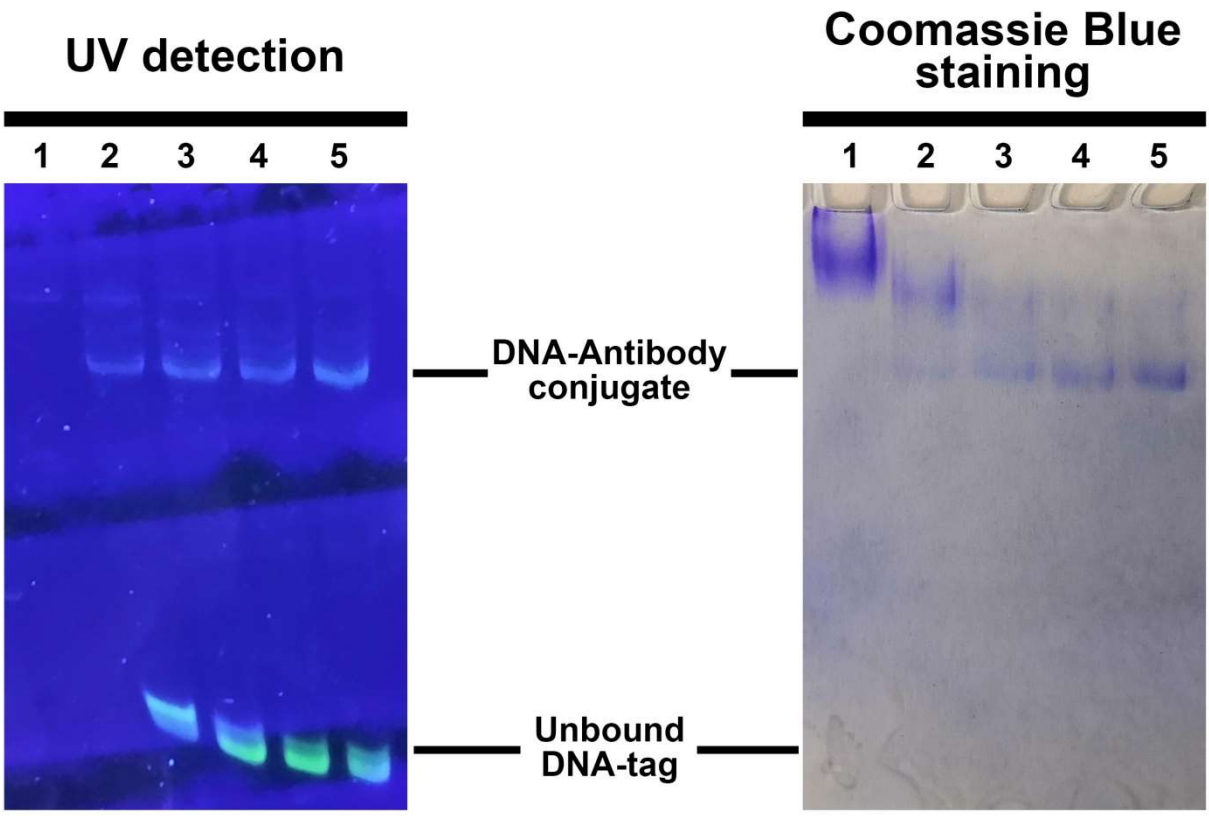

***Figure 2.7**. Gel Electrophoresis of DNA-antibody conjugates obtained with different conjugation protocols. Lane1: Native IgG. Lane2: product conjugated with DNA at 4°C without purification after the first step. The upper band corresponds to the DBCO-modified antibody. Lane3: SPAAC reaction performed at 4°C. Lane4: SPAAC reaction performed at 25°C. Lane5: SPAAC reaction performed at 37°C.*

Using UV, three bands of dsDNA were detected corresponding to i) the unreacted DNA-tag1 (the two bands with higher mobility) and ii) the DAC. The native antibody is not visible with UV detection because it is not stained by SYBR green. The intensity of the band corresponding to the antibody-DNA conjugate increases by raising the conjugation temperature (lane 1 to lane 3). This result is also confirmed by Coomassie brilliant blue staining. For this reason, a temperature of 37°C was chosen as the best condition to perform the SPAAC reaction. In the lower region of the gel, there are two different UV detectable bands. We hypothesize that the band with slightly higher mobility corresponds to unreacted DNA-capture1 itself, while the band with lower mobility corresponds to DNA-capture that has reacted with the remaining DBCO-NHS ester that is still present in the mixture despite the first purification.

A second aliquot of antibody was conjugated following the same protocol (SPAAC reaction at 4°C), skipping the first purification step. Using this procedure, only a small amount of antibody is effectively conjugated to DNA, while the majority of it is modified only with DBCO

(see the upper band in Figure 2.7, lane2). The low reaction yield is probably due to the presence of DBCO-NHS ester in excess that quenches azido groups of oligonucleotides during the conjugation step.

The low reaction yield and the presence of DNA-capture1 in lanes 3, 4 and 5 indicate that purification steps are essential and need improvement. Therefore the cutoff of centrifugal filters was optimized. We used a 100 kDa cutoff for both the purification steps, and then we compared the purity of the samples by gel electrophoresis (Figure 2.8). The two bands of non-conjugated DNA, although still present, are less intense, and the quality of the tagged antibody is compatible with its use in immunoassays.

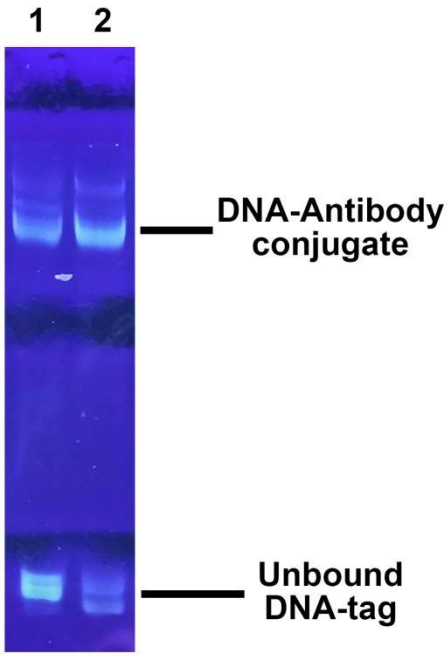

***Figure 2.8**. Gel Electrophoresis of DNA-antibody conjugates obtained using two different purification protocols: aliquot "A" (lane1) and "B" (lane2).*

Once completed the optimization, a robust, reliable synthesis for DACs was obtained. As demonstrated by gel electrophoresis (see Figure 2.8), the protocol leads to the synthesis of DACs with 1:1 ratio between antibody and DNA. All involved reactions require short handling times, relatively cheap reactants, and inexpensive lab equipment, making the conjugation protocol easy to be reproduced in biological laboratories by personnel without a strong background in organic synthesis. During this Ph.D., this optimized protocol has been applied to a large variety of different antibodies and proteins (e.g., streptavidin), always giving satisfactory results (data not shown).

The obtained protocol was used to generate the conjugate between antiCD63 and DNAtag1, from now on called antiCD63-tag1. Then, the first thing to be evaluated was whether this DAC could be effectively immobilized on DNA-capture1 (the complementary sequence of DNA) through DNA-directed immobilization or not.

For this reason, a microarray experiment was devised, and RT-IRIS was chosen for measurement. RT-IRIS is a label-free technique that provides information regarding the accumulation of biological mass on the surface of microarray spots. DNAcapture1 was printed on microarray chips at different concentrations (namely 0.5, 5, 10, and 25 μM), and two different negative controls: COCU8, a sequence of DNA not complementary to antiCD63-DNAtag1 and native antiCD63 itself, which are not supposed to interact with the DAC.

Then microarray chips were assembled in a microfluidic cartridge and incubated with three increasing concentrations of antiCD63-DNAtag1 (0.5, 5, and 10 μg/mL), and biomass accumulation signals (expressed as pg/mm^2) are reported in Figure 2.9.

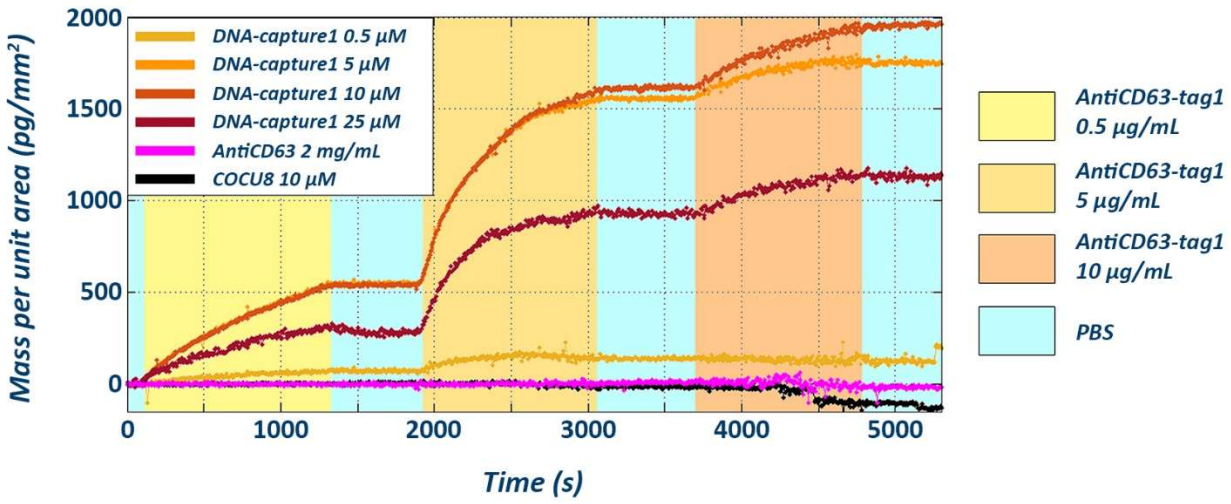

***Figure 2.9**. Real-time IRIS analysis of mass accumulation of DNA-directed antibodies. Mass accumulation over time on spots of antiCD63, COCU8 and DNA-capture1 spotted at 0.5, 5, 10, and 25 μM concentration.*

As expected, no mass is accumulated on negative controls while the signal increase on DNAcapture1 spots, confirming that the DNA-antibody conjugate can be effectively immobilized through DDI and that the interaction is sequence selective (no signal is registered on COCU8 spots).

Different concentrations of DNA-capture1 printed on the surface can immobilize different amounts of antiCD63-tag1. In particular, only small quantities of DAC are immobilized on

0.5 µM spots, and the saturation is reached when 5 µg/mL DAC is used for incubation (no signal increase is observed using higher concentrations). Increasing the concentration of printed DNA to 5 and 10 µM led to a sensibly higher amount of DAC immobilized on the surface, up to 2 ng/mm^2.

Not surprisingly, a further increase in the concentration of DNA-capture1 to 25 µM caused a decrease in the amount of DAC immobilized on the surface through DDI. This phenomenon is probably due to a crowding effect that limits the accessibility of DNA probes on the surface of the microarray chip.

Based on these results, we determined that the best concentrations for subsequent microarray experiments was 5 µM for DNA-capture1 and 5 µg/mL for antiCD63-tag1.

Once demonstrated the immobilization of antiCD63-tag1 on its complementary DNA strand, we investigated its ability to bind CD63+ EVs even if conjugated with DNA. To shed light on this, we performed a different microarray test. Polyclonal rabbit IgG (used as a negative control), native antiCD63, and DNAcapture1 were printed on microarray chips as described in Section 2.2.5. Chips, divided into three groups, were incubated with increasing concentrations of EVs (namely 10^8, 10^9, and 10^{10} particles/mL), and analyzed on ExoView R100 using the SP-IRIS technique and results are shown in Figure 2.10.

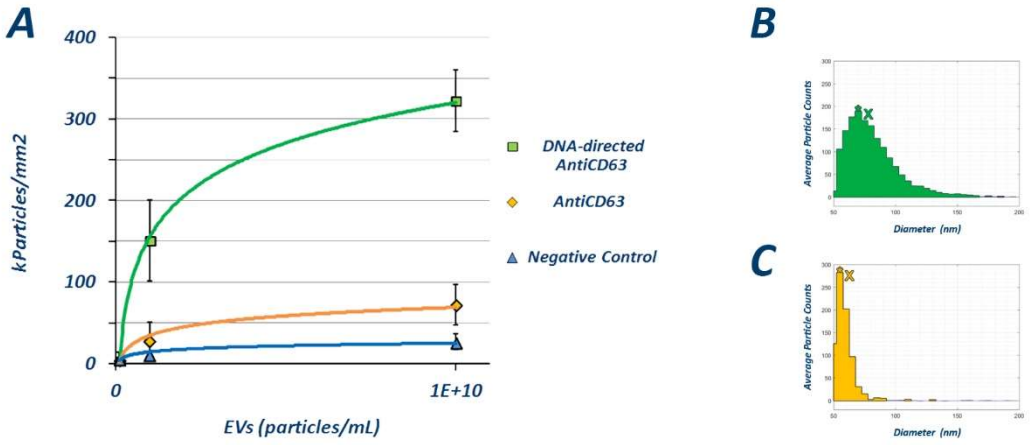

***Figure 2.10**. a) Immobilization rate for EVs on DNA-directed antiCD63, unmodified antiCD63 and negative control. b) Size distribution of EVs captured through DNA-directed antiCD63 and c) unmodified antiCD63*

Surprisingly, DNA-directed antiCD63 not only retained its ability to capture EVs after conjugation with DNA, but it was more effective in binding extracellular vesicles in comparison with native antiCD63 printed on the chip through conventional immobilization. This result further confirmed the beneficial effect of the dsDNA linker between the antibody

and the surface, which was already known to promote a better exposure and accessibility of antigen-binding sites[60].

The better exposure led to capture a higher number of EVs, and bind particles of larger size compared with unmodified antiCD63 (see Figure 2.10b-c).

Table 2.1 summarizes the experimental data obtained in the experiments. The antibody density was measured with the IRIS set-up. The antiCD63 density was measured at the beginning of the experiment while, for antiCD63-DNAtag1, we report the difference between the initial mass and that accumulated on 5 μM DNAcapture1 spot after the incubation with 5 μg/mL DAC). EVs counts were obtained with SP-IRIS experiments incubating the chips with solutions containing 10^{10} particles/mL.

The results clearly show that using the DDI approach, even if a sensibly lower amount of antibody is immobilized on the surface in comparison with conventionally immobilized antibody (around 2.5 times lower) a higher number of EVs is captured (4.5 times the number captured on conventionally immobilized antiCD63). Based on these data, it appears that under the herein described experimental conditions, the binding capacity per unit mass of the same antibody improves by 11 times adding a DNA linker to space the protein from the surface.

IMMOBILIZATION STRATEGY	ANTIBODY DENSITY (pg/mm^2)	CAPTURED EVs (kParticles/mm^2)
Amine Coupling (2 mg/mL)	3879 ± 3	72.4 ± 24.9
DNA-Directed Immobilization (5 μM)	1558 ± 5	322.4 ± 37.8

***Table 2.1**. Comparison between immobilization densities and EV-capture efficiencies for antiCD63 immobilized on the surface through amine coupling and DNA-directed immobilization (data come from experiments described in sections 2.1.7 and 2.1.8), (Mean ± standard deviation of three independent measures).*

CHAPTER 3

ANTIBODY MICROARRAY FABRICATION USING DNA-DIRECTED IMMOBILIZATION OF ANITIBODIES

1. Advantages of DNA-directed immobilization of antibodies

The microarray concept was first introduced by Roger P. Ekins, who developed the so-called multi-analyte immunoassay in 1989[71]; it refers to the miniaturization of thousands of assays on a single substrate. During the following decade, DNA microarrays became widely adopted to simultaneously determine the expression levels of thousands of mRNA. However, gene expression profiling does not always reflect actual protein expression[72]. Since proteins are the key players in most biological processes, there was a need for high-throughput technologies to provide insights into protein functions and interactions. Protein microarrays were developed to fulfill this need[73].

Despite their success, the potential of protein microarrays is still limited by several technological challenges. While DNA is a highly stable oligomer that possesses well- defined physicochemical properties almost independent from its sequence, the term protein represents a heterogeneous class of biomolecules, generally more labile than DNA, displaying different characteristics[74]. Moreover, proteins must retain their tertiary (or even quaternary) structure to maintain their biological activity. Thus, choosing an appropriate immobilization strategy that ensures protein availability and correct surface orientation is crucial. While nucleic acids are commercially available with various chemical groups linked to their 5' and 3' ends that allow optimal surface orientation, proteins are more heterogeneous, making it difficult to devise immobilization protocols of general applicability. Different immobilization approaches were developed (involving site-directed mutagenesis, heterobifunctional crosslinkers, and affinity tags), but, in all the cases mentioned above, the protocol had to be optimized for each protein[75].

To extend to proteins the technological robustness of DNA immobilization, the DNA-directed immobilization (DDI) approach was developed in 1994 by Niemeyer et al.[58]. DDI enables the translation of a DNA array into a protein array thanks to Watson-Crick base pairing between surface-immobilized capture-DNAs and DNA-tagged antibodies[59].

Recent works have demonstrated that DNA linkers are excellent spacers to enhance the availability of antibody binding sites for bio-nanoparticle capture by decreasing the steric hindrance around the protein[60]. Due to these peculiar advantages, during the last two decades, DNA-directed immobilization has been exploited in different fields, including proteomic studies, cell, and microorganism arrays[59,76–78].

All systems based on microarray technology require optimization of spot morphology. Morphological features such as coffee rings, crystallization, or other non-uniform structures prevent accurate detection of particles. However, optimizing spotting conditions is time and material consuming, as many parameters must be varied to obtain homogeneous regions. Moreover, the entire optimization process needs to be repeated every time a new protein is spotted on silicon chips.

A different immobilization strategy based on DDI was developed to bind proteins, in particular, antibodies. DDI can be implemented in any platform based on protein microarrays.

DNA-directed immobilization exploits arrays of DNA-capture probes to immobilize proteins conjugated with complementary DNA-tag sequences. Thus, it is possible to fabricate a single array of multiple DNA-capture sequences that, once spot morphology is optimized, can be turned into multiple antibody microarrays through DNA-directed immobilization of diverse antibodies, without the need to optimize spotting conditions for every single antibody.

2. Development of antibody microarrays for extracellular vesicles' detection using DDI

In addition to these findings, the work described in previous Chapter demonstrated that the presence of the DNA linker enormously improved the capacity of antiCD63 to bind EVs. For this reason, besides the development of a separation protocol for EVs, the DDI approach was evaluated as a strategy to fabricate antibody microarrays for the detection and characterization of EVs.

The performance of antibody microarrays generated by DDI was compared with that of commercially available antibody microarrays, where antibodies are covalently immobilized

on the sensor's surface. In particular, ExoView™ R100 was chosen as model instrument for the comparison.

ExoView™ R100 is an instrument commercialized by NanoView Biosciences (Boston, MA, USA) and is based on SP-IRIS technology. The instrument combines label-free and fluorescence detection of EVs previously captured on an antibody microarray platform[79]. The technique allows to digitally measure the number of particles captured by the different antibodies arrayed on the surface, particularly anti-tetraspanins (CD9, CD41a, CD63, and CD81) antibodies and isotype IgG negative controls. The integration on the same sensing platform of a fluorescence detection module completes the information. After capturing EVs, the chip is incubated with a mix of antibodies, each labeled with a different fluorophore. Colocalization of fluorescence and label-free signals provides the protein expression profile of both surface and luminal proteins.

Advantages in fabricating antibody microarrays through DDI, especially regarding the detection of EVs, were demonstrated and described in the following Sections.

2.1 Materials

Ammonium sulfate ($(NH_4)_2SO_4$), dibenzocyclooctyne-N-hydroxysuccinimidyl ester (DBCO-NHS ester), phosphate buffer saline tablets (PBS), Trizma base, 37% chloric acid (HCl), sodium phosphate (Na_3PO_4), sucrose monolaurate, sodium chloride (NaCl), ethanolamine, trehalose dehydrate and Amicon Ultra centrifugal filters (MWCO 100K) were purchased from Sigma Aldrich (St. Louis, MO, USA). All solvents were used as received. MCP-2 copolymer was purchased from Lucidant Polymers (Sunnyvale, CA, USA). Mouse anti-human CD9 IgG (clone MEM-61) and mouse anti-human CD63 IgG (clone MEM-259) were provided by Hansa BioMed Life Sciences Ltd (Tallinn, Estonia). Cy3-labeled rabbit anti-mouse IgG was purchased from Jackson ImmunoResearch (Baltimore, PA, USA). Oligonucleotides were synthesized by MWG-Biotech AG (Ebevsberg, Germany): see Section 2.1.1 for oligonucleotide sequences. Oligonucleotides were freeze-dried and resuspended in DI water at a final concentration of 100 μM before use. Untreated silicon chips with 100 nm thermal grown oxide (14 x 14 mm) were supplied by SVM, Silicon Valley Microelectronics Inc. (Santa Clara, CA, USA). NV10B silicon chips were supplied by NanoView Biosciences (Boston, MA, USA). Both chips were pretreated using a HARRICK Plasma Cleaner, PDC-002 (Ithaca, NY, USA), connected to an oxygen line. Spotting was performed using SciFLEXARRAYER S12 (Scienion, Berlin, Germany). Centrifugation was carried out using Eppendorf MiniSpin (Eppendorf, Hamburg, Germany). Fluorescence

images were obtained using the ScanArray Lite confocal laser scanner and analyzed using ScanArray Express software (Perkin Elmer, MA, USA). Interferometric analysis of EVs was performed using ExoView™ R100 for image acquisition and NanoViewer 2.6.0 software for analysis (NanoView Biosciences Inc., MA, USA). Nanoparticle Tracking Analysis was performed with NanoSight NS300 using 3.2 Dev Build 3.2.16 software (Malvern Instruments Ltd, Malvern, United Kingdom).

2.1.1 Oligonucleotide sequences

- *DNA-capture1:* 5'-NH_2-ACTTAGGACTCAGTACAGGATAGACTTGATATCGGTTGGA 3'
- *DNA-tag1:* 5'-Azide-AAAAATCCAACCGATATCAAGTCTA-3'
- *DNA-capture2:* 5'-NH_2-ATCCGACCTTGACATCTCTACCACTGCGACTAACTCTGTA-3'
- *DNA-tag2:* 5'-Azide-AAAAATACAGAGTTAGTCGCAGTGG-3'
- *DNA-capture3*: 5'-NH_2-ATATGTACCCACCGCATTCTCAGTCTGTTCATTCGTAGGC-3'
- *DNA-tag3*: 5'-Azide-AAAAAGCCTACGAATGAACAGACTG-3'
- *DNA-stabilizer3*: 5'-AGAATGCGGTGGGTACATAT-3'
- *DNA-capture4*: 5'-NH_2-AAAAAAAAAAAAAAAAAAAAACTCCAGTGCCAAGTACGAT -3'
- *DNA-tag4*: 5'-Azide-AAAAAATCGTACTTGGCACTGGAGT-3'
- *DNA-stabilizer4*: 5'-TTTTTTTTTTTTTTTTTTTT-3'
- *DNA-capture5*: 5'-NH_2-AAAAAAAAAAAAAAAAAAAATAATCTAATTCTGGTCGCGG-3'
- *DNA-tag5*: 5'-Azide-AAAAACCGCGACCAGAATTAGATT-3'

2.1.2 DACs synthesis

DACs were synthesized using protocol described in Chapter 2, Section 2.1.2.
Using this protocol antiCD63 antibody was conjugated with either DNA-tag1 or DNA-tag3. AntiCD9 antibody was tagged with either DNA-tag2 or DNA-tag4, while a polyclonal rabbit IgG was conjugated to DNA-tag5.

2.1.3 DDI selectivity

Nine silicon chips were pretreated with oxygen plasma for 10 min: the oxygen pressure was set to 1.2 bars with a power of 29.6 W. To coat the chips, MCP-2 copolymer was dissolved in DI water to a final concentration of 2% w/v and then diluted 1:1 with a solution of ammonium sulfate 1.6 M. The chips were immersed into each solution for 30 min, then rinsed with DI water, dried under a nitrogen stream, and finally cured at 80°C for 15 minutes. DNA-capture1 and DNA-capture2, dissolved at 0.5, 10 and 25 μM concentration in 150 mM sodium phosphate buffer, pH 8.5, containing 0.01% w/v sucrose monolaurate and antiCD9,

antiCD63 dissolved at 1 mg/mL concentration in PBS containing 50 mM trehalose were spotted in quadruplicate on the chips using a noncontact microarray spotter (sciFLEXARRAYER S12, Scienion, Berlin) equipped with an 80 µm nozzle.

Four hundred pL drops of spotting solution were deposited at room temperature and 65% humidity. Immediately after spotting, the chips were stored overnight in a sealed chamber filled at the bottom with sodium chloride saturated water (40 g/100 mL H_2O). After incubation, the chips were treated with a blocking solution of ethanolamine (50 mM in 0.1 M Tris/HCl buffer pH 9), at room temperature for 1 h. Then chips were rinsed with bidistilled water and dried.

The chips were incubated, in triplicate, either with 5 µg/mL solutions of antiCD9-tag1 and antiCD63-tag2 prepared as described in Section 2.1.2 or with PBS (as the negative control) for 1 h at room temperature. The chips were washed 10 min in PBS, rinsed with bidistilled water, dried under nitrogen stream and then incubated with a 10 µg/mL solution of Cy3-labeled rabbit anti-mouse IgG in PBS for 1 h at room temperature. The chips were washed 10 min in PBS, rinsed with bidistilled water, and dried under a nitrogen stream. Fluorescence images were acquired using ScanArray Lite confocal laser scanner with 65% laser power and 55% PMT.

2.1.4 DNA-probe spotting optimization

Three ExoView™ R100 silicon chips layered with 55 nm silicon oxide were coated using MCP-2 copolymer as described in section 2.1.3. DNA-capture3 alone or mixed in equimolar ratio with an oligonucleotide called DNA-stabilizer was diluted at different concentrations (5,10 and 25 µM for DNA-capture alone; 5+5, 10+10 and 25+25 µM for DNA-capture mixed with DNA-stabilizer) in the spotting buffer (150 mM sodium phosphate buffer, pH 8.5, containing 0.01% sucrose monolaurate). The DNA solutions were printed on coated silicon chips as described in section 4.1.2. The chips were then scanned for label-free particle detection using the ExoView™ R100 instrument and analyzed.

2.1.5 Separation and characterization of HEK EVs

2.1.5.1 HEK-derived sEVs separation by ultracentrifugation. Three days conditioned media from HEK-293 cells were harvested and centrifuged at 500 x g for 25 minutes. Supernatants were filtered with 0.22 mm filters (Merck Millipore) and centrifuged in a SorvallTM WX Ultracentrifuge (ThermoFisher Scientific, WX Ultra 100 #75000100) at 150.000 x g for 90 minutes at 4°C with a SureSpinTM 630 swinging bucket rotor (ThermoFisher Scientific) to

pellet EVs. After the supernatant was carefully removed, EV-containing pellets were resuspended in PBS and directly used for subsequent analysis.

2.1.5.2 HEK-derived sEVs characterization using Nanoparticle Tracking Analysis. The sample obtained as reported in paragraph 2.1.5.1 was analyzed using Nanosight NS300 (Malvern Panalytical, Malvern, UK). Videos were analyzed by the in-built NanoSight Software NTA 3.2 Dev Build 3.2.16. The Camera type, Camera level, and Detect Threshold were sCMOS, 14 and 4, respectively. The number of completed tracks in NTA measurements was 5 (a 60 seconds movie was registered for each measurement). The sample was diluted in PBS to a final volume of 1 mL. The ideal concentration was assessed by pre-testing the optimal particle per frame value (20-100 particles per frame).

2.1.6 EVs capture on antibodies immobilized by conventional and DDI approach

Three SP-IRIS silicon chips were coated and spotted as described in section 2.1.3. Polyclonal rabbit IgG, mouse antiCD63 IgG and DNA-capture3 mixed with DNA-stabilizer3 (25 + 25 μM) were printed on silicon chips. After the chips were blocked, they were incubated with a 5 μg/mL solution of antiCD63-tag3 in PBS for 1 h at room temperature. The chips were washed 10 min in PBS, rinsed with bidistilled water, dried, mapped and pre-scanned using ExoView™ R100. Then the chips were incubated with EVs isolated from HEK cell culture media ($5*10^9$ particles/mL in PBS) for 2.5 h at room temperature. To compare conventional immobilization with DDI, three commercial microarray chips, part of the ExoView Tetraspanin Plasma kit, were also included in this experiment. Also in this case, the chips were incubated with EVs isolated from HEK cell culture media ($5*10^9$ particles/mL in PBS) for 2.5 h at room temperature. After incubation, all chips were washed for 10 min in PBS, rinsed with bidistilled water, dried and incubated for 1 h at room temperature with fluorescently labeled antiCD81 solution, obtained by diluting 1:1000 in PBS the stock solution supplied with ExoView Tetraspanin Plasma kit (NanoView Biosciences, Boston, USA). The chips were then washed 10 min in PBS, rinsed with bidistilled water and dried. Silicon chips were analyzed using ExoView™ R100 to get post-scan data.

2.1.7 Linear dependence of capture on EVs concentration

Eighteen silicon SP-IRIS chips were coated and spotted with DNA-capture3 mixed with DNA-stabilizer3 (25 + 25 μM) as described in section 2.1.3. After the blocking, the chips were incubated with a 5 μg/mL solution of antiCD63-tag3 in PBS for 1 h at room temperature.

The chips were washed 10 min in PBS, rinsed with bidistilled water, dried, mapped and analyzed using ExoView™ R100 to obtain pre-scan images. Then the chips, in triplicate, were incubated either with PBS or with increasing concentrations of EVs isolated from HEK cell culture media (namely $5*10^8$, $1*10^9$, $5*10^9$, $1*10^{10}$ and $5*10^{10}$ particles/mL in PBS) for 2.5 h at room temperature. After incubation, all chips were washed for 10 min in PBS, rinsed with bidistilled water, dried and incubated for 1 h at room temperature with fluorescently labeled antiCD81 solution, obtained by diluting 1:1000 in PBS the stock solution supplied with ExoView Tetraspanin Plasma kit (NanoView Biosciences, Boston, USA). The chips were then washed 10 min in PBS, rinsed with bidistilled water and dried. Silicon chips were analyzed using ExoView™ R100 to get post-scan data.

2.1.8 Multiplexing analysis of EVs on antibody microarray generated by DDI

Three silicon SP-IRIS chips were coated and spotted with 3 different mixtures of DNA-capture and DNA-stabilizer strands (25 + 25 μM, namely DNA-capture3 mixed with DNA-stabilizer3, and DNA-capture4 and 5, both mixed with DNA-stabilizer4) as described in section 2.4. After the blocking, the chips were incubated with antiCD63-tag3, antiCD9-tag4, and polyclonal rabbit IgG-tag5, each 5 μg/mL in PBS for 1 h at room temperature. The chips were washed 10 min in PBS, rinsed with bidistilled water, dried, mapped, and analyzed using ExoView™ R100 to obtain pre-scan images. Then the chips were incubated with EVs isolated from HEK cell culture media ($5*10^9$ particles/mL in PBS) for 2.5 h at room temperature. After incubation, chips were washed for 10 min in PBS, rinsed with bidistilled water, dried and incubated for 1 h at room temperature with fluorescently labeled antiCD81 solution, obtained by diluting 1:1000 in PBS the stock solution supplied with ExoView Tetraspanin Plasma kit (NanoView Biosciences, Boston, USA). The chips were then washed 10 min in PBS, rinsed with bidistilled water, and dried. Silicon chips were analyzed using ExoView™ R100 to get post-scan data.

3. Results and Discussion

Driven by the interest in diagnostic use of EVs, many methods to analyze them and their cargo were developed in the last few years. Several detection techniques, both label-based (e.g., nanoparticle tracking analysis, flow cytometry, digital PCR, microscopic imaging, and

DNA-PAINT) and label-free (Raman spectroscopy, atomic force microscopy, infrared spectroscopy, and interferometric imaging), were developed[80].

New approaches to analyze EVs based on a protein microarray platform were introduced recently. Antibodies printed onto a substrate, either a glass slide or a silicon chip capture EVs through their surface or surface-associated proteins. Once captured on the surface, EV profiling can be performed by label-free or fluorescence detection with labeled selected antibodies such as antiCD9, -CD63, and -CD81.

Recently, Nanoview Biosciences (Boston, MA, USA) has introduced ExoView™ R100, an instrument that provides EVs counting and phenotyping at single-particle level by combining interferometric and fluorescent detection on an antibody microarray platform[79].

Since the EV field is in continuous and rapid evolution, the discovery of new potential biomarkers requires the ability to functionalize a microarray diagnostic platform with new antibodies constantly. Optimizing the spotting procedure is a time-consuming process that limits, or even hinders, the multiplexing potential of antibody microarrays. In the process of covalent immobilization, the antibodies must be dissolved in amine-free buffers at the proper concentration. Additives such as glycerol or residual ammonium sulfate, often present in commercial products, lead to poor immobilization. In addition, protein/peptide molecules are known to interact strongly with a wide variety of solid surfaces through hydrophobic, electrostatic, and hydrogen bond interactions. The presence of a rigid linker prevents the formation of attractive interaction with the solid surface favoring the folding of the protein into its native state. The DNA-directed immobilization strategy allows transforming DNA microarrays into protein microarrays, offering a solution to most protein immobilization problems. Furthermore, once the spot morphology of several single- stranded DNAs is optimized, the same microarray can be used for all the proteins of interest.

For all these reasons, we evaluated the applicability of DDI to generate antibody microarrays for the analysis of EVs. Firstly, we studied the possibility to fabricate multiplexed antibody microarrays through DDI. To do so, silicon chips were printed with unmodified antibodies (namely antiCD9 and antiCD63) and with DNA probes (DNA-capture1 to immobilize antiCD9-tag1 and DNA-capture2 to bind antiCD63-tag2) using a noncontact microarray spotter. The DNA probes, dissolved in printing buffer at 3 different concentrations, 0.5, 10, and 25 μM, were spotted on nine chips that were divided into three groups (three replicates each) and incubated with 5 μg/mL antiCD9-tag1, antiCD63-tag2, and PBS as the negative control.

Surface immobilized antibodies were scanned for fluorescence detection after incubation with Cy3-labeled rabbit anti-mouse IgG. The results in Figure 3.1 indicate each DNA-antibody conjugate binds specifically to its complementary surface-immobilized DNA (Figure 3.1a-b). Incubation with PBS, the negative control, demonstrates the absence of nonspecific interactions between a fluorescently-labeled secondary antibody and surface DNA (Figure 3.1c).

These results show that increasing the concentration of spotted oligonucleotide from 10 to 25 μM leads only to a slight increment of captured antibody. At 25 μM, the amount of antibody captured by DDI is similar to that captured by the antibody covalently bound to the chip.

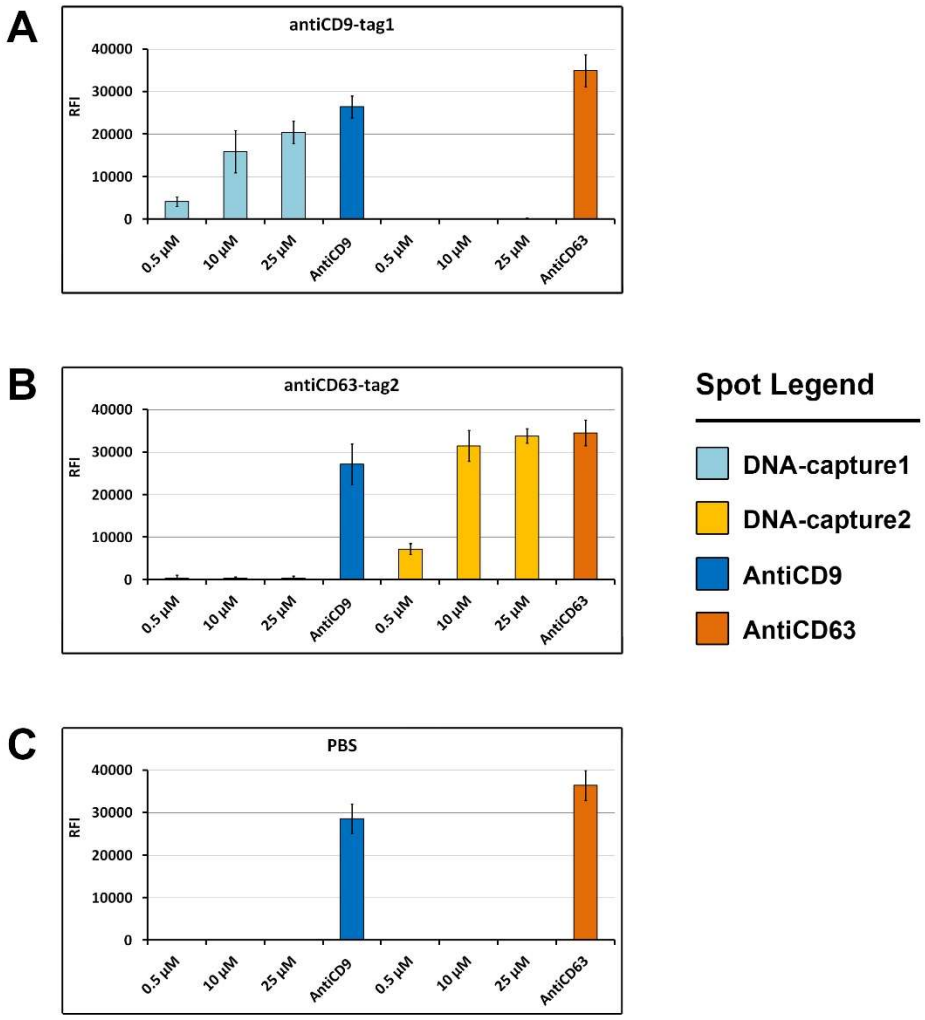

***Figure 3.1**. Antibody capture on DNA-capture strands through DDI. Fluorescence data for a) chips incubated with antiCD9-tag1, b) chips incubated with antiCD63-tag2 and c) chips incubated with PBS.*

As already mentioned, spot morphology is of utmost importance in microarray applications. This is even more crucial for SP-IRIS technique. Morphologies aberrations led to irregular spots with wrinkled surfaces that are erroneously detected as particles by the instrument even before incubating with EVs. This phenomenon causes misleading and unreliable data. For this reason, we optimized spot morphology.

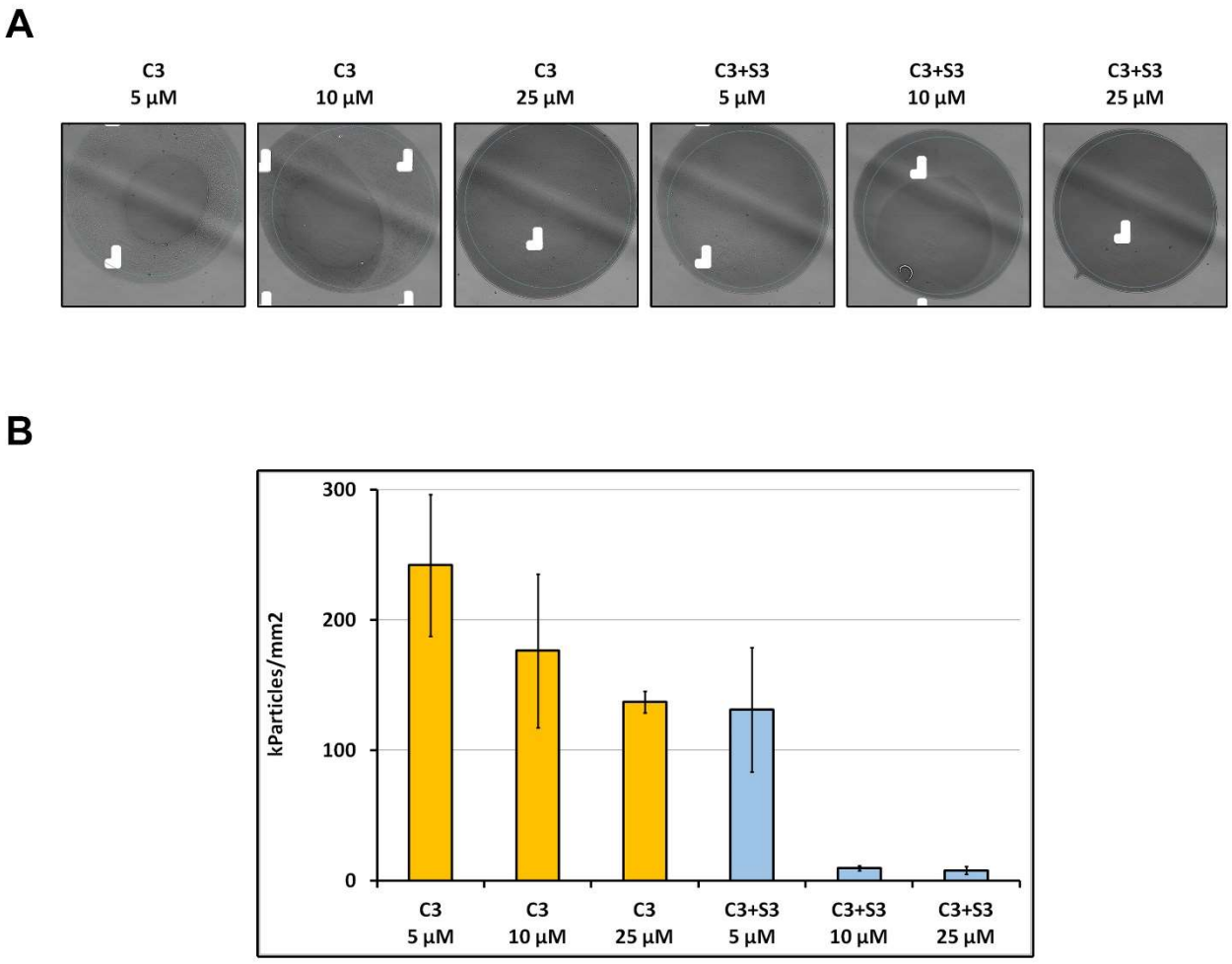

***Figure 3.2**. a) Label free images of DNA spotted under different conditions. b) Density of particles detected by ExoView™ R100 during pre-scan step using different spotting conditions. Both DNA-capture3 alone (C3) and DNA-capture3 prehybridized with DNA-stabilizer3 (C3+S3) were printed on chip at three different concentrations.*

To produce homogeneous spots, we investigated different options. First, we spotted three different concentrations of oligonucleotide DNA-capture3 (5, 10 and 25 µM) on silicon chips. The DNA-capture probe is a 40-*mer* oligonucleotide where 20 bases at 3' end are complementary to the antibody tag sequence. The 5' end bears the amino-linker, and it is used to bind the oligonucleotide to the surface covalently. Unfortunately, these solutions of oligonucleotides do not provide spots suitable for detection on ExoView™ R100. They are

inhomogeneous, with regions of different density and, most importantly, they are not flat (see Figure 3.2a).

In an attempt to improve spot morphology, the 20-*mer* portion of the DNA-capture probe at the 5' end was hybridized in solution, before spotting, with a complementary oligonucleotide called DNA-stabilizer that was added in equimolar ratio to the probe.

Generally, an increased concentration of DNA-capture led to lower particle counts. Moreover, adding the DNA-stabilizer to the DNA-capture caused a significant reduction of particle density in the pre-scan (Figure 3.2b). A possible explanation is that the stabilizer, which is complementary to the region of DNA close to the surface, produces a dsDNA region with a lower propensity to aggregate with nearby oligonucleotides. In addition, its enhanced rigidity in comparison with ssDNA leads to a better orientation of the DNA strand.

Based on spot morphology (shape and homogeneity) and lower number of background particles detected during the pre-scan, 25 μM DNA-capture prehybridized with DNA-stabilizer at the same concentration was chosen as the best condition for printing DNA on microarray chips for further experiments.

We then tested the performance of antibody microarrays fabricated via DDI for EV-capturing. DNA-capture3 was spotted on silicon chips coated with MCP-2 using optimized spotting conditions and DDI of antiCD63-tag3 was performed. Then the system was tested using sEVs derived from HEK-293 cell line, obtained through ultracentrifugation whose quality, and Nanoparticle Tracking Analysis assessed the concentration (NTA, data not shown). The linearity of the dose/response curve was demonstrated with silicon chips functionalized with antiCD63 immobilized via DDI and incubated with increasing concentrations of EVs (from $5*10^8$ to $5*10^{10}$ particles/mL), as described in Section 2.1.7. Subsequent incubation with fluorescently-labeled antiCD81 was also performed, and the analysis of label-free and fluorescence signals on the chips was carried out using ExoView™ R100 (see Figure 3.3a). For all the concentrations tested, a good correspondence between label-free and fluorescent signals was observed. We evaluated the linearity within this range of concentrations (Figure 3.3b-c). While we can fit fluorescent signals with a straight line comprising all the experimental points, the number of vesicles detected label-free at the highest concentration tested (i.e. $5*10^{10}$ particles/mL) reaches saturation. We expected this result since digital counting of the nanoparticles is impossible if their density on the surface is too high, while fluorescence is less affected by this phenomenon.

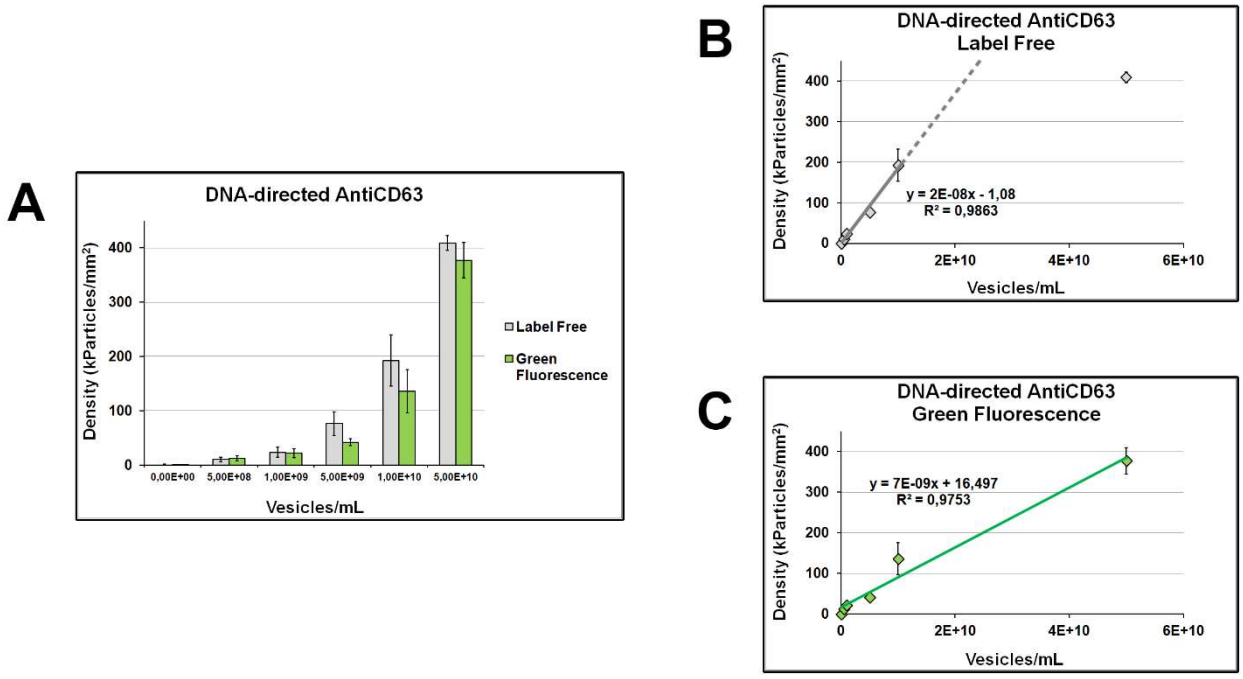

***Figure 3.3**. Label free and fluorescence detection of single extracellular vesicles captured on microarray chip using DNA-directed antiCD63 when incubated at different concentrations (a). Linear regressions of the same data are shown for label free (b) and fluorescence (c) detection.*

Then, we compared the performance of antibody microarray generated by DDI to that of the ExoView Tetraspanin Plasma kit (i.e. the commercially available antibody microarray). The chips were incubated using EVs and analyzed as described in Section 2.1.6. Label-free particle counts and fluorescence signals are shown in Figure 3.4, and compared with results obtained using the DDI approach. In general, signals detected with ExoView kit showed a higher standard deviation, than those provided by DDI chips except for antiCD9 spots.

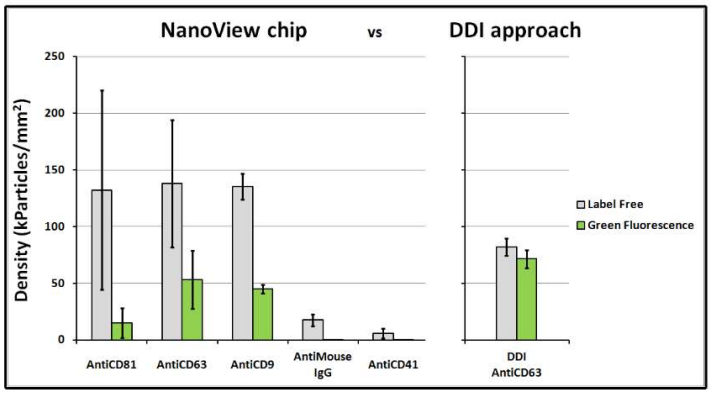

***Figure 3.4**. Particles captured from HEK-derived EVs on (left panel) commercial antibody array or (right panel) DDI-based antibody microarray, detected using label free interferometry (gray bars) and fluorescence (green bars).*

No signals were detected on the negative control spots (mouse IgG) and on antiCD41a (a marker for platelet-derived vesicles, which are not supposed to be found in EVs isolated from cell culture media), while a high number of particles was detected on the other anti-tetraspanins antibodies (CD9, CD63 and CD81). Combining ExoView™ R100 fluorescent and label-free counts, we assessed the number of colocalized vesicles, which are particles that were simultaneously detected by the two modes. This is an important indication of the quality of the analysis. Particles that present only label-free signals may be extracellular vesicles but also protein aggregates and other entities that are erroneously recognized as particles. Likewise, fluorescent signals may come from EVs smaller than 50 nm but from non-specific interactions between the fluorescent antibody and the surface.

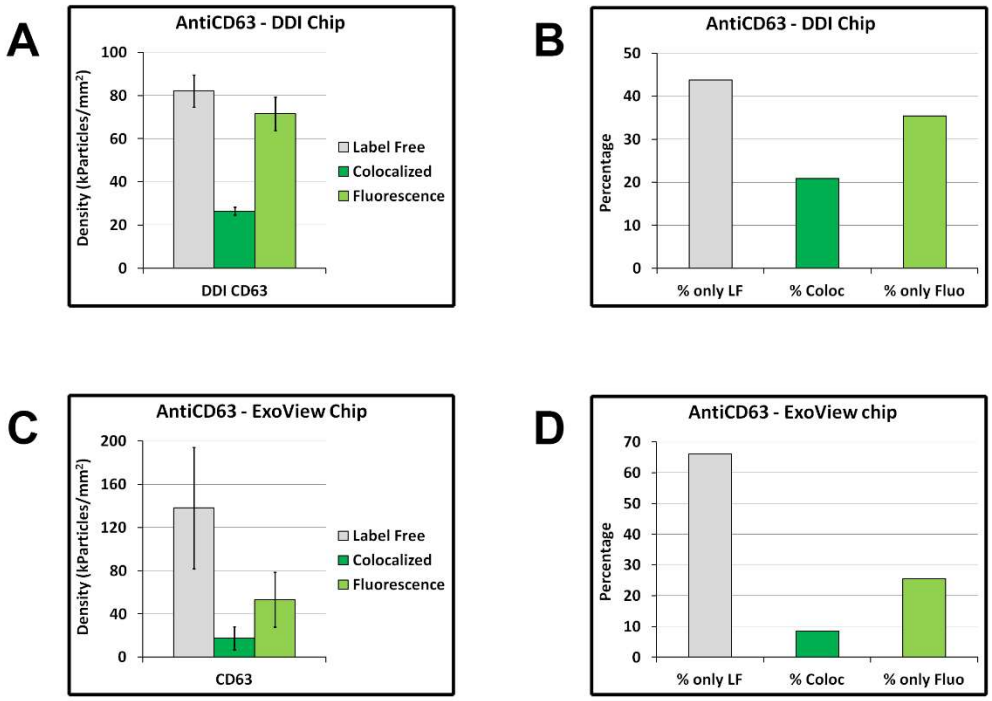

***Figure 3.5**. Label free and fluorescence detection of EVs captured on microarray chip using either DNA-directed antiCD63 (a and b) and covalently immobilized antiCD63 (c and d). a;c) Dark green data represents colocalized particles, which are particles detected by label free and fluorescence detection modes simultaneously. B;d) Percentage* of label free only, fluorescent only and colocalized signals obtained incubating the chips with 5*10^9 EVs/mL.*

(*) For percentage measurement the density of colocalized particles has been subtracted from total label free and fluorescence densities and measured as follows:

- **Total label free particle density (L)**
- **Total fluorescence particle density (F)**

- **Colocalized particle density (C)**
- **Total particle density (T) = (L - C) + (F - C) + C**
- **Label free percentage = [(L – C) / T] * 100**
- **Fluorescence percentage = [(F – C) / T] * 100**
- **Colocalized percentage = (C / T) * 100**

The number of fluorescent and label-free particles detected on antiCD63 spots is reported in Figure 3.5, together with the number of so-called colocalized particles that are vesicles seen simultaneously by both detection modes. By comparing the results obtained with the different immobilization approaches, we demonstrated that, while colocalized and fluorescence signals are quite similar in the two cases, the label-free signal in the ExoView chip is almost double that obtained with the custom array. The percentage of colocalized particles on ExoView chip is 8.4% (lower than the 20.8% registered using DDI). Since the two types of chips were incubated with the same sample, the observed difference might indicate a greater specificity of antiCD63 when it is immobilized on the surface through DDI. We also considered the size distribution of the fraction of particles detected simultaneously as label and label-free particles on ExoView and on our custom chips. On both types of substrates, the number of particles captured by the isotype control (mouse IgG) is negligible, while antitetraspanins antibodies capture particles of EVs-compatible size (see Figure 3.6).

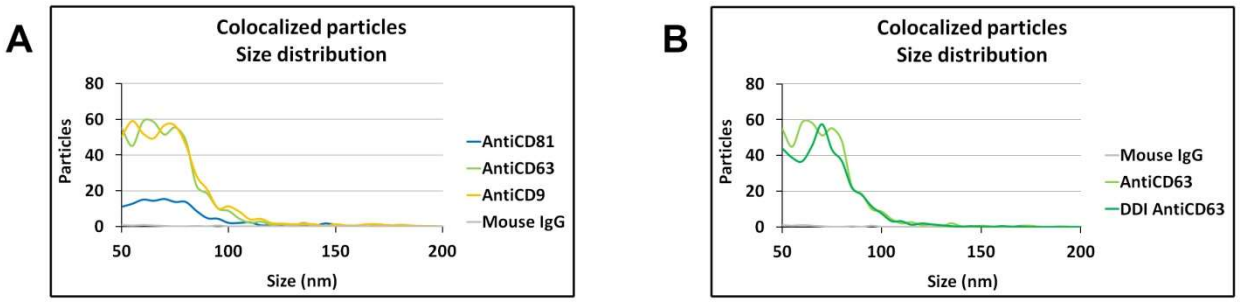

***Figure 3.6**. a) Size distribution of colocalized purified EVs captured on ExoView chip by antitetraspanins antibodies and isotype control. b) Size distribution of colocalized EVs captured by antiCD63 printed on microarray (light green line) or DNA-directed (dark green line) on custom array.*

Finally, to demonstrate how multiplexed antibody microarrays can be fabricated using the DDI approach, silicon SP-IRIS chips were functionalized with 3 DNA-capture sequences to immobilize antibodies tagged with different DNA-tags (namely antiCD63-tag3, antiCD9-tag4 and polyclonal rabbit IgG-tag5 as negative control) as described in section 2.1.8. After DNA-

directed immobilization of antibodies, the chips were incubated with $5*10^9$ particles/mL EVs purified from HEK-293 cell line culture media and then with Cy3-labeled antiCD81 and analyzed using ExoView™ R100. Results are shown in Figure 3.7, and compared with those obtained with the experiment on commercial chip described in section 2.1.6. The results obtained using the DDI approach substantially replicate the ones obtained with commercial chip (no signal is detected on negative control, while antitetraspanin antibodies capture EVs), confirming that DNA-directed immobilization strategy is suitable for generating a multiplexing analytical platform.

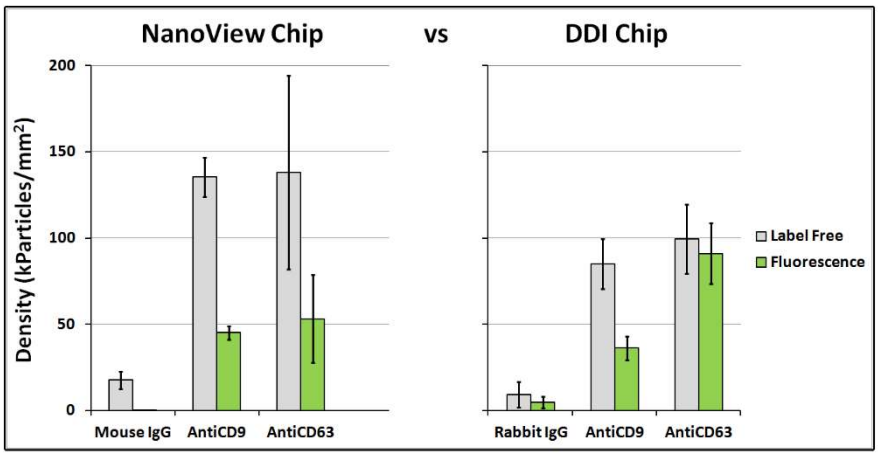

***Figure 3.7**. Particles captured from HEK-derived EVs on negative control antibody, antiCD9 and antiCD63 immobilized via (left panel) conventional spotting or (right panel) DNA-directed immobilization. Particles are detected using both label free interferometry (gray bars) and fluorescence (green bars).*

Within this work, 5 DNA capture-tag pairs were successfully used to perform DDI, but many more sequences can be used on the same platform, with the only limitation represented by the need for selectivity between DNA tags and the arrayed strands. Moreover, since the DNA is only used to direct the protein on the chip and is not involved in the target recognition, the choice of a particular DNA-tag for antibody conjugation does not affect the analysis.

In conclusion, DNA-directed immobilization of proteins was confirmed as a viable method for transforming DNA microarrays into antibody microarrays. The conditions to spot DNA on silicon chips were optimized.

DDI approach was successfully exploited to capture EVs from diluted samples demonstrating similar or even better detection performance in EVs immunocapturing than conventional antibody microarrays.

Additionally, the herein proposed approach extends to protein arrays the technological advantages of DNA microarrays (ease of fabrication, lower costs and longer stability) offering a freely customizable platform that can be functionalized with any antibody of interest without optimizing the spotting of each antibody.

CHAPTER 4

IMMUNO-AFFINITY SEPARATION OF EXTRACELLULAR VESICLES USING DNA-DIRECTED IMMOBILIZATION OF ANTIBODIES

1. Use of DDI in combination with enzymatic cleavage of DNA linker

Double stranded DNA is an excellent linker for antibodies on solid surfaces since it enhances the availability of antibody binding sites for biological nanoparticles capture by decreasing the steric hindrance surrounding the protein[60]. In Chapters 2 and 3 we demonstrated that EV-binding capacity of antiCD63 IgG sensibly improves when the antibody is anchored on the surface through DNA-directed immobilization.

Additionally, the interaction between DNA strands in the linker is non-covalent and reversible, meaning that one can potentially remove the antibody from the surface in a mild and stimulus-controlled way. This is particularly important because once the antibody has captured the EV, their interaction is hard to revert. The detachment requires low pH, high ionic strength and/or detergents, conditions known to damage EVs[29]. For this reason, it is more convenient to work on the DNA linker to enable the release of intact EVs.

Different options to revert the interaction between the DNA strands are available, including changes of physical properties (e.g., heating and sonicating) or chemical conditions (such as alkaline treatment, use of formamide, and DMSO). Unfortunately, both options are not compatible with the stability of EVs.

For this reason, a different approach has been chosen: the use of endonucleases, a class of enzymes that catalyzes the cleavage of dsDNA, is compatible with EVs (see Figure 4.1). In particular, the choice fell on DNase I, an endonuclease that randomly cuts dsDNA and requires only divalent cations (in particular calcium and magnesium) as cofactors to catalyze the reaction[81]. The enzyme displays maximum efficacy when working at 37°C. The presence of divalent cations and the operational temperature are fully compliant with the release of intact EVs, thus enabling their further characterization using imaging techniques such as SP-IRIS, Nanoparticle Tracking Analysis, TEM and Nanoscale Flow Cytometry.

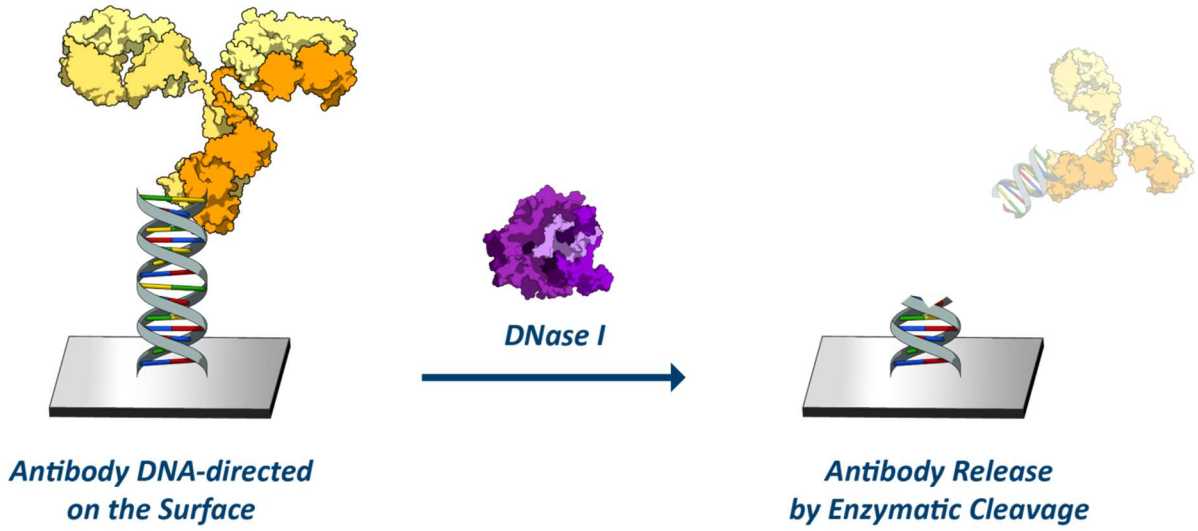

***Figure 4.1**. Schematic representation of DNase I-mediated release of antibodies immobilized via DDI.*

To achieve this challenging goal, namely the immuno-affinity separation of EVs from complex biological fluids followed by their enzymatic release using DNase I, DDI protocols developed in previous Chapters were transferred onto magnetic beads.

2. Development of reversible DNA-directed immobilization of antibodies for extracellular vesicles' separation

In the first place, we evaluated the possibility to detach antibodies, previously immobilized via DDI, exploiting the enzymatic cleavage of dsDNA-linker mediated by DNase I. To this extent, microarray experiments were first devised and demonstrated that i) antibodies are effectively released from the surface upon incubation with the enzyme, and ii) the system is also able to provide reversible immuno-capturing of EVs.

Subsequently, we transferred the process to magnetic beads. In particular, we chose streptavidin-coated magnetic beads as the most appropriate substrate due to their commercial availability and ease of functionalization through biotinylated biomolecules[82]. Magnetic beads were functionalized using biotin-labeled DNA-capture1 and captured antiCD63-tag1 via DDI as represented in Figure 4.2a.

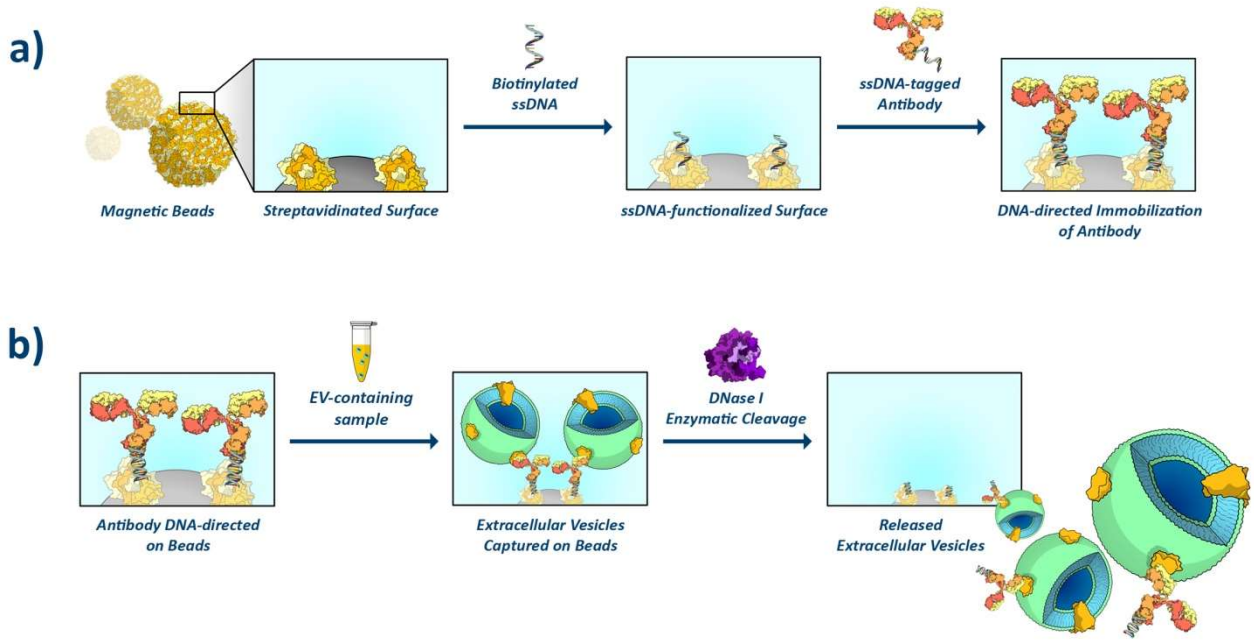

***Figure 4.2**. Schematic representation of DDI-based approach on magnetic beads. a) Beads functionalization and b) extracellular vesicles separation from biological samples.*

Once functionalized, antiCD63-decorated magnetic beads were incubated with samples of increasing complexity containing EVs. We initially used EVs pre-enriched through ultracentrifugation, then HEK-293 cell culture supernatant, and finally human blood plasma. The catalytic activity of DNase I promoted the cleavage of the DNA linker (see Figure 4.2b), and the separated EVs were finally analyzed using different techniques to test system efficiency and selectivity.

2.1 Materials

Phosphate buffer saline tablets (PBS), Tris, 37% chloric acid (HCl), sodium phosphate (Na_3PO_4), sucrose monolaurate, sodium chloride (NaCl), magnesium chloride ($MgCl_2$), calcium chloride ($CaCl_2$), ethanolamine, trehalose dehydrate, ethylenediaminetetraacetic acid (EDTA), Tween 20, glycerol, sodium dodecyl sulfate (SDS), bromophenol blue, DNase I from bovine pancreas, and IgGs from rabbit serum were purchased from Sigma Aldrich (St. Louis, MO, USA). Sodium azide mouse anti-human CD63 (clone MEM-259) was provided by HansaBioMed Life Sciences Ltd (Tallinn, Estonia). CellTrace™ CFSE reagent was purchased from Thermofisher Scientific (Waltham, MA, USA). Alexa Fluor® 488-conjugated antiCD63 antibody was purchased from R&D Systems (Minneapolis, MN, USA). Phycoerythrin (PE) labeled antiCD63 antibody was purchased from Exbio, Vestec, Czech Republic). Unreacted CFSE reagent and fluorescent antibodies were removed using

Nanosep MWCO 300K spin columns (Pall Corporation, New York, USA). Amine magnetic beads (0.5 µm in diameter) were purchased from Abraxis Inc. (Warminster, PA, USA). MCP-2 copolymer was purchased from Lucidant Polymers, LLC (Sunnyvale, CA, USA). Oligonucleotides were synthesized by MWG-Biotech AG (Ebevsberg, Germany): see Section 2.1.1 for oligonucleotide sequences. DNA-capture1 was modified with a biotin linker at 5' end, while DNA-tag1 was modified with a C3-azido linker at 5' end. Oligonucleotides were freeze-dried and resuspended in de-ionized water (DI water) at a final concentration of 100 µM before use. NV10B silicon chips for SP-IRIS measurements were supplied by NanoView Biosciences (Boston, MA, USA). Both chips were pretreated using a HARRICK Plasma Cleaner, PDC-002 (Ithaca, NY, USA), connected to an oxygen line. Spotting was performed using SciFLEXARRAYER S12 (Scienion, Berlin, Germany). Nanoparticle Tracking Analysis was performed with NanoSight NS300 using 3.2 Dev Build 3.2.16 software (Malvern Instruments Ltd, Malvern, United Kingdom). Nanoscale Flow Cytometry (nanoFCM) measurements were carried out using flow nanoanalyser model U30E (nanoFCM Co. LTD, Nottingham, UK), a dedicated nanoparticle flow analyser, which detects down to 40-45nm EVs at the single-particle level. Data were analysed using the NF Profession software version 1.0.

2.1.1 Oligonucleotide sequences

- *DNA-tag1*: 5'-AAAAAGCCTACGAATGAACAGACTG-3'
- *DNA-capture1*: 5'-ATATGTACCCACCGCATTCTCAGTCTGTTCATTCGTAGGC-3'

2.1.2 Synthesis of antiCD63-tag1

AntiCD63-tag1 was synthesized starting from azide free mouse antiCD63 IgG and azido-modified DNAtag1. To a mouse antiCD63 IgG solution in PBS (100 µL, 1 mg/mL) 2.46 µL of DBCO-NHS ester 4 mM (15 equivalents) were added and the mixture was allowed to react 30 min at room temperature. The reaction was quenched in 5 min at room temperature by adding 10 µL of 1 M Tris/HCl pH 8.0. Unreacted DBCO-NHS ester was removed through centrifugation on Amicon Ultra 100 MWCO filters (3 × 5 min at 12.000×*g*). After centrifugation, the volume was adjusted to 100 µL with PBS. DNA-antibody conjugation was performed by adding 6.67 µL (1 equivalent) of azido modified DNA-tag1 from a 100 µM stock solution to 100 µL of DBCO-modified antibody (1 mg/mL). The reaction mixture was incubated overnight at 37 ◦C. Unreacted DNA-tags were removed through centrifugation on Amicon Ultra 100 MWCO filters (3 × 5 min at 12.000×*g*). After centrifugation, the volume

was adjusted to 99 µL with PBS. Finally, 1 µL of 2% w/v sodium azide solution was added as a preservative (up to a final azide concentration of 0.02%)

2.1.3 Separation of EVs from HEK-293 cell culture medium by ultracentrifugation

HEK-293 cells were seeded on 150 mm dishes in DMEM culture medium supplemented with 10% EV-depleted FCS (obtained by recovering the supernatant after ultracentrifugation of the FCS at 150.000 x g for 17 h), 2 mM L-Glutamine, 100 U/mL penicillin, and 100 µg/mL streptomycin-sulfate. After 72 h incubation, the culture medium was collected and centrifuged at 450 x g for 25 min to remove cell debris. The obtained supernatant was filtered through 0.22 µm filter and then ultracentrifuged at 150.000 x g for 2 hours at 4°C (Beckman Coulter). The EV-containing pellet was finally resuspended in PBS.

2.1.4 Microarray chips functionalization

Proteins were dissolved at 2 mg/mL in 50 mM trehalose in PBS, while DNAcapture1 was dissolved in 150 mM sodium phosphate buffer containing 0.01% sucrose monolaurate at pH 8.5. Depending on the detection technique used, the different probes were spotted onto the surface of different silicon/silicon oxide chips. All chips were coated with MCP-2 and spotted using a noncontact microarray spotter (sciFLEXARRAYER S12, Scienion, Berlin) equipped with an 80 µm nozzle. 400 pL of solution were spotted at room temperature and 65% humidity. Immediately after spotting, the chips were stored overnight in a sealed chamber filled at the bottom with sodium chloride saturated water (40 g/100 mL H_2O). After incubation, they were treated with a blocking solution of ethanolamine (50 mM in 0.1M Tris/HCl buffer pH 9) at room temperature for 1 h. Then chips were rinsed with bidistilled water and dried under a nitrogen stream.

2.1.5 Enzymatic release of extracellular vesicles from microarray chip

5 µM DNAcapture1 spots were deposited on three SP-IRIS chips as described in Section 2.1.4. Chips were incubated with a 5 µg/mL solution of antiCD63-DNAtag1 for 1 h at room temperature to perform DDI. Chips were washed 10 min in PBS, rinsed with bidistilled water, and dried. Pre-scan images of the chips were acquired. Chips were incubated with a $1*10^9$ particles/mL solution of EVs isolated from HEK-293 cell culture media, as described in 2.1.3 (isolated sample was diluted in PBS to reach the desired concentration). The incubation was carried out at room temperature in a humid chamber for 2.5 h. The chips were then washed for 10 min in PBS, rinsed with bidistilled water, and dried. Chips were then incubated with a

250 mKunitz/µL solution of DNAse I from bovine pancreas in 10 mM Tris/HCl pH 7.5 buffer, containing 5 mM $MgCl_2$ and 130 µM $CaCl_2$. The incubation was performed in a humid chamber at 37°C for 1 h, and then the chips were washed 15 min PBS, rinsed with bidistilled water, and dried. Finally, post-scan images were acquired.

2.1.6 HEK-293 derived extracellular vesicles separation using DNA-Directed Immobilization of antiCD63 on magnetic beads

2.1.6.1 Separation of EVs from HEK-293 cell culture medium by ultracentrifugation: HEK-293 cells were seeded on 150 mm dishes in DMEM culture medium supplemented with 10% EV-depleted FCS (obtained by recovering the supernatant after ultracentrifugation of the FCS at 150.000 x g for 17 h), 2 mM L-Glutamine, 100 U/mL penicillin and 100 µg/mL streptomycin-sulphate. After 72 h incubation, the culture medium was collected and centrifuged at 450 x g for 25 min to remove cell debris. The obtained supernatant was filtered through 0.22 µm filter and then ultracentrifuged at 150.000 x g for 2 hours at 4°C (Beckman Coulter). The EV-containing pellet was resuspended in PBS.

2.1.6.2 Magnetic beads functionalization using DDI: DNA tagged antibodies were immobilized on the surface of magnetic beads and used to immuno-capture EVs. Prior to their use, streptavidin-coated magnetic beads (Dynabeads M-270 Streptavidin, Invitrogen) were washed three times with binding and washing buffer (B&W) (5 mM Tris-HCl, pH 7.5; 0.5 mM EDTA; 1 M NaCl) according to the manufacturer's protocol. Then 500 µg of beads were added to 100 µL of 1 µM biotinylated DNA-capture1 solution. The suspension was stirred for 30 min at 23°C, then the solution was removed and the beads were washed twice with B&W buffer, then once with PBS.
Oligonucleotide modified beads (500 µg) were incubated with 100 µL of ssDNA-antibody 160 µg/mL (depending on the experiment, beads were modified either with antiCD63-tag1 or with rabbit IgG-tag1) for 1h at 25°C, then the solution was removed and the beads were washed twice in PBS.

2.1.6.3 Separation of HEK-293 derived EVs isolated via ultracentrifugation using magnetic beads: DNA-directed antiCD63-tag1 functionalized magnetic beads (500 µg) were incubated with 250 µL EVs isolated from HEK-293 cell line by ultracentrifugation. After 2.5 h of incubation at room temperature under stirring, the tube was placed on a magnetic stand, the supernatant removed, and the beads were washed twice with PBS. Then beads were

incubated with 50 µL of 250 mKunitz/µL solution of DNase I from bovine pancreas in 10 mM Tris/HCl, pH 7.5 buffer, containing 5 mM $MgCl_2$ and 130 µM $CaCl_2$. At the end of the incubation, which was performed at 37°C for 1 h under stirring, the beads were separated using a magnetic stand and the buffer was recovered, and analyzed by nanoFCM. As negative control, the same experiment was repeated on magnetic beads functionalized using DNA-directed rabbit IgG-tag1.

2.1.6.4 Separation of EVs from HEK-293 cell culture supernatant using magnetic beads: HEK-293 cell culture supernatant was centrifuged for 4 min at 400 x g to remove cell debris and for 30 min at 10.000 x g to pellet large EVs. Then DNA-directed antiCD63-tag1 functionalized magnetic beads (500 µg) were added to 10 mL of this conditioned medium and incubated for 2.5 h at room temperature under stirring, followed by overnight incubation at 4°C. The tube was placed on a magnetic stand, the supernatant removed, and the beads were washed three times with PBS. Then beads were incubated with 50 µL of 250 mKunitz/µL solution of DNase I from bovine pancreas in 10 mM Tris/HCl, pH 7.5 buffer, containing 5 mM $MgCl_2$ and 130 µM $CaCl_2$. At the end of the incubation, which was performed at 37°C for 1 h under stirring, the beads were separated using a magnetic stand, the supernatant diluted 1:3 using PBS and analyzed by TEM microscopy.

2.1.7 Plasma derived extracellular vesicles separation

2.1.7.1 Plasma collection: Blood samples were obtained from healthy blood donors in non-fasting conditions at the Department of Clinical Immunology at Aalborg University Hospital. Blood samples were collected in a bag system LQT6283LE (Macopharma, France) using CPDA as anticoagulant and centrifuged at 4800 x g for 10 min to separate plasma. The plasma was removed, aliquoted, and stored at -40°C. Before analysis, plasma was centrifuged at 10.000 x g for 10 min, and then filtered through 0.22 µm syringe filters (Corning, NY, USA).

2.1.7.2 Magnetic beads for conventional immunocapturing (CIC): Carboxylated magnetic beads (Abraxys Inc., Warminster, PA, USA) were covalently functionalized with antiCD63 (clone MEM259, HansaBioMed, Estonia) via conventional amine coupling according to manufacturer's protocol. 10 µL of 2.5 mg/mL functionalized magnetic beads (0.5 µm in diameter) were added to 500 µL of plasma and incubated for 4 h at 25°C and 1400 rpm. Then the beads were washed twice with 1 mL of PBS. Ten µL of elution buffer

(HansaBioMed, Tallinn, Estonia) was added to the beads to release EVs, and the solution was vortexed for 30 s. After 5 min, the solution was vortexed again for 30 s and finally, 40 µL of PBS were added.

2.1.7.3 Ultracentrifugation: plasma sample was centrifuged at 10000 x g for 10 min to remove debris and aggregates. The supernatant was collected, diluted 1:2 with PBS, and filtered through 0.22 µm syringe filters (Corning, NY, USA). The clarified medium was then centrifuged at 150.000 x g at 4°C for 90 min (Beckman Coulter TL-100 Ultracentrifuge, TLA-100.3 fixed angle rotor) to sediment extracellular vesicles. The supernatant was carefully removed, and the pellet was resuspended in PBS and stored at -20°C until used.

2.1.7.4 Capture and release of EVs from magnetic beads using DDI: DNA-directed antiCD63-tag1 functionalized magnetic beads (500 µg) were incubated with 250 µL plasma. After 2.5 h of incubation at room temperature under stirring, the tube was placed on a magnetic stand, the supernatant removed, and the beads were washed twice with PBS. Then beads were incubated with 50 µL of 250 mKunitz/µL solution of DNase I from bovine pancreas in 10 mM Tris/HCl, pH 7.5 buffer, containing 5 mM $MgCl_2$ and 130 µM $CaCl_2$. At the end of the incubation, which was performed at 37°C for 1 h under stirring, the beads were separated using a magnetic stand and the buffer was recovered, and used in subsequent analysis.

2.1.8 Characterization of released extracellular vesicles

2.1.8.1 Nanoscale Flow Cytometry (nanoFCM) Analysis: Optimizations performed to achieve increased sensitivity in detecting single nanoparticles in flow have previously been described [83–85]. A continuous wave 40mW 488 laser excitation source causes nanoparticles to scatter and emit light, which is then split by dichroic beam splitters to arrive at three single-photon counting modules (SPCM). Bandpass filters placed before each SPCM detector, allow to simultaneously detect side scatter (SS – 488/10) and fluorescence (green channel – 525/40) of a single event. For each channel, thresholds were set to three times the standard deviation of detected background signal. Events and respective intensities were recorded for each peak higher than set thresholds. Samples were read for 1 minute at a rate under 12.000 events/min to avoid swarm effect and consequently, co-detection of two or more events. Size and concentration estimations were performed based on previous research [83–85], using a Silica nanospheres cocktail (68 ± 2 nm, 91 ± 3 nm, 113 ± 3 nm, and

155 ± 3 nm; S16M-Exo; nanoFCM Co. LTD, UK) and 200nm Counting standard nanospheres (S08210; nanoFCM Co. LTD, UK). For staining reactions with primary fluorescent antibodies, $1x10^9$ particles were incubated with optimized concentrations of AlexaFluor® 488-conjugated antiCD63 (diluted 1:5 in PBS) or phycoerythrin labeled antiCD63 (diluted 1:25 in PBS) for 1h at 37°C. Unbound antibodies were washed off by performing buffer exchange with PBS using Nanosep MWCO 300K spin columns.

2.1.8.2 EVs staining using CFSE: After assessing particle concentration by unstained nanoFCM measurement, each CFSE staining reaction consisted of $1x10^9$ particles, with CellTrace™ CFSE reagent at 10uM in PBS following the manufacturers protocol. Excess dye was removed by performing buffer exchange with PBS, using Nanosep MWCO 300K spin columns.

2.1.8.3 Nanoparticle Tracking Analysis: All samples were analyzed using Nanosight NS300 (Malvern Panalytical, Malvern, UK) configured with 532 nm laser. Videos were analyzed by the in-build NanoSight Software NTA 3.2 Dev Build 3.2.16. The Camera type, Camera level, and Detect Threshold were sCMOS, 14 and 4, respectively. A syringe pump with constant flow injection was used. The number of completed tracks in NTA measurements was 5 (a 60 seconds movie was registered for each measurement). All samples were diluted in PBS to a final volume of 1 mL. The ideal concentration was assessed by pre-testing the optimal particle per frame value (20-100 particles per frame).

2.1.8.4 TEM Microscopy: Transmission electron microscopy (TEM) was performed on isolated sEVs, resuspended in PBS, to analyze their ultrastructural morphology. The sEV suspension was mixed with paraformaldehyde to 2% final concentration and applied onto a formvar/carbon coated cooper grid. The grids were washed twice with PBS, incubated with 1% glutaraldehyde and stained with 2% uranyl acetate. Dried samples were visualized the same day with a Thermo Scientific Talos F200X electron microscope, at 200kV accelerating voltage.

2.1.8.5 Western Blot Analysis: For tetraspanin detection, sample was lysed in non-reducing sample buffer (62.5 mM Tris–HCl pH 6.8, 10% glycerol, 2% SDS, and 0.04% bromophenol blue) and boiled for 5 min at 95°C. Then, samples were loaded on Any kD™ Mini-PROTEAN® TGX™ Precast Protein Gel (Biorad Laboratories Inc., Hercules, CA, USA). For

the detection of other proteins, sample was lysed in reducing sample buffer (62.5 mM Tris–HCl pH 6.8, 10% glycerol, 2% SDS, 1.25% 2-mercaptoethanol and 0.01% bromophenol blue) and boiled for 5 min at 95°C. Then, samples were loaded on Any kD™ Mini-PROTEAN® TGX™ Precast Protein Gel (Biorad Laboratories Inc., Hercules, CA, USA). After protein separation, stain free images of the gels were acquired using Chemidoc XRS+ (Biorad Laboratories Inc., Hercules, CA, USA), and then electro-transferred onto a nitrocellulose membrane. Stain free images of nitrocellulose membrane was acquired to confirm successful protein transfer. Nonspecific binding sites were blocked with 5% (w/v) skimmed milk in T-TBS (150mM NaCl, 20mM Tris-HCl pH 7.4, and 0.5% Tween 20). Membranes were incubated overnight at 4°C with the following antibodies: anti-CD63 (1:1000, #556019, BD Pharmingen, CA, USA), anti-CD9 (1:1000, #M-L13; BD Pharmingen), anti-Alix (1:1000, #sc-271975, Santa Cruz, CA, USA) and anti-TSG101 (1:1000, #4A10, Novusbio). After several washes in T-TBS, membranes were incubated with goat anti-mouse IgG conjugated to horse-radish peroxidase (1:3000, #170-6516, BioRad Laboratories Inc., CA, USA) for 1 h. Positive immunoreactive bands were detected by the enhanced chemiluminescence method (Clarity Western ECL Substrate, Biorad Laboratories Inc., Hercules, CA, USA) and images acquired using Chemidoc XRS+. Membrane used for Alix detection was then stripped using an acidic buffer (200 mM glycine-HCl pH 2.2, 1% SDS and 1% Tween 20). After several washings with T-TBS and PBS, membrane was blocked with 5% (w/v) skimmed milk in T-TBS (150mM NaCl, 20mM Tris-HCl pH 7.4, and 0.5% Tween 20) and incubated overnight at 4°C with anti-Calnexin (1:1000, #C7617, Sigma-Aldrich, MO, USA). After several washes in T-TBS, membranes were incubated with goat anti-mouse IgG conjugated to horse-radish peroxidase (1:3000, #170-6516, BioRad Laboratories Inc., CA, USA) for 1 h. Positive immunoreactive bands were detected by the enhanced chemiluminescence method (Clarity Western ECL Substrate, Biorad Laboratories Inc., Hercules, CA, USA) and images acquired using Chemidoc XRS+. Stain free and chemiluminescence bands were analyzed using Image Lab software version 6.1 and protein enrichment after DDI-based separation was measured based on these data.

3. Results & Discussion

To know whether the incubation with DNase I can provide the effective release of antibodies anchored via DDI, and consequently the separation of EVs from complex media, we devised preliminary microarray tests.

A series of chips was functionalized with DNA-directed antiCD63 and incubated with EVs separated from a cell culture supernatant via ultracentrifugation as described in Section 2.1.5. Then, the chips were treated with a 250 mKunitz/µL solution of DNase I at 37°C for 1 hour, and the results, detected using SP-IRIS technique, are shown in Figure 4.3.

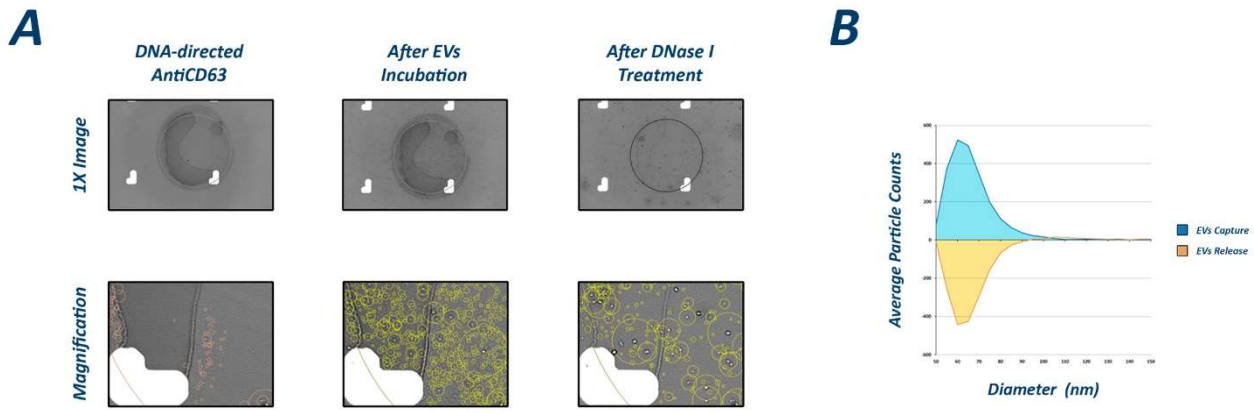

***Figure 4.3**. a) Pictures of the same spot of DNA-directed antiCD63 before and after incubation with EVs and after DNase I treatment (upper boxes) and relative enlargements (bottom boxes). b) Size distribution of EVs captured and released from DNA-directed antiCD63 spots.*

Figure 4.3a shows high-resolution images of single spots. The upper boxes report the spots of antibodies immobilized via DNA linker (left), incubated with EVs (center), and treated with DNase I (right). The lower boxes show magnifications of the same spots in the various steps of the experiment. In the magnified pictures each particle is highlighted with a colored circle. Only a few particles are present on antiCD63-DNAtag1. They can be ascribed to spot roughness since the instrument does not detect surface antibodies. After incubation with EVs, the number of particles corresponding to single vesicles immuno-captured on the surface arouse. The presence of EVs is also confirmed by the size distribution of bound vesicles (see Figure 4.3b, blue curve) that perfectly matches the size of a small EV population.

Finally, after the treatment with DNase I, the spot nearly disappeared from the surface. The released particles have a negative size distribution (Figure 4.3b, orange curve) that overlaps the distribution of particles initially captured, confirming that DNase I has cut the dsDNA linker. This experiment proves that the proposed strategy effectively produces a reversible immuno-affinity capture that can be then transferred onto magnetic beads.

Further experiments validated the suitability of magnetic beads functionalized with DNA-directed antibodies as an effective immuno-affinity separation tool. EVs were separated from complex biological fluids, and characterized to confirm the release of intact EVs compatible with analysis by imaging techniques.

Figure 4.2 depicts the schematic protocol used for magnetic bead separations. Briefly, magnetic beads coated with streptavidin were functionalized using biotinylated DNA-capture1 to allow the subsequent immobilization of antiCD63-tag1 through DDI, thus obtaining a system where antiCD63 is immobilized on magnetic beads through a dsDNA linker. Then, the magnetic particles were incubated with EVs and, subsequently, DNase I. The immuno-affinity capture on DNA-directed antiCD63, followed by enzymatic cleavage of dsDNA linker, allows releasing vesicle-antibody complexes.

We tested magnetic beads, functionalized with antiCD63 using DDI, in EV separation from samples of increasing complexity. All the samples containing EVs were filtered over 0.22 μm filters before being used to incubate magnetic beads in order to select small extracellular vesicles (sEVs). In fact, the instruments used in this thesis for the analysis of EVs (i.e. nanoFCM and SP-IRIS) can characterize particles with a size up to 200 nm. For this reason, in the next paraghraphs, we refer to small EVs.

Firstly, the selectivity of the method has been tested by incubating beads with EVs separated from HEK-293 cell culture supernatant through ultracentrifugation. After DNase I-mediated release and removal of beads using a magnetic stand, the sample was analyzed by Nanoscale Flow Cytometry (nanoFCM).

nanoFCM is a high-resolution flow cytometry method for analyzing and sorting individual EVs larger than 40 nm. It uses high sensitivity multiparametric scattered light and fluorescence measurements to count and size single nanoparticles at a single particle level[86]. EVs isolated through ultracentrifugation from HEK-293 cell culture media were analyzed by nanoFCM. Preliminary experiments to assess the percentage of CD63 positive (CD63+) EVs were performed by combining label-free and fluorescence analyses (the results are shown in Figure 4.4).

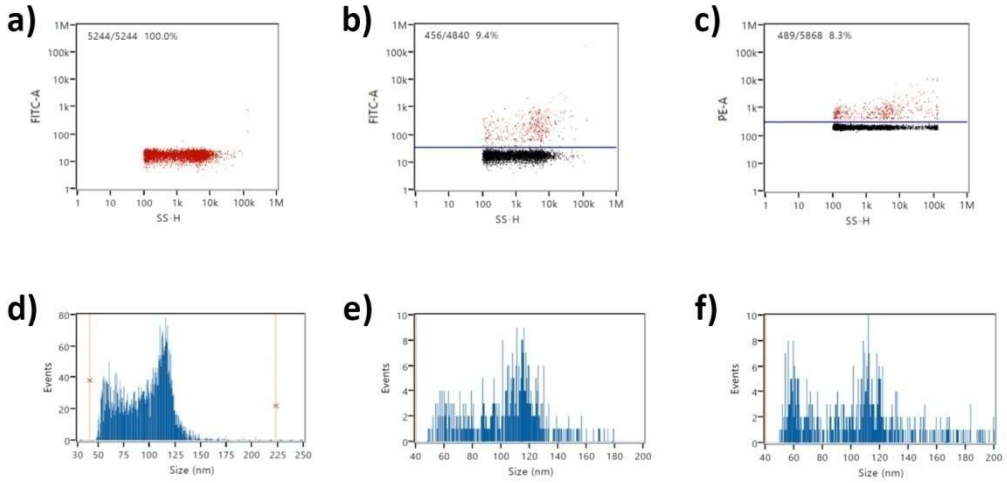

***Figure 4.4**. Nanoscale Flow Cytometry analysis of EVs isolated from HEK cell culture media using ultracentrifugation. Plots for unstained vesicles, as well as EVs labeled with AlexaFluor488 and phycoerithryn conjugated antiCD63 are reported in a, b and c, respectively). The size distribution of the same samples is shown in the bottom panels (d, e and f, respectively).*

Initially, unlabeled EVs were analyzed using only side scattering signals in order to gather information about the whole population (i.e. particle concentration in the sample and size distribution of the vesicles) and to set detection thresholds for fluorescent detection (Figure 4.4a,d). Then two aliquots of the same sample were incubated with antiCD63 IgG labeled either with AlexaFluor488 or with phycoerythrin (Figure 4.4b and c, respectively) and analyzed by both scattering and fluorescence. While side scattering allows the detection of all the EVs contained in the sample, antibody-mediated fluorescent detection provides information only about CD63+ vesicles (two different antiCD63 IgGs were used in order to exclude clone-specific artifacts). The two antibodies showed similar results, indicating that around 9% of total vesicles in the sample expose CD63 on their surface.

To analyze the sample obtained from DDI-based immuno-affinity separation of EVs using nanoFCM, the vesicles have to be stained for fluorescent detection. For this purpose EVs separated from HEK cells were stained using the protein-binding dye 5(6)-Carboxyfluorescein diacetate N-succinimidyl ester or CFDA-SE (from now on referred to as CFSE) following the protocol described in Section 2.1.8.2. The CFSE structure is depicted in Figure 4.5. It is the activated ester of carboxyfluorescein, where the phenolic groups are protected as acetic esters. The presence of acetic esters (highlighted in green in the figure) confers peculiar characteristics to this dye, making it optimal for EVs detection using nanoFCM. In fact, acetic esters, besides quenching fluorescence, enhance the lipophilicity of the molecule allowing the dye to cross lipid bilayer membrane. Inside EVs some esterases

catalyze the cleavage of acetic esters freeing the phenolic groups of fluorescein and thus producing a double effect: after deprotection, fluorescein emits fluorescence and becomes more hydrophilic, so that it cannot pass EVs' membrane anymore. As a result, CFSE produces a fluorescent staining of EVs only when vesicles are intact. Moreover, CFSE staining does not induce aggregation or artifacts that alter the nanoFCM analysis of EVs [86].

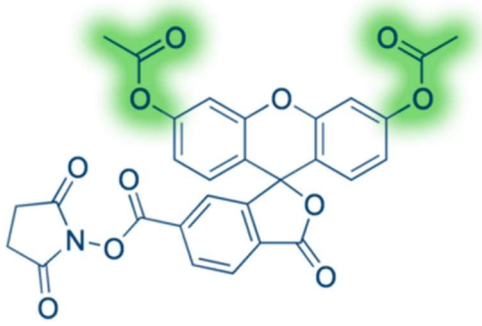

***Figure 4.5**. Chemical structure of 5(6)-Carboxyfluorescein diacetate N-succinimidyl ester (CFSE). Acetic ester protecting groups are highlighted in green.*

After staining with CFSE, the EVs were analyzed by nanoFCM, revealing that around 70% of total vesicles was successfully stained (see Figure 4.6a-b). CFSE-stained EVs were incubated with magnetic beads functionalized with DNA-directed antiCD63. The captured vesicles were released upon incubation with DNase I. The EVs recovered using the DDI approach were analyzed by nanoFCM. As a negative control, the same experimental procedure was repeated on magnetic beads functionalized with DNA-directed rabbit IgG, and the results are summarized in Figure 4.6c.

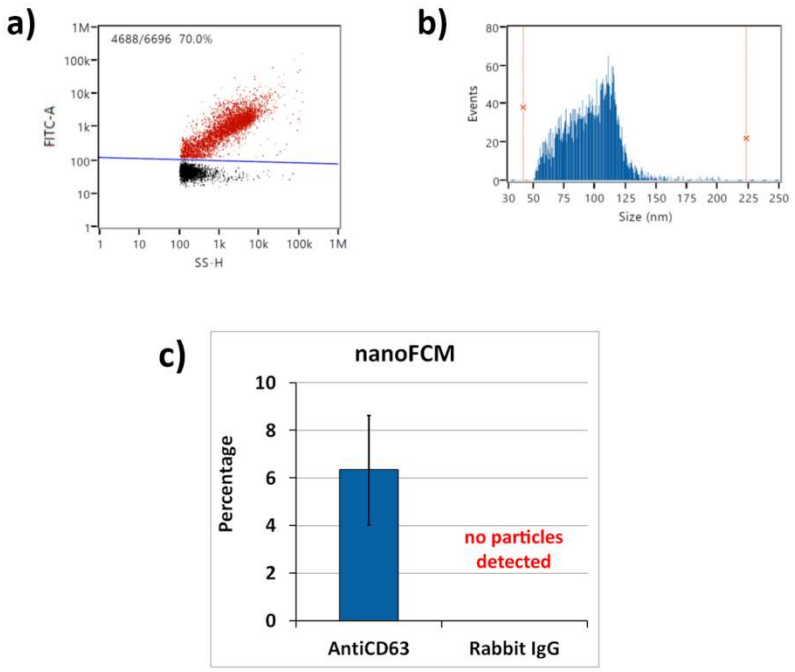

***Figure 4.6**. Nanoscale Flow Cytometry analysis of EVs stained using CFSE (a) and their size distribution (b). Nanoscale Flow Cytometry analysis of CFSE-stained EVs captured on ssDNA-antiCD63 and ssDNA-rabbit IgG and released using DNase I (c). Results are reported as percentage of total input EVs recovered after DDI-based immuno-affinity separation. EVs are effectively captured and released only when beads are functionalized with antiCD63, while no particle is detected repeating the experiment using rabbit IgG.*

The negative control confirms the selectivity of the proposed method. In fact, when magnetic beads are functionalized with rabbit IgG via DNA-directed immobilization no EVs are detected by nanoFCM. Contrarily a good number of vesicles is recovered from beads functionalized using antiCD63.

In addition, nanoFCM detect only intact EVs since both scattering light and fluorescence emission reveal only vesicles that are surrounded by a lipid bilayer membrane. Moreover the recovery of 6% of total input EVs, despite seeming low as a percentage, is an excellent result since only 9% of total vesicles were CD63+ (with an overall 66.7% yield of recovery).

The next step towards separating EVs from biological fluids of higher complexity was their isolation from HEK-293 cell culture supernatant. Magnetic beads were functionalized with DNA-directed antiCD63 as described in previous Sections and incubated overnight at 4°C with 10 mL of supernatant (previously centrifuged to remove cell debris and larger vesicles). The sample recovered from the beads after incubation with DNase I was analyzed by TEM microscopy, which highlighted the presence of intact vesicles, ranging from 50 to 150 nm in diameter, surrounded by integral lipid bilayer membranes (see Figure 4.7).

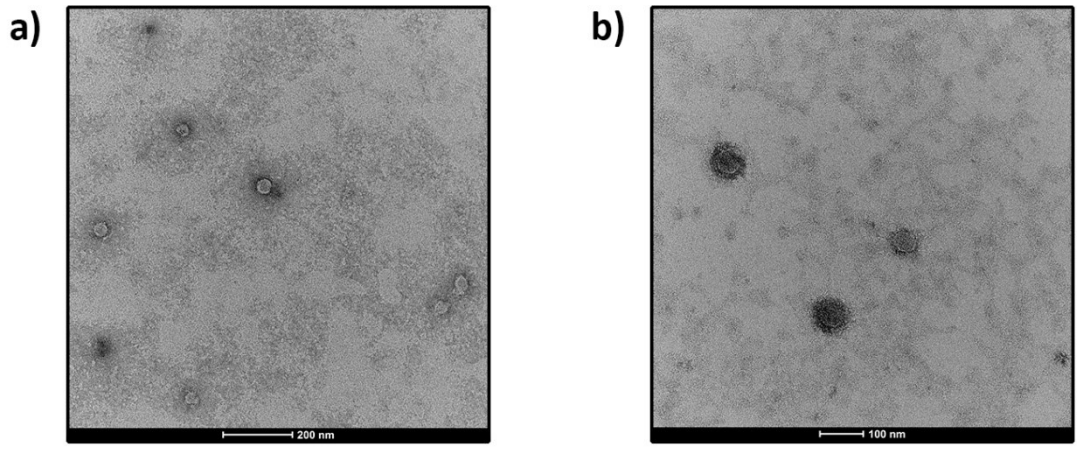

***Figure 4.7**. Transmission electron microscopy (TEM) analysis of sample recovered with DDI approach. The pictures, taken using different magnifications, are representative of the whole sample. a) Bar indicates 200 nm. b) Bar indicates 100 nm.*

These results confirms that DDI-based approach maintains its efficacy increasing the complexity of the sample matrix. Additionally, the described experiment suggests the possible application of this method for EVs separation starting from large-volumes and low-concentrated sources, such as urine.

The herein described method was finally applied to recover EVs from human blood plasma. Plasma samples were recollected from healthy donors and processed as described in Section 2.1.7.1, and a DDI-based approach was applied to separate EVs from other contaminants. After a DNase I treatment, samples recovered from the beads were characterized with different techniques: NTA, TEM microscopy and Western Blot.

Nanoparticle Tracking Analysis (see Figure 4.8) revealed in the sample derived from plasma after immuno-affinity separation of EVs on magnetic beads (orange curve) the presence of nanoparticles with a size distribution that is fully compatible with a population of small EVs, characterized by a high number of particles ranging from 75 to 200 nm in diameter. Most of the particles larger than 200 nm came from release buffer since they can also be found in DNase I-containing release buffer (blue curve).

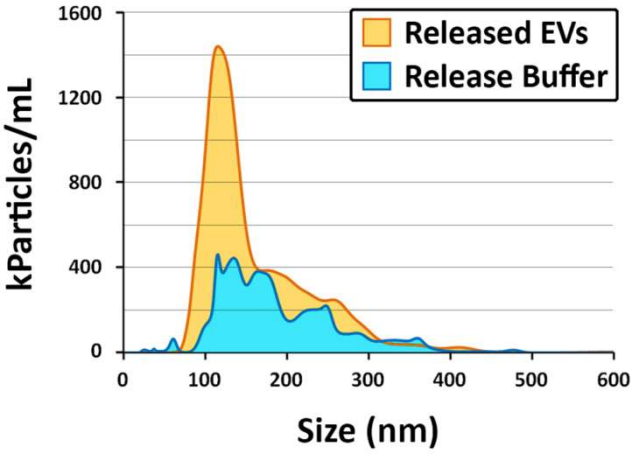

***Figure 4.8**. NTA analysis of EVs recovered from magnetic particle functionalized by DDI approach (orange curve) and DNase I containing buffer (blue curve). Each curve represents the mean of five measurements.*

TEM microscopy, performed on the sample highlighted the presence of intact and round-shaped EVs successfully released from magnetic beads (see Figure 4.9).

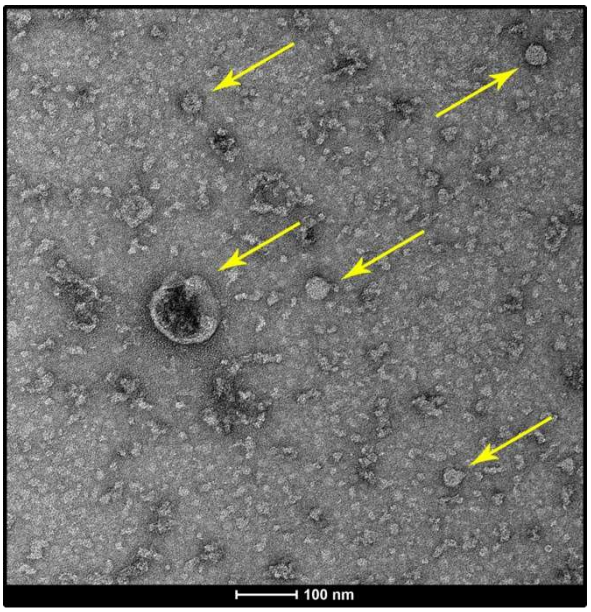

***Figure 4.9**. TEM microscopy of released EVs. Yellow arrows indicate intact EVs.*

To demonstrate that nanoparticles separated using DDI-based approach were EVs, we performed Western Blot analysis to evaluate the enrichment in EV-related proteins. Four different separation experiments were carried out, and the released solutions were pooled together. To enable complete characterization of the samples, antiCD63 in excess and DNase I were removed using spin columns. The solution recovered from the beads, the starting plasma, and the antiCD63-tag1 were loaded in an acrylamide gel and analyzed by

Western Blot to assess the degree of purification and exclude the presence of antiCD63-tag1 as a contaminant. As shown in Figure 4.10, all EV-related markers produce stronger signals in DDI separated EVs in comparison with plasma despite the total proteins loaded in the two lanes were the same (as obtained from stain-free detection of proteins on electrophoresis gels, data non shown), confirming a significative enrichment of EV-related proteins. The bands present in the region of Calnexin (used as negative control) overlap with those belonging to Alix and might result from its incomplete stripping. Compared to other EV markers, Calnexin is only minimally enriched (3.1 times versus the 42.4 times of CD9). Thus, the WB confirms the successful separation of CD63+ sEVs from plasma.

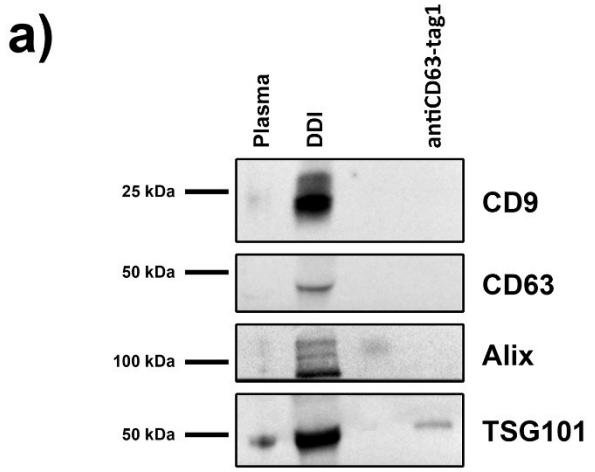

b)

MARKER	ENRICHMENT (folds of increase)
CD9	42.44
CD63	29.14
Alix	12.75
TSG101	6.66

***Figure 4.10**. a) Western Blot analysis of Plasma, EVs purified using DDI-based approach and antiCD63-tag1, which is a possible contaminant of DDI sample. b) Folds of enrichment for EV-related proteins.*

Finally, the DNase I-based method was compared to conventional separation methods for EVs. The same human blood plasma was processed to separate EVs with both ultracentrifugation (UC) and conventional immuno-affinity capturing (CIC) as described in Sections 2.1.7.2 and 2.1.7.3. CIC was performed on magnetic beads exposing amino groups on the surface that were functionalized with antiCD63 (the same clone, obtained from the same supplier, used for the synthesis of antiCD63-tag1) via classical amine-coupling reaction.

NTA analyzed EVs purified with UC and CIC, and results, compared with those obtained using the DDI approach, are illustrated in Figure 4.11.

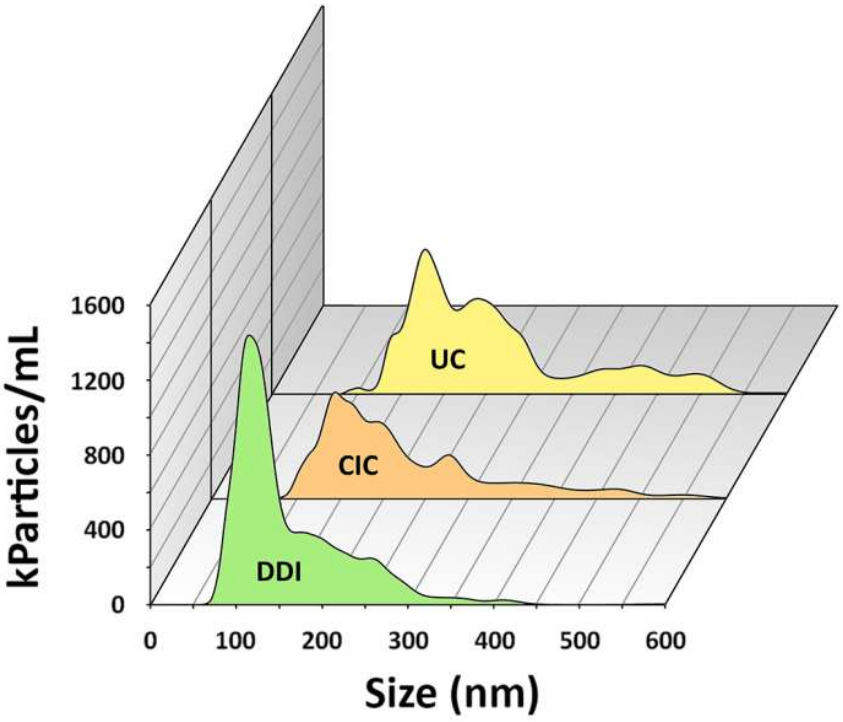

***Figure 4.11**. Nanoparticle Tracking Analysis of EVs separated by immuno-capturing on magnetic beads functionalized with antibodies bound by DNA directed (DDI), covalent immobilization (CIC) and by ultracentrifugation (UC). The area under the curves does not represent the actual sample concentration, since the samples were differently diluted in order to obtain a final concentration of 20-100 particles per frame.*

Only the sample separated by immuno-affinity capture with DNA-directed immobilized antibodies has the typical size distribution of sEVs, while the profile of the other two samples looks different and shows the presence of larger particles (400-500 nm) that might result from the aggregation of small vesicles induced by the harsh release treatment of CIC or high centrifugal forces exerted by UC.

In conclusion, the use of DNA-directed immobilization of antiCD63, coupled with the enzymatic release mediated by DNase I, produce an effective separation of EVs. This approach demonstrated its efficacy both on purified samples and complex biological fluids. In particular, the release of EVs works under mild conditions that preserve the structural integrity of biological nanoparticles, as extensively demonstrated by analysis using imaging techniques. This feature represents a substantial improvement in comparison with commercially available separation kits based on immuno-affinity precipitation of EVs.

CHAPTER 5

APTAMER-MEDIATED IMMOBILIZATION OF ANTIBODIES – DEVELOPMENT ON MICROARRAY

1. Introduction

During the last decade a number of methods for EV separation from biological fluids have been developed, including ultracentrifugation, ultrafiltration, size exclusion chromatography, polymer-induced precipitation, phase separation as well as affinity precipitation, and microfluidics[87]. Since many of these separation methods rely on the physical properties of EVs to separate them from complex biological matrices, they are eligible for EV-harvesting but cannot be applied to isolate a specific subpopulation of EVs.

Immuno-affinity precipitation of extracellular vesicles exploits surface-bound antibodies directed against EVs surface markers to precipitate them from complex mixtures selectively. Immuno-affinity precipitation provides EVS with unrivaled purity and selectivity, also allowing the separation of specific subpopulations[87,88]. This level of purity is particularly important when a single and low represented type of EV is responsible for a precise biological response or is the source of the biomarker of interest.

Despite the great potential of immuno-affinity precipitation for EV separation, its implementation in diagnostics is still limited by a critical drawback. In fact, despite superior selectivity the overall yield is quite low compared to other separation methods. This is mainly due to the reduced capacity of the solid phase used (usually magnetic beads or resins) and to difficulties in detaching EVs from antibodies after the capture step. Low pH or high ionic strength buffers are typically used to displace an antigen from its antibody, but unfortunately, both these conditions may damage EVs[87]. While the rupture of EVs might be acceptable in analysis like western blot, it indeed impairs their detection using innovative imaging technologies that are able to characterize vesicles at single-particle level (e.g., high resolution flow cytometry, nanoparticle tracking analysis, interferometric imaging)[80].

A possible loophole is described by Zhang et al.[39], who developed an affinity precipitation strategy for EVs separation where aptamers replace antibodies as affinity capture agents. Aptamers are single-stranded oligonucleotides that bind targets (ions, protein complexes and even entire cells) with high affinity and specificity[38]. The authors exploited the double

nature of aptamers that are both able to capture their targets and hybridize with complementary oligonucleotides. Aptamers alone display 3D structures that confer affinity towards their target. They lose their folding and assume a double helix conformation upon interaction with a complementary oligonucleotide, causing target release. Zhang et al. described an aptamer-based affinity separation where a DNA aptamer directed against CD63 (a tetraspanin exposed on EV surface) is used to capture EVs on magnetic beads. The subsequent incubation with the complementary strand of DNA causes the nondestructive release of vesicles from magnetic beads.

Despite the remarkable advantages of aptamers towards antibodies (low costs of production, ease of chemical modification, relatively small size)[89] their use is still limited, and few examples of their application can be found in literature, in most cases involving a restricted number of well-characterized aptamers (e.g., thrombin- and ATP-binding aptamers)[90]. This may depend on concerns about their stability in biological media, lower degree of acceptability among the scientific community compared to antibodies and difficulties in finding aptamers directed against a desired target[38].

For this reason, we describe here an innovative immuno-affinity precipitation strategy that exploits a combination of aptamers and antibodies to overcome their respective drawbacks (i.e., availability and difficult release of the target). More precisely, *StrepApt5*, a streptavidin-binding DNA aptamer[91], is immobilized on magnetic beads and used to anchor streptavidin to the surface. Then, biotinylated antibodies are immobilized on the beads exploiting the strong interaction between streptavidin and biotin (Figure 5.1a).

In this way, a platform for immuno-precipitation of EVs can be generated combining the selectivity and specificity of easily available antibodies and the effective release mediated by the aptamer. After EVs are captured on the beads by antibody recognition of its antigen, the same vesicles can be released under mild conditions by adding the sequence of DNA complementary to StrepApt5 (cDNA, see Figure 5.1b).

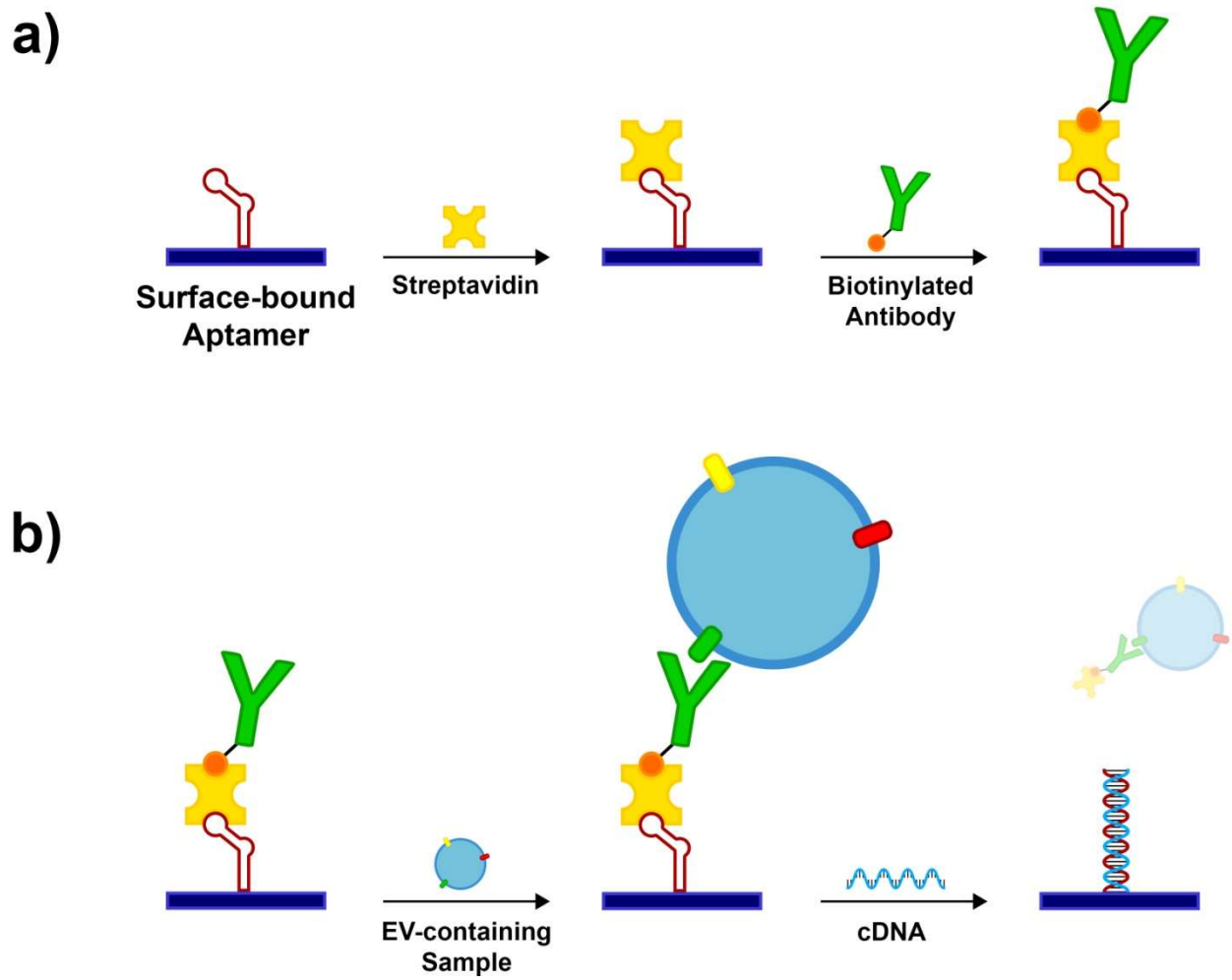

Figure 5.1. *Schematic representation of StrepApt5-mediated immobilization of antibodies on solid surfaces (a) and its use in EVs capture and release experiment using cDNA to promote detachment from the surface (b).*

This approach was developed on microarray chips. We detail protocols and experiments in the following Sections.

2. Protocol development on microarray chips

In order to test the suitability of reversible aptamer-mediated immobilization of antibodies, and its ability to capture EVs and separate them from complex biological fluids, a series of experiment was designed. In particular, we performed microarray tests to select optimal conditions for capture and release experiments.

2.1 Materials

Ammonium sulfate ($(NH_4)_2SO_4$), phosphate buffer saline tablets (PBS), Trizma base, 37% chloric acid (HCl), sodium phosphate (Na_3PO_4), sucrose monolaurate, sodium chloride (NaCl), ethanolamine, trehalose dehydrate, magnesium chloride ($MgCl_2$), NHS-PEG_4-biotin, Amicon Ultra 100MWCO centrifugal filters, streptavidin and polyclonal rabbit IgG were purchased from Sigma Aldrich (St. Louis, MO, USA). Mouse antihuman CD9 IgG (clone MEM-61) and biotinylated mouse antihuman CD9 IgG (clone MEM-61) were a kind gift of Hansa BioMed Life Sciences Ltd (Tallinn, Estonia). Cy3-labeled Fab_2 fragment rabbit antimouse IgG and Cy3-labeled Fab fragment goat antihuman IgG were purchased from Jackson ImmunoResearch (Baltimore, PA, USA). Oligonucleotides were synthesized by MWG-Biotech AG (Ebevsberg, Germany): see Section 2.1.1 for oligonucleotide sequences. StrepApt5, 20A-StrepApt5 and COCU8 were modified in 5' position with a C6 amino-linker, only StrepApt5 was also modified in 5' position with dibenzocyclooctine (DBCO) linker. cDNA and COCU11 were labeled with Cy5 at 5' end. Oligonucleotides were freeze-dried and resuspended in de-ionized water (DI water) at a final concentration of 100 μM before use. StrepApt5 and 20A-StrepApt5 underwent a folding procedure before immobilization on solid supports: aptamer solutions were heated at 95°C for 8 min, transferred into ice at -20°C for 10 min and finally left at room temperature for 15 min.

Untreated silicon chips with 100 nm thermal grown oxide (14 x 14 mm) were supplied by SVM, Silicon Valley Microelectronics Inc. (Santa Clara, CA, USA). NV10B silicon chips were supplied by NanoView Biosciences (Boston, MA, USA). Both chips were pretreated using a HARRICK Plasma Cleaner, PDC-002 (Ithaca, NY, USA), connected to an oxygen line. MCP-2 and MCP-6 copolymers were purchased from Lucidant Polymers Inc. (Sunnyvale, CA, USA). Spotting is performed using SciFLEXARRAYER S12 (Scienion, Berlin, Germany). Fluorescence images were obtained using the ScanArray Lite confocal laser scanner and analyzed using ScanArray Express software (Perkin Elmer, MA, USA). Interferometric and fluorescence analyses of EVs were performed exploiting SP-IRIS technique using ExoView™ R100 for image acquisition and nanoViewer 2.6.0 software for analysis (NanoView Biosciences Inc., MA, USA). This instrument measures the number of single particles (ranging from 50 to 200 nm in diameter) captured on the chip surface as well as their size distribution. Nanoparticle Tracking Analysis was performed with NanoSight NS300 using 3.2 Dev Build 3.2.16 software (Malvern Instruments Ltd, Malvern, United Kingdom).

2.1.1 Oligonucleotide sequences

- *StrepApt5*: 5'-GGGAACGCACCGATCGCAGGTTTCCC-3'
- *20A-StrepApt5*:
5'-AAAAAAAAAAAAAAAAAAAAGGGAACGCACCGATCGCAGGTTTCCC-3'
- *cDNA*: 5'-ACCTGCGATCGGTGCGTTCCC-3'
- *COCU8*: 5'-GCCCACCTATAAGGTAAAAGTGA-3'
- *COCU11*: 5'-TCACTTTTACCTTATAGGTGGGC-3'

2.1.2 General preparation of microarray supports

Different silicon supports were employed in various experiments. We used silicon chips (14 x 14 mm) layered with 100 nm of thermal grown silicon dioxide in experiments requiring fluorescent detection, and NV10B silicon chips layered with 55 nm of thermally-grown silicon dioxide for SP-IRIS experiments using Exoview™ R100. All the silicon supports were pretreated with oxygen plasma to clean and activate the surface. The oxygen pressure was set to 1.2 bar with a power of 29.6 W for 10 min. Then we dipped the chips into a 1% w/v solution of MCP-2 in 0.9 M aqueous ammonium sulfate. The slides, immersed into the coating solution for 30 min at room temperature were rinsed in bidistilled water, dried under a nitrogen stream, and then cured at 80 °C for 15 min.

Chips were spotted using a noncontact microarray spotter (sciFLEXARRAYER S12, Scienion, Berlin) equipped with an 80 μm nozzle; 400 pL of solution were spotted at room temperature and 65% humidity.

To prepare spotting solutions, proteins were dissolved at 1 mg/mL in 50 mM trehalose in PBS, while amino-modified oligonucleotides were dissolved at different concentrations (5, 10, and 25 μM) in a solution of 150 mM sodium phosphate buffer containing 0.01% sucrose monolaurate at pH 8.5. After spotting, the chips were stored overnight in a sealed chamber filled at the bottom with sodium chloride saturated water (40 g/100 mL H_2O). Finally, chips were treated with a blocking solution of ethanolamine (50 mM in 0.1M Tris/HCl buffer pH 9 and 2 mM $MgCl_2$) at room temperature for 1 h, rinsed with bidistilled water, and dried.

2.1.3 System development using microarray supports

2.1.3.1 Optimization of aptamer concentration: 3 silicon chips were prepared and spotted with StrepApt5 and 20A-StrepApt5 (both the aptamers were deposited on the surface at 3 different concentrations, namely 5, 10, and 25 μM) and 0.1 mg/mL Cy3-labeled Fab fragment goat antihuman IgG as a positive control as described in 2.1.2. Chips were incubated with 1 mg/mL streptavidin in 2 mM $MgCl_2$ in PBS (hereinafter referred to as PBS-

M) for 1 h at room temperature. Chips were washed 10 min in PBS-M, rinsed with 2 mM $MgCl_2$, and dried under nitrogen stream.
A second incubation was performed using 15 μg/mL biotinylated antiCD9 in PBS-M and carried out for 30 minutes at room temperature. Chips were washed 10 min in PBS-M, rinsed with 2 mM $MgCl_2$, and dried under a nitrogen stream. Then chips were incubated with 10 μg/mL Cy3-labeled Fab fragment rabbit antimouse IgG in PBS-M for 1 h at room temperature. Chips were washed 10 min in PBS-M, rinsed with 2 mM $MgCl_2$, and dried under a nitrogen stream. Fluorescence images were acquired using ScanArray Lite confocal laser scanner with 65% laser power and 65% PMT.

2.1.3.2 Biotin-labeled antiCD9 capture and release: 9 silicon chips were prepared and functionalized with 1 mg/mL streptavidin, 1 mg/mL antiCD9, 10 μM COCU8, 10 μM StrepApt5 and 0.1 mg/mL Cy3-labeled Fab fragment goat antihuman IgG as positive control as described in 2.1.2. Chips were incubated with 1 mg/mL streptavidin in PBS-M for 1 h at room temperature. Chips were washed 10 min in PBS-M, rinsed with 2 mM $MgCl_2$, and dried under a nitrogen stream. Then chips were incubated with 15 μg/mL biotin-labeled antiCD9 in PBS-M for 30 min at room temperature, washed 10 min with PBS-M, rinsed with 2 mM $MgCl_2$, and finally dried under a nitrogen stream.
Then chips were divided into 3 groups. The first group was incubated with PBS-M for 30 minutes at room temperature, rinsed with 2 mM $MgCl_2$, and dried with a nitrogen stream.
The second group was incubated with 1 μM Cy5-labeled cDNA in PBS-M for 30 min at room temperature, washed 10 min in PBS-M, rinsed with 2 mM $MgCl_2$, and finally dried under a nitrogen stream.
The third group was incubated with 1 μM Cy5-labeled COCU11 in PBS-M for 30 min at room temperature, washed 10 min in PBS-M, rinsed with 2 mM $MgCl_2$, and finally dried under a nitrogen stream.
Finally, all chips were incubated with 10 μg/mL Cy3-labeled Fab fragment rabbit antimouse IgG in PBS-M for 1 h at room temperature. Chips were washed 10 min in PBS-M, rinsed with 2 mM $MgCl_2$, and dried under a nitrogen stream.
Fluorescence images of all chips were acquired using ScanArray Lite confocal laser scanner with 65% laser power and 65% PMT for both red and green fluorescence.

2.1.4 Extracellular vesicles capture on microarray

2.1.4.1 Separation of EVs from HEK-293 cell culture medium by ultracentrifugation: HEK-293 cells were seeded on 150 mm dishes in DMEM culture medium supplemented with 10% EV-depleted FCS (obtained by recovering the supernatant after ultracentrifugation of the FCS at 150.000 x g for 17 h), 2 mM L-Glutamine, 100 U/mL penicillin and 100 µg/mL streptomycin-sulfate. After 72 h incubation, the culture medium was collected and centrifuged (1500 rpm) for 25 min to remove cell debris. The obtained supernatant was filtered through 0.22 µm filter and then ultracentrifuged at 150.000 x g for 2 hours at 4° C (Beckman Coulter). The EV containing pellet was resuspended in PBS.

2.1.4.2 EVs characterization by Nanoparticle Tracking Analysis: sample was analyzed using Nanosight NS300 (Malvern Panalytical, Malvern, UK) configured with 532 nm laser. Videos were analyzed by the in-built NanoSight Software NTA 3.2 Dev Build 3.2.16. The Camera type, Camera level, and Detect Threshold were sCMOS, 14 and 4, respectively. A syringe pump with constant flow injection was used. The number of completed tracks in NTA measurements was 5 (a 60 seconds movie was registered for each measurement). The sample was diluted in PBS to a final volume of 1 mL. The ideal concentration was assessed by pre-testing the optimal particle per frame value (20-100 particles per frame).

2.1.4.3 EVs characterization by Transmission Electron Microscopy: Transmission electron microscopy (TEM) was performed on isolated EVs, resuspended in PBS, to analyze their ultrastructural morphology. According to proper dilution, the sample was adsorbed to 300 mesh carbon-coated copper grids (Electron Microscopy Sciences, Hatfield, PA, USA) for 5 min in a humidified chamber at room temperature. EVs on grids were then fixed in 2% glutaraldehyde (Electron Microscopy Sciences, Hatfield, PA, USA) in PBS for 10 min and then briefly rinsed in bidistilled water. Grids with adhered EVs were examined with a Philips CM 100 transmission electron microscope TEM at 80kV, after negative staining with 2% phosphotungstic acid, brought to pH 7.0 with NaOH. The images were captured by a Kodak digital camera.

2.1.4.4 Synthesis of biotinylated rabbit IgG: polyclonal rabbit IgG was dissolved into PBS at a final concentration of 1 mg/mL. To 100 µL of the so obtained solution, 3.15 µL of freshly prepared 8.5 mM NHS-PEG_4-biotin in PBS (40 equivalents) were added, and the solution was allowed to react 30 min at room temperature. The reaction was quenched by adding 10

μL of 1 M Tris-HCl pH 8. After 5 minutes at room temperature, the unreacted biotin-linker was removed using Amicon Ultra 100MWCO centrifugal filters (4 x 5 minutes at 12,000 x g, adding PBS to a final volume of 500 μL before each centrifugation). The final volume was set to 100 μL by adding PBS and the concentration (0.83 mg/mL) was assessed by Bradford protein assay.

2.1.4.5 Extracellular vesicles capture and release: 15 silicon chips were functionalized with 1 mg/mL polyclonal rabbit IgG, 1 mg/mL antiCD9, 1 mg/mL streptavidin and 10 μM StrepApt5 as described in 2.1.2. Chips were incubated with 1 mg/mL streptavidin in PBS-M for 1 h at room temperature. Chips were washed 10 min in PBS-M, rinsed with 2 mM $MgCl_2$ and dried. 9 chips were then incubated with 15 μg/mL biotin-labeled antiCD9 in PBS-M for 30 min at room temperature, while the remaining chips were incubated with 15 μg/mL biotinylated polyclonal rabbit IgG in PBS-M (as negative control) under the same conditions. All chips were washed 10 min in PBS-M, rinsed with 2 mM $MgCl_2$ and dried. Chips were scanned using ExoView™ R100.
Three chips, functionalized with biotin-labeled antiCD9, were incubated with PBS-M for 2.5 h at room temperature, while the remaining chips were divided into two groups and incubated with different concentrations of HEK-derived EVs in PBS-M ($5*10^{10}$ and $1*10^{9}$ particles/mL) for 2.5 h at room temperature. Chips were washed 10 min in PBS-M, rinsed with 2 mM $MgCl_2$, dried and scanned using ExoView™ R100. Chips incubated using the lowest concentration of EVs were subsequently incubated with a mix of fluorescently-labeled antibodies (Cy3-labeled antiCD81 and Cy5-labeled antiCD63, each 1 μg/mL in PBS-M) for 1 h at RT, washed 10 min with PBS-M, rinsed with 2 mM $MgCl_2$, dried and scanned using ExoView™ R100. The same chips were finally incubated with 10 μM cDNA in PBS for 1 h at RT, washed 10 min in PBS, rinsed in 2 mM $MgCl_2$, dried, and scanned using ExoView™ R100.

3. Results & Discussion

Immuno-precipitation of EVs is a powerful technique for their separation from biological matrices such as body fluids. It consists on using surface-bound antibodies and it is one of few examples of separation methods that can provide vesicles with a particular phenotype,

selecting a specific EV fraction on the basis of its membrane composition. Despite this great potential, conventional immuno-precipitation methods possess a common drawback related to the difficulties in releasing the antigen from the antibody after separation. Typically buffers with low pH (usually glycine pH 2-3) or high ionic strength (e.g., 2 M NaCl or 5 M LiCl) are used to revert the interaction between the antibody and its antigen, but unfortunately, both these conditions may damage EVs altering downstream analyses[87,88].

With the aim of developing an immuno-precipitation strategy for EVs that exploits nondestructive release under mild conditions Zhang et al. described a method where aptamers replace surface-bound antibodies[39].

Aptamers are short, single-stranded nucleic acids that bind with high affinity and specificity targets upon folding into tertiary structures. They have a number of advantages over antibodies: shorter production time, lower costs of manufacturing, no batch-to-batch variability, ease of chemical modification, better thermal stability, and the ability to bind non-immunogenic targets[92].

Zhang et al. used a DNA aptamer directed against CD63 (a transmembrane protein commonly found on the surface of extracellular vesicles) to address EVs and immobilize them on the surface of magnetic beads. After EV capturing, the author exploited the ability of nucleic acids to bind their complementary strand to release vesicles. In fact, upon interaction with its complementary strand of DNA, the antiCD63 aptamer loses its tertiary structure to form the double helix because of Watson-Crick interaction with nucleobases on the complementary strand, causing the release of EVs from magnetic beads under mild and nondestructive conditions. The authors also repeated the same protocol using an antiMUC1 aptamer to provide a successful separation of cancer-derived EVs.

Even though aptamers were initially considered promising in diagnostics and therapy, they demonstrated to be much less efficient than expected, and only a few examples of their application are reported in the literature. The examples involve a restricted number of well-characterized aptamers (e.g., thrombin- and ATP-binding aptamers)[38,90].

A possible explanation may be that the aptamer selection protocol requires a specific buffer, whose character is of utmost importance for a correct aptamer folding. Any change in its composition may alter aptamer tertiary structure and hence its affinity towards the target. This aspect becomes particularly important with biological samples that do not always match selection buffer requirements, thus impairing or at least limiting aptamer application in bioassays.

Moreover, aptamer's use conditions need to be optimized for each specific application since their behavior in the presence of both target and complementary strands may change depending on the experimental setup and aptamer characteristics. While in some cases the interaction between a DNA aptamer and its complementary DNA can produce a double helix causing target release[93], the opposite may also occur[90].

In this work, we propose an innovative immuno-precipitation strategy that overcomes limitations from the use of antibodies (i.e., difficult target release) and aptamers (reduced number of targets available and unpredictable behavior), by using them in combination.

The proposed method (see Figure 5.1) generates surfaces functionalized with StrepApt5, a DNA aptamer that binds streptavidin with high affinity (K_d = 35 nM) occupying two biotin binding sites[91]. The aptamer-functionalized surface is then used to bind streptavidin, obtaining a surface that can immobilize biotinylated entities, in the specific case antibodies. Using this strategy, we developed an immuno-precipitation platform that combines antibody and aptamers advantages, also limiting specific drawbacks. Specifically, the reduced number of targets available for aptamers would no longer be a problem since the affinity capture is mediated by biotinylated antibodies, which are either commercially available or easily synthesizable using biotinylation kits, provided by a large number of suppliers for different applications.

In addition, the use of StrepApt5 to mediate streptavidin immobilization on the surface provides a system that is stable during the target capture step (the aptamer stably retains its tertiary structure in 2 mM $MgCl_2$ in PBS) and enables a straightforward release of the target upon incubation with the strand of DNA complementary to the aptamer (cDNA), as shown in Figure 5.1b.

To prove the effectiveness of this method, its applicability has been firstly demonstrated on microarray platforms and then transferred on magnetic beads to provide EV-separation from biological matrices.

First of all, as a proof of concept, we demonstrated the possibility to immobilize biotinylated antibodies in a reversible way using StrepApt5-anchored streptavidin in microarray tests.

Silicon chips were coated using MCP-2, a member of a family of copolymers widely used in biosensing[64,94,95]. MCP-2 is the commercial name for copoly (DMA-NAS-MAPS), a *ter*-copolymer of *N,N*-dymethilacrylamide (DMA) (97% in moles), *N*-acryloyloxysuccinimide (NAS) (2% in moles), and 3-(trimethoxysilyl)propyl methacrylate (MAPS) (1% in moles), which forms a 3-D layer for the immobilization of biomolecules with retained capture efficiency and suppression of non-specific binding[63].

To demonstrate the possibility to immobilize streptavidin and subsequently biotinylated antibodies on aptamer-functionalized surfaces, silicon chips were spotted with StrepApt5 and 20A-StrepApt5 as described in section 2.1.3.1. In particular, 20A-StrepApt5 is an oligonucleotide where the streptavidin-binding sequence is outdistanced from the surface by a 20-mer adenine tail on the 5' end. It was used to evaluate the effect of the distance between aptamer and the surface. Both the oligonucleotides were printed on chips at 3 different concentrations (5, 10, and 25 μM) and sequentially incubated with streptavidin, biotinylated antiCD9, and Cy3-labelled Fab_2 fragment rabbit antimouse IgG to provide fluorescent detection. Results in Figure 5.2 clearly show the same trend for both aptamers, where the highest degree of immobilization is reached when the DNA is spotted at a concentration of 10 μM, using lower or higher concentrations the fluorescent signal decreases.

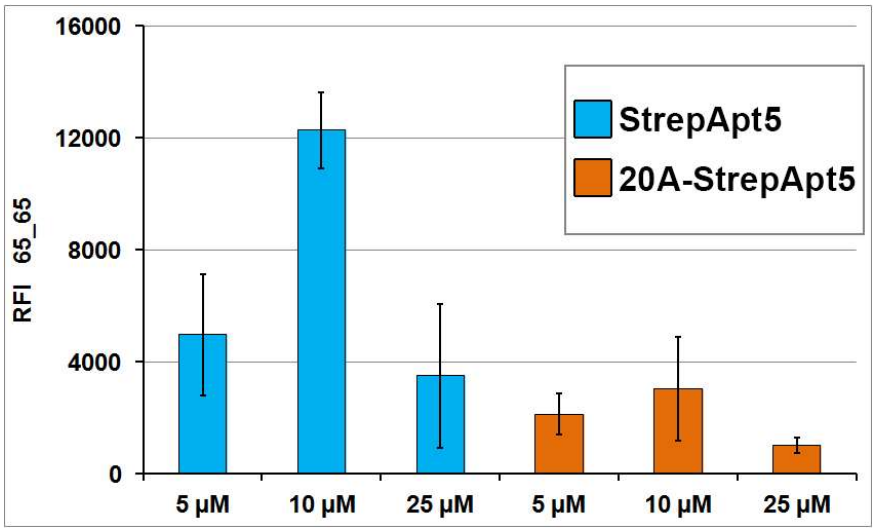

***Figure 5.2**. Fluorescent detection of biotinylated antiCD9 immobilized on aptamer-bound streptavidin. Blue bars represent streptavidin immobilized on three different concentrations of StrepApt5. Orange bars represent streptavidin immobilized on three increasing concentrations of 20A-StrepApt5. Immobilized biotinylated antiCD9 was revealed upon incubation with Cy3 labeled secondary antibody. The results are the mean of three independent experiments, error bars represent standard deviation.*

The aptamer possesses a critical density, where the immobilization of streptavidin reaches a maximum. At this critical density the aptamer retains an appropriate folding, while lower concentrations produce lower signals. Instead, at higher densities interactions between complementary regions in adjacent strands occurs, hindering correct aptamer folding and thus limiting streptavidin immobilization. The results also show how the presence of the spacer in 20A-StrepApt5 reduces streptavidin immobilization levels, probably because the

spacer promotes interaction between contiguous strands. Based on this experiment, 10 μM StrepApt5 was chosen as the best spotting condition to be used in the following experiments.
A simple experiment demonstrated the reversibility of antibody-streptavidin immobilization on aptamer, and its specificity. Silicon chips were coated using MCP-2 and functionalized with streptavidin, antiCD9, StrepApt5, and COCU8 (an ssDNA sequence that does not bind StrepApt5, used as the negative control). The chips were sequentially incubated with streptavidin, biotinylated antiCD9, and Cy3-labeled Fab_2 rabbit antimouse IgG. Then chips were divided in 3 groups: the first was analyzed without performing additional incubations, the second was incubated with Cy5-labeled cDNA (which is complementary to StrepApt5) while the third was incubated with Cy5-labeled COCU11 (the strand of DNA complementary to COCU8). The experimental scheme is summarized in Figure5.3A. Using this experimental protocol, Cy3 fluorescence signal (green) appears when antiCD9 is immobilized on the surface, while Cy5 fluorescence signal (red) appears upon annealing of complementary DNA strands. For this reason, StrepApt5 spots that are green after antibody immobilization turn red upon cDNA-mediated release.
The results of Figure 5.3B show that using this approach, biotinylated antiCD9 can be immobilized on aptamer-bound streptavidin with high density (around half of the antibody immobilized on streptavidin directly printed on the surface) and effectively released through incubation with cDNA. Moreover, the bottom panel demonstrates that the release is sequence-selective. In fact, when the chip is incubated with COCU11, the non biotinylated antibody is released from StrepApt5.
We, therefore, demonstrated that using streptavidin immobilized on StrepApt5 it is possible to generate a platform for selective capture and release of biotinylated antibodies. Even if the amount of antibody immobilized with this approach is sensibly lower in comparison with the direct immobilization of the same antibody on the surface (around 25%), we demonstrated in Chapter 3 that a lower density of antibodies, as long as they are better exposed, could improve immuno-capturing of EVs[96].

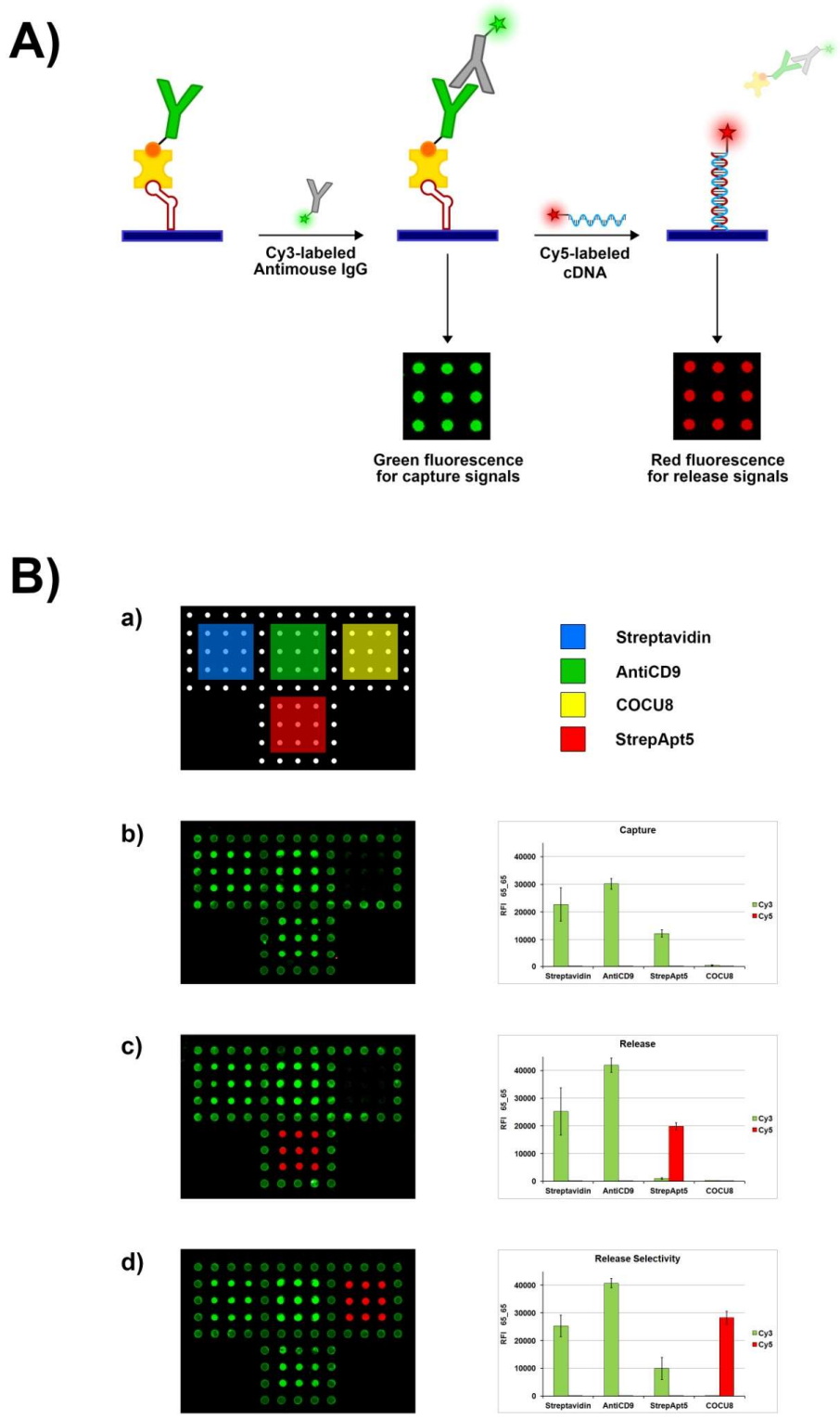

Figure 5.3. *(A) Schematic representation of experimental outline. Biotin-labeled antiCD9 immobilized on aptamer-bound streptavidin is revealed upon incubation with Cy3 labeled secondary antibody, producing green fluorescence signal. Cy5-labeled cDNA was used to release antibody-streptavidin complex from the aptamer, causing the switch from green to red fluorescence. (B) Overview of results. a) Spotting scheme. b) Capture experiment, chips not incubated with cDNA. c) Release experiment, chips incubated with cDNA to release the antibody. d) Chips incubated with COCU11 to prove selectivity of release step.*

The ability of aptamer-directed antibodies to capture EVs was evaluated using Exoview™ R100, a commercial platform developed by Nanoview Biosciences (Boston, MA, USA) that can detect and size extracellular vesicles digitally using label free interferometry. Silicon chips were coated using MCP-2 and functionalized with rabbit IgG, antiCD9, streptavidin, and StrepApt5 as described in Section 2.1.4.5. The chips were incubated with 1 mg/mL streptavidin and then with a biotinylated antibody (either antiCD9 or rabbit IgG). Both streptavidin and aptamer spots on the microarray surface captured biotinylated antibodies. Chips were incubated with EVs purified from HEK-293 cell culture supernatant by ultracentrifugation diluted with PBS-M to a final concentration of $5*10^{10}$ particles/mL, and finally analyzed using label free interferometry. As a negative control, chips functionalized with biotinylated antiCD9 were incubated with PBS-M under the same conditions and analyzed. Results (see Figure 5.4a) show that EVs are efficiently captured on StrepApt5 spots only when the chips are functionalized with antiCD9 and incubated with EVs. On the contrary, only low background signals are obtained when the aptamer's spot is incubated with rabbit IgG or only with PBS-M (i.e. PBS added with 2 mM $MgCl_2$).

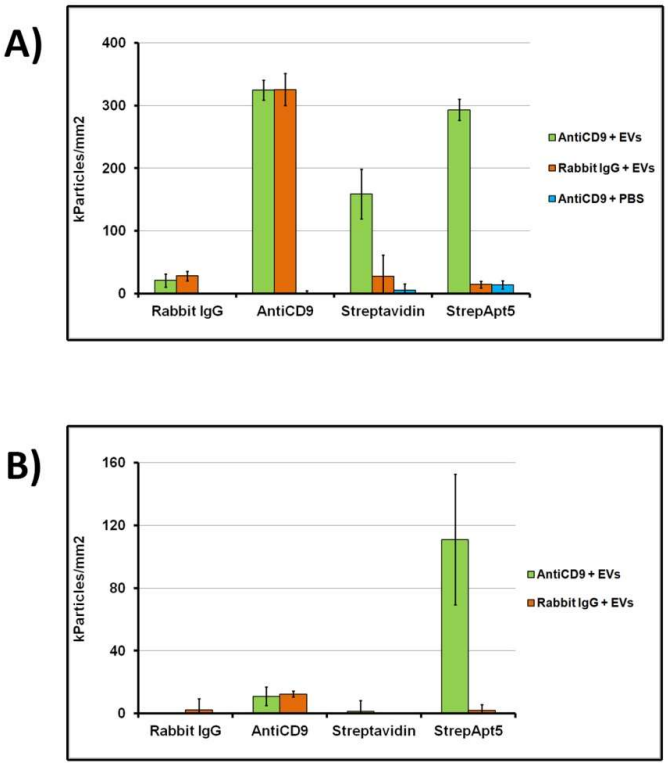

***Figure 5.4**. Number of EVs detected by label free interferometry on microarray chips. Streptavidin and StrepApt5 spots are functionalized either with antiCD9 or rabbit IgG as described in Section 2.1.4.5. a) Results for chips incubated with PBS-M or $5*10^{10}$ particles/mL EVs. b) Results for chips incubated with $1*10^{9}$ particles/mL EVs.*

Since the number of EVs captured on antiCD9, either conventionally immobilized on chips or aptamer-directed on the surface, is relatively high (suggesting a saturation of the signal), the same experiment was repeated incubating chips with a lower concentration of EVs (i.e. $1*10^9$ particles/mL) and the results are shown in Figure 5.4b. Under these experimental conditions, the selectivity is confirmed. The aptamer-directed antiCD9 shows improved affinity for EVs compared to antiCD9 conventionally immobilized on the surface or captured on the surface only by streptavidin.

To demonstrate that EVs captured on the surface could actually be released from the surface upon incubation with cDNA, silicon chips used for EVs capture at the lowest concentration were incubated with a mix of fluorescently-labeled antibodies. Figure 5.5, left panel, shows high resolution fluorescence image of a single spot of StrepApt5. High fluorescence levels of both Cy5 and Cy3 fluorescence are detected on the spot, confirming that the particles immobilized on the aptamer-directed antiCD9 are EVs. The chip was then incubated with cDNA and as shown in Figure 5.5, right panel. The fluorescence signal dramatically decreased, proving that the EVs captured on the surface using the aptamer-mediated approach can be effectively released from the spot.

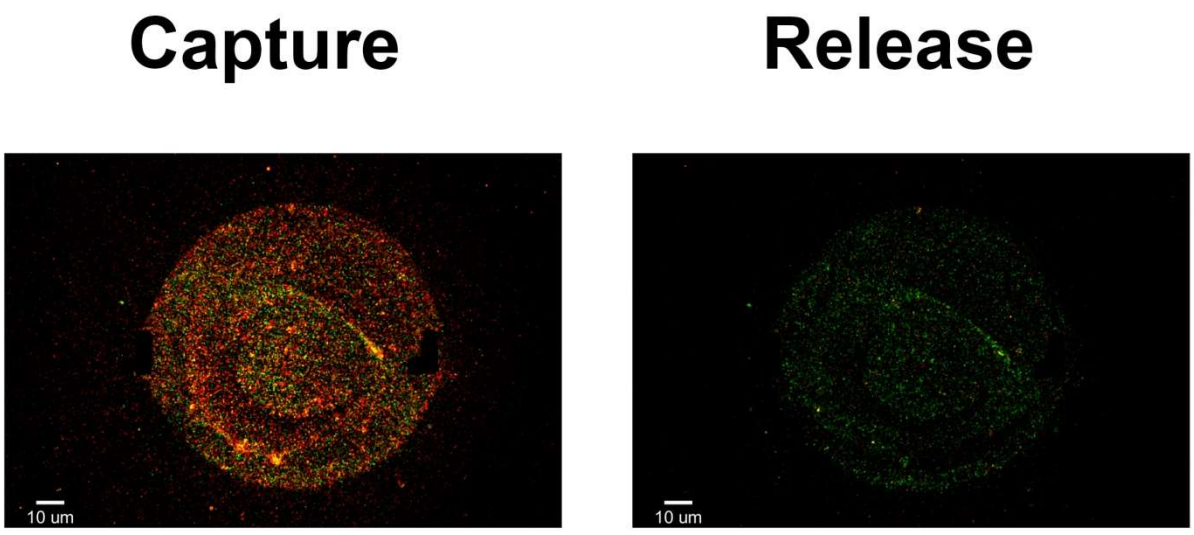

***Figure 5.5**. Green and red fluorescence signals on StrepApt5 spots after EV-capture step and after cDNA-mediated release.*

In conclusion, a universal and reversible immune-affinity platform was generated using this strategy, which can be functionalized with different antibodies depending on experimental needs.

CHAPTER 6

DEVELOPMENT AND CHARACTERIZATION OF CUSTOM AZIDE-EXPOSING SILICA BEADS

1. Coating of silica beads using MCP-6

Once the protocol for the reversible aptamer-directed immobilization of antibodies was developed on microarrays, and proved to be effective in providing a reversible immuno-affinity capture of EVs, it was transferred to micro-particles.

The critical step in the development was the choice of an appropriate protocol to immobilize StrepApt5 on the surface of beads. It was impossible to label the aptamer with a biotin moiety to promote the interaction with streptavidin-coated beads. Therefore, covalent immobilization of the aptamer had to be considered. We decided to avoid the use of N-acylation reactions for the immobilization. This chemistry exploits the reaction between amines and activated carboxylic acids to form stable amides and has been extensively applied to immobilize biological probes on solid surfaces[97,98]. Despite the wide range of applications of this approach, based on previous expertise, it provides unsatisfactory and poorly reproducible results, especially when the reaction takes place in aqueous media.

We selected strain-promoted azide-alkyne cycloaddition (SPAAC), a reaction that involves azide groups and alkyne moieties and leads to the formation of stable triazole rings. This click chemistry reaction is compatible with biological environments, and possesses faster kinetics in comparison with N-acylation reaction. In particular, SPAAC was chosen instead of its copper-catalyzed counterpart (CuAAC) because copper may promote the radical cleavage of DNA increasing the protocol's variability. In fact, SPAAC reaction does not require the use of copper but implies tensioned alkynes like dibenzocyclooctine (DBCO) that, being forced into 8-membered ring, possess higher energy. Therefore it is more reactive[62].

To apply SPAAC for immobilization purposes, aptamer and beads need to be functionalized with DBCO and azide moieties. While DNA sequences can be easily labeled with both azide and DBCO and are commonly commercially available, micro-particles with suitable properties in terms of size, coating and functionalization are difficult to find. Generally, it is

harder to find beads that expose DBCO groups on the surface; we opted for DBCO-labeled aptamers and azide-bearing micro-particles.

Different beads functionalized with azide groups were purchased and tested (all involving the presence of an azide-containing self-assembled monolayer). They returned unsatisfactory results in terms of DNA immobilization (data not shown). In this work, we developed a coating that exposes an azide moiety to allow the proper immobilization of StrepApt5. The customized coating was required to immobilized the aptamer at a precise density, which is crucial for its efficacy.

In particular, silica beads (1 µm in diameter) were coated using MCP-6. MCP-6 (see structure in Figure 6.1), a DMA-based copolymer obtained from MCP-2 through post-polymerization reaction with 3-azide-1-propylamine as described in [99]. In particular, it retains MCP-2 optimal properties (i.e., excellent immobilization of bioprobes with good exposure and antifouling properties) while displaying azide groups on the surface.

Silica beads were chosen due to multiple factors, including their commercial availability, low costs, and ease of recovery by centrifugation at low g speed. In addition, silica beads expose silanols on their surface that react with trimethoxysilyl ethers on MCP-6, a providing covalent and stable coating.

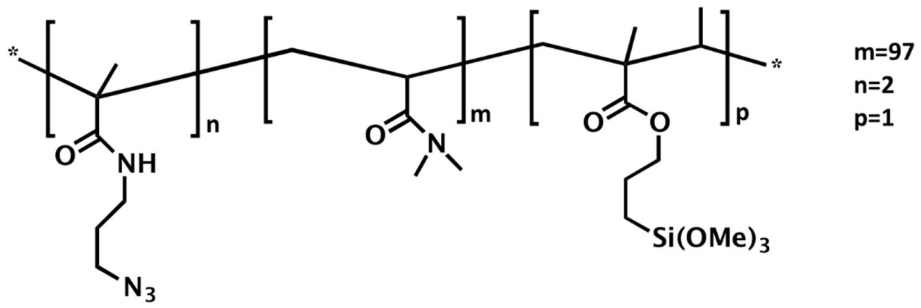

***Figure 6.1**. Chemical structure of MCP-6.*

In the following Sections we report the silica bead coating procedure and their characterization.

1.1 Materials

Ammonium sulfate ($(NH_4)_2SO_4$), dibenzocyclooctyne-N-hydroxysuccinimidyl ester (DBCO-NHS ester), phosphate buffer saline tablets (PBS), streptavidin, Dimethylacrylamide (DMA), N-succinimidyl acrylate (NAS), 3-(trimethoxysilyl)propyl methacrylate (MAPS), 3-azide-1-propylamine, bovine serum albumin (BSA), sodium dodecyl sulphate (SDS), Tris, HCl,

polyclonal rabbit IgG, Amicon Ultra 30 MWCO and 100 MWCO centrifugal filters were purchased from Sigma Aldrich (St. Louis, MO, USA). Bradford Protein Assay Dye Concentrate was purchased from Bio-Rad (Hercules, CA, USA). Goat antirabbit IgG was purchased from Jackson ImmunoResearch (Baltimore, PA, USA). Oligonucleotides were synthesized by MWG-Biotech AG (Ebevsberg, Germany): see Section 1.1.1 for oligonucleotide sequences. COCU8 was modified either with DBCO-linker or biotin at 5' end, COCU11 was labeled with Cy5 at 5' end and DNA-capture1 was labeled with biotin at 5' end. Oligonucleotides were freeze-dried and resuspended in de-ionized water (DI water) at a final concentration of 100 μM before use. Silica microbeads were purchased from Bangs Laboratories Inc (Fishers, IN, USA). Spectrofluorimetric analysis was performed using a Jasco FP-550 spectrofluorometer equipped with thermo-stated Peltier cell holder. Bradford protein assay were performed using a Thermo Labsystems Multiskan Ascent microplate spectrophotometer. ζ-Potential measurements were performed on a Zetasizer Nano ZS Instrument (Malvern Instruments Corp., Malvern, UK) and samples were loaded in a Zetasizer nano series Dip Cell Kit (Malvern Instruments Corp., Malvern, UK).

1.1.1 Oligonucleotide sequences

- *COCU8*: 5'-GCCCACCTATAAGGTAAAAGTGA-3'
- *COCU11*: 5'-TCACTTTTACCTTATAGGTGGGC-3'
- *DNA-capture1:* 5'-NH_2-ACTTAGGACTCAGTACAGGATAGACTTGATATCGGTTGGA 3'

1.1.2 Polymers synthesis

1.1.2.1 Synthesis of MCP-2: copoly (DMA-NAS-MAPS), is composed of DMA (97% mole percent), N-succinimidyl acrylate (NAS) (2% mole percent), and 3-(trimethoxysilyl)propyl methacrylate (MAPS, 1% mole percent). The polymer was synthesized by free radical polymerization as reported elsewhere [100]. Briefly, after degassing anhydrous THF with helium, DMA, NAS, and MAPS were added to the reaction flask so that the total monomer feed was 20% w/v. The reaction mixture was heated to 65°C for two hours in the presence of AIBN. The crude material was cooled to room temperature and diluted 1:1 with dry THF; the solution was then precipitated in petroleum ether (10 times the volume of the reaction mixture) to eliminate unreacted monomers, filtered on a Büchner funnel, and dried under vacuum at room temperature.

1.1.2.2 Synthesis of MCP-6: MCP-2 was modified by reaction with 3-azido-1-propylamine, as reported elsewhere [95]. To introduce the azide groups, a 20% w/v solution of the copolymer was prepared by dissolving it in dry THF. 3-azido-propylamine was added in 2.5 molar excess with respect to the moles of NAS. The concentration of NAS functionalities along the polymer chain is 40 mM. The mixture was stirred for 5 h at room temperature and then diluted 1:1 with anhydrous THF. The polymers were precipitated in petroleum ether (10 times the volume of the reaction mixture), filtered on a Büchner funnel and dried under vacuum at room temperature.

1.1.3 Coating of silica microspheres using MCP-6

Silica microspheres (10% w/v, diameter = 1 µm) were sonicated in a water bath for 10 min and stirred using a vortex shaker 30 sec to ensure proper resuspension. Then 50 µL (= 5 mg) were transferred into a 1.5 mL tube and washed twice with MQ water. After each washing or incubation step beads were separated from supernatant by centrifugation. Beads were resuspended in 1 mL solution of MCP-6 (1% w/v in 0.9 M ammonium sulphate) and incubated 30 min at 25°C under stirring followed by 30 min at 25°C without stirring. Beads were washed twice with 1 mL of MQ water and used for further experiments.

1.1.4 Analysis of MCP-6 coated silica microspheres by ζ-Potential

ζ-potential measurements were carried out at a wavelength of 633 nm with a solid state He-Ne laser at a scattering angle of 173°, at 298 K on diluted samples (0.01-0.1 mg/mL particles) at pH 7. Each result was averaged from at least three measurements.

1.1.5 Antifouling properties evaluation

20 mg of silica microspheres were coated with MCP-6 as described in section 1.1.3. Beads were washed with 1 mL of PBS and then incubated overnight at 37°C under stirring with 1 mL of a 50 mg/mL solution of BSA in PBS. Beads were washed three times with PBS, resuspended in 150 µL of 0.1% SDS, and incubated 10 min at 95°C. After centrifugation, the supernatant was recovered. The washing step with SDS was repeated two additional times, and all supernatants were pooled and concentrated on an Amicon Ultra 30 MWCO centrifugal filter (10 min at 12,200 g) to a final volume of around 20 µL. The same procedure was repeated on 20 mg of uncoated silica microspheres as a negative control. The concentration of BSA released by the beads upon SDS-mediated denaturation was assessed by a Bradford protein assay.

1.1.6 Immobilization of oligonucleotides on MCP-6 coated silica microspheres

1.1.6.1 Immobilization of oligonucleotides: 5 mg of MCP-6 coated silica microspheres were washed in 1 ml of PBS and resuspended in 100 µL of DBCO-modified COCU8 in PBS (different concentrations ranging from 1 to 20 µM were tested) and incubated overnight at 37°C under stirring. Beads were washed twice with 1 mL of water and once with 1 mL of PBS.

1.1.6.2 Hybridization with COCU11: 5 mg of beads functionalized with COCU8 were resuspended in 100 µL of Cy5-labeled COCU11 in PBS (at the same concentration used for COCU8 during immobilization step) and incubated for 1 h at 25°C under stirring. Beads were centrifuged and supernatant was recollected. Beads were washed twice with 100 µL of PBS, after each beads were centrifuged and supernatant recollected. Supernatants were pooled together and, only in samples where the concentration of DNA used during incubation was 5 µM or higher it was diluted 1:10 using PBS. 150 µL of pooled supernatants (diluted or not) were mixed with 350 µL of PBS and the fluorescence emission intensity at 658 nm was measured using using a Jasco FP-550 spectrofluorimeter in 1 cm quartz cuvettes.

1.1.7 Immobilization of streptavidin on MCP-6 coated silica microspheres

1.1.7.1 Synthesis of DBCO-modified streptavidin: to 1 mL of 1 mg/mL streptavidin in PBS, 9 µL of 4 mM DBCO-NHS ester were added (6.7 equivalents). The solution was allowed to react 30 min at room temperature. The reaction was quenched by adding 100 µL of Tris-HCl 1 M pH 8. After 5 min at room temperature, the solution was transferred to Amicon Ultra 30 MWCO centrifugal filters, and the excess of DBCO-NHS ester was removed by centrifugation. The final volume was adjusted to 1 mL by adding PBS.

1.1.7.2 Streptavidin immobilization: 10 mg of MCP-6 coated silica microspheres were resuspended in 500 µL of 1 mg/mL DBCO-modified streptavidin and incubated overnight at 37°C under stirring. Beads were then washed 3 times with 1 mL of PBS and finally resuspended in 100 µL of PBS.

1.1.7.3 Capture of biotinylated oligonucleotides: 1 mg of streptavidin-coated silica microspheres, prepared as described in section 1.1.7.2, were resuspended in 200 µL of 3 µM biotinylated COCU8 in PBS for 30 min at 25°C under stirring. Beads were washed twice with 1 ml of MQ water and once with 1 mL of PBS. As a negative control, 1 mg of streptavidin-

coated silica microspheres were used to immobilize biotinylated DNA-capture1 following the same experimental procedure. Both the aliquots were resuspended in 100 µL of 6 µM Cy5-labeled COCU10 in PBS and incubated for 1 h at 25°C under stirring, then beads were centrifuged and the supernatant was recollected. Beads were washed twice with 100 µL of PBS, and after each step, the supernatants were recollected. Pooled supernatants were diluted 1:10 using PBS and 150 µL of the diluted solution were added to 350 µL of PBS and the fluorescence emission intensity at 658 nm was measured using a Jasco FP-550 spectrofluorimeter in 1 cm quartz cuvettes.

1.1.8 Immobilization of antibodies on MCP-6 coated silica microspheres

1.1.8.1 Synthesis of DBCO-modified rabbit IgG: to 500 µL of 1 mg/mL rabbit IgG in PBS, 12.3 µL of 4 mM DBCO-NHS ester were added (15 equivalents). The solution was allowed to react 30 min at room temperature. The reaction was quenched by adding 50 µL of Tris-HCl 1 M pH 8. After 5 min at room temperature, the solution was transferred to Amicon Ultra 100 MWCO centrifugal filters, and the excess of DBCO-NHS ester was removed by centrifugation. The final volume was adjusted to 500 µL by adding PBS.

1.1.8.2 Rabbit IgG immobilization: 10 mg of MCP-6 coated silica microspheres were resuspended in 500 µL of 1 mg/mL DBCO-modified rabbit IgG and incubated overnight at 37°C under stirring. Beads were then washed 3 times with 1 mL of PBS and finally resuspended in 100 µL of PBS. As a negative control, 10 mg of MCP-6 coated silica microspheres were incubated overnight with PBS at 37°C under stirring, washed 3 times with 1 mL of PBS, and finally resuspended in 100 µL of PBS.

1.1.8.3 Interaction with secondary antibody: the two aliquots of beads prepared as described in section 1.1.8.2 were resuspended in 40 µL of 0.5 mg/mL goat antirabbit IgG in PBS and incubated for 1 h at 25°C under stirring. After centrifugation, the supernatant was recollected. Beads were washed once with 40 µL of PBS and supernatant was recollected. Supernatants were pooled, and goat antirabbit IgG concentration was measured by Bradford protein assay.

2. Results & Discussion

MCP-6 has proven to be highly efficient in coating glass and silicon microarray chips. In fact, this polymer interacts with these materials through both covalent (i.e. condensation of surface silanols with MAPS monomer) and non-covalent interactions (e.g. H-bonds and Wan der Waals forces).

Accordingly, the coating of silica beads that expose free silanols on their surface) was expected to proceed straight. To obtain a stable coating, silica microbeads were immersed into a solution of the polymer (1% w/v) in 0.9 M ammonium sulfate. The salt acts like salting-out agent that, by limiting the polymer's solubility in water, promotes its adsorption on the surface of the beads. After 1 h incubation, silica beads were recovered by centrifugation and washed twice with water to afford MCP-6-coated particles.

The presence of the polymeric coating was demonstrated by Zeta-Potential measurement. Uncoated and MCP-6 coated silica microbeads were dispersed and diluted in a NaCl solution and analyzed. The measured Zeta-Potentials were -72 mV and -12.1 mV for uncoated and MCP-6 coated beads, respectively. This result confirmed the successful coating of the beads. In fact, while bare silica presents a high density of negative charges on its surface, these charges are partially masked after coating with MCP-6 (negatively charged silanols react with MAPS resulting in covalent bonds with neutral charge). The high difference between Zeta-Potential for uncoated and coated beads (around 60 mV) suggests a high-performance coating of the beads.

Subsequently, to demonstrate that once adsorbed onto silica beads, MCP-6 retains its peculiar antifouling behavior (i.e., it shows a low non-specific binding of biomolecules on its surface), coated beads were incubated overnight with 50 mg/mL BSA in PBS at 37°C. As the negative control, uncoated silica beads were treated in the same way.

After incubation with BSA, beads were incubated with 0.1% SDS for 10 min at 95°C in order to break non-specific interaction between albumin and beads. Supernatants were recovered, and BSA concentration was measured by Bradford protein assay. The results are shown in Figure 6.2.

a)

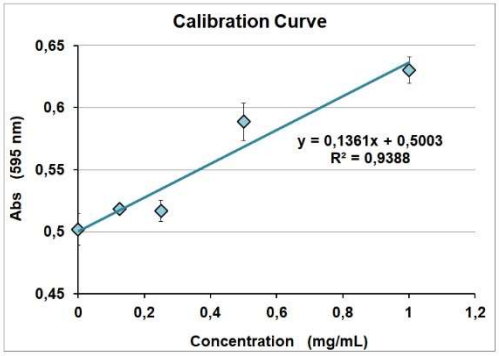

b)

	Uncoated silica	MCP-6 coated silica
BSA (mg/mL)	5.23*	- 0.70**

***Figure 6.2**. BSA quantification by Bradford protein assay. a) Calibration Curve for BSA, b) concentration of BSA released from beads after SDS treatment.*

** Higher than calibration curve maximum concentration.*

*** Lower than zero, probably under the limit of detection for Bradford assay.*

As highlighted in the figure, MCP-6-coated and uncoated silica beads behave differently: uncoated beads release a high concentration of BSA after treatment with SDS, confirming literature evidences supporting a strong non-specific adsorption of proteins onto silica surfaces[101,102]. Contrarily, the MCP-6 coating confers antifouling properties to silica beads since no trace of BSA can be detected (-0.70 mg/mL suggests an extremely low level of BSA adsorption, under the limit of detection of the assay).

Once demonstrated that MCP-6 to provides a homogeneous and stable coating of silica microbeads, we evaluated its ability to provide efficient immobilization of biological probes. In particular, the immobilization rate for oligonucleotides, streptavidin and antibodies was assessed, covering a wide panel of biological molecules.

The immobilization of biological probes was evaluated using indirect assays. Probe-functionalized beads were incubated with their biological counterparts. The depletion of the counterparts in solution was measured. By difference, it was possible to know the amount of analyte captured on the surface, hence the quantity of immobilized probe. We are aware that such an indirect measurement could potentially underestimate the amount of probe that is bound to the surface. However, it well represents the amount of accessible probe (i.e., the quantity of probe that could actually take part in biomolecular recognition of targets) on the surface, which is what actually impacts on the overall performance of an assay.

First of all, we evaluated the ability of MCP-6-coated silica microbeads to immobilize DBCO-modified antibodies. Polyclonal rabbit IgG was functionalized with DBCO groups and incubated overnight with beads to provide efficient immobilization. Negative control was carried out, incubating beads overnight with only PBS. After several washing steps, both

sets of beads were incubated with a secondary antibody (goat antirabbit IgG) and its concentration before and after the incubation with beads was evaluated through a Bradford protein assay (see Figure 6.3). The secondary antibody was entirely captured on the surface of antibody-functionalized beads (1.89 µg/mg of resin) while a sensibly lower amount was captured on the negative control (0.40 µg/mg of resin, around 5 times lower).

a)

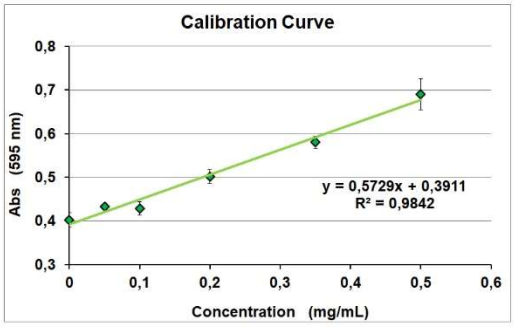

b)

	MCP-6 coated silica	Negative control
Secondary antibody (µg/mg of resin)	1.89	0.40

Figure 6.3*. Antibody quantification by Bradford protein assay. a) Calibration Curve for goat antirabbit IgG, b) concentration of goat antirabbit IgG captured on rabbit IgG-functionalized silica beads. The amount of captured IgG was calculated subtracting its concentration after the experiment with its initial concentration.*

Similarly, we evaluated the immobilization of streptavidin on MCP-6-coated silica microbeads. DBCO-modified streptavidin was synthesized as described in Section 1.1.7.1 and used to incubate overnight MCP-6-coated silica beads. Streptavidin immobilization yield was assessed measuring the amount of biotinylated ssDNA that was effectively captured on the surface of beads. Streptavidin-coated beads were incubated with biotinylated-COCU8. As a negative control, a second set of beads was functionalized with biotin-labeled DNA-capture1. Both sets of beads were incubated with Cy5-labeled COCU11 (a sequence of DNA complementary only to COCU8) and the depletion of fluorescence – which corresponds to the amount of COCU11 immobilized on the surface through interaction with COCU8 - was measured with a spectrofluorimeter (see Figure 6.4). In particular, it was calculated that 255 pmoles per mg of resin are immobilized through hybridation with COCU8, no COCU11 is captured by the negative control.

a)

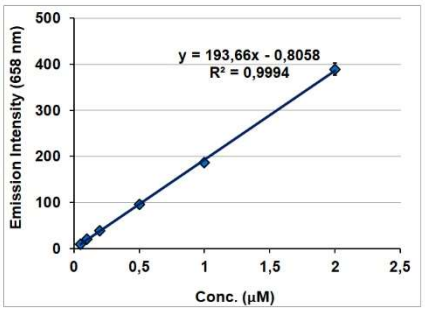

b)

	MCP-6 coated silica	Negative control
Captured Cy5-COCU11 (pmol/mg of resin)	255	/

***Figure 6.4**. Spectrofluorimetric measurement of Cy5-labeled COCU11. a) Calibration Curve for Cy5-COCU11 and b) amount of pmoles of Cy5-COCU11 captured per mg of silica microbeads on the positive and negative control.*

This result is important since it demonstrates that biotynilated DNA is specifically captured by streptavidin bound to MCP-6 coated silica beads. Additionally, the binding capacity of biotinylated ssDNA is slightly higher than that of commercially available beads (e.g., the reported binding capacity for Dynabeads™ Streptavidin M-270 is 200 pmol per mg of beads).

Finally, also binding capacity for direct ssDNA immobilization was measured. For this purpose, 5 mg of MCP-6 coated beads were incubated overnight with 100 µL of DBCO-modified COCU8 at different concentrations (namely 1, 2, 5, 10, and 20 µM) at 37°C. After washing, the beads were incubated with 100 µL of Cy5-labeled COCU11 (at the same concentration used for COCU8 immobilization) for 1 h at 25°C. After incubation the supernatant was recovered, properly diluted and fluorescence emission evaluated by spectrofluorimeter, and COCU11 concentration inferred using a calibration curve. The measured concentration was subtracted to starting concentration to assess the amount of COCU11 captured on functionalized beads and the value used as an indirect measure of COCU8 bound to MCP-6 beads. Results are shown in Figure 6.5.

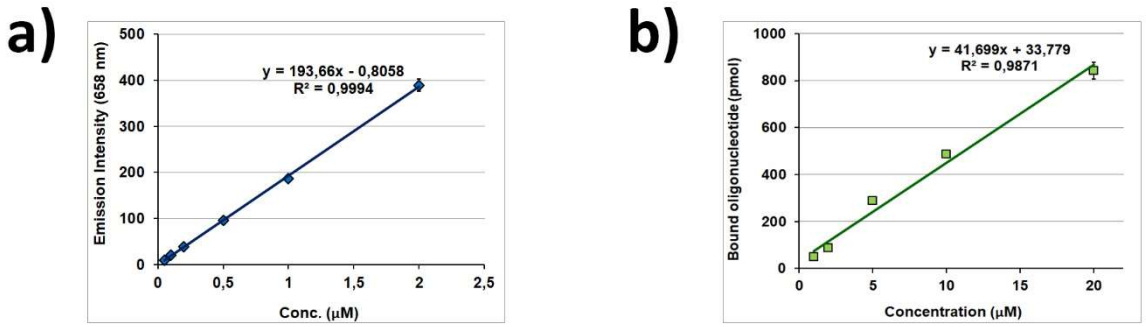

***Figure 6.5**. a) calibration curve for Cy5-labeled COCU11. b) Correlation between pmoles of ssDNA immobilized on 5 mg of MCP-6 coated beads and ssDNA concentration used.*

As it can be noticed, there is a linear correlation between the concentration of DBCO-modified COCU8 used for the immobilization on MCP-6 coated beads, and the amount of ssDNA effectively immobilized on the surface. Since the molecular weight of DBCO-modified COCU8 and the total surface of 5 mg silica beads are known (8000 g/mol and $3.75*10^9$ μm^2, respectively) the density of DNA probes on the surface can be easily calculated and is reported in Table 6.1.

Concentration* (µM)	1	2	5	10	20
Density (ng/mm^2)	0.11	0.18	0.61	1.04	1.80

***Table 6.1**. Correlation between concentration and density of immobilized ssDNA on the surface. *Concentration used during incubation to immobilize COCU8 on the surface.*

In conclusion, we developed an effective strategy for the coating of silica microbeads. MCP-6 was chosen to provide the functional coating that exposes of azido groups. Different biological probes have been successfully labeled with DBCO groups and immobilized onto coated silica particles, exploiting SPAAC reactions. Antibodies, streptavidin, and ssDNA have been used to functionalize silica beads and proved to be still able to interact with their biological counterparts (secondary antibody, biotinylated ssDNA, and complementary DNA, respectively).

Data acquired during the development of silica microbeads as solid supports were used to effectively exploit the immobilization of StrepApt5 and achieve a reversible aptamer-mediated antibody immobilization on beads, as described in the next Chapter.

CHAPTER 7

SEPARATION OF EXTRACELLULAR VESICLES BY APTAMER-MEDIATED IMMOBILIZATION OF ANTIBODIES

1. Silica beads functionalization with StrepApt5

Having demonstrated that silica micro particles coated with MCP-6 can provide an effective immobilization of DBCO-modified biological probes, including ssDNA, the possibility to immobilize StrepApt5 was evaluated, as well as the ability to perform reversible aptamer-mediated antibody immobilization on the surface of beads.

1.1 Materials

Ammonium sulfate ($(NH_4)_2SO_4$), phosphate buffer saline tablets (PBS), Trizma base, 37% chloric acid (HCl), sodium phosphate (Na_3PO_4), sucrose monolaurate, sodium chloride (NaCl), ethanolamine, trehalose dehydrate, magnesium chloride ($MgCl_2$), NHS-PEG_4-biotin, Amicon Ultra 100MWCO centrifugal filters, streptavidin and polyclonal rabbit IgG were purchased from Sigma Aldrich (St. Louis, MO, USA). Bradford Protein Assay Dye Concentrate was purchased from Bio-Rad (Hercules, CA, USA). Goat antirabbit IgG was purchased from Jackson ImmunoResearch (Baltimore, PA, USA). Oligonucleotides were synthesized by MWG-Biotech AG (Ebevsberg, Germany): see Section 1.1.1 for oligonucleotide sequences. StrepApt5 was modified at 5' end with DBCO-linker, cDNA was used both unmodified and labeled with Cy5 at 5' end. Oligonucleotides were freeze-dried and resuspended in de-ionized water (DI water) at a final concentration of 100 μM before use. StrepApt5 underwent a folding procedure before immobilization on solid supports: aptamer solutions were heated at 95°C for 8 min, transferred into ice at -20°C for 10 min and finally left at room temperature for 15 min.

Silica microbeads were purchased from Bangs Laboratories Inc (Fishers, IN, USA). Spectrofluorimetric analysis was performed using a Jasco FP-550 spectrofluorometer equipped with thermo-stated Peltier cell holder. Bradford protein assay were performed using a Thermo Labsystems Multiskan Ascent microplate spectrophotometer.

1.1.1 Oligonucleotide sequences

- *StrepApt5*: 5'-GGGAACGCACCGATCGCAGGTTTCCC-3'
- *cDNA*: 5'-ACCTGCGATCGGTGCGTTCCC-3'

1.1.2 Beads functionalization with StrepApt5

Silica microbeads (diameter = 1μm, 10% content in solids) were sonicated 10 min and stirred using a vortex shaker 30 sec in order to achieve optimal resuspension. 50 μL (= 5 mg) were transferred in a 1.5 ml tube and centrifuged to pellet beads (30 sec at 12,000 rpm). The same procedure was repeated after every washing or incubation step to remove supernatant from beads. Beads were washed twice with bidistilled water and then incubated with a MCP-6 solution (1% w/v) in 0.9 M ammonium sulfate for 1 h at 25°C under stirring. Beads were washed twice with bidistilled water and once with PBS added with 2 mM $MgCl_2$ (hereinafter referred to as PBS-M). Then, beads were resuspended in 100 μL of 10 μM DBCO-modified StrepApt5 in PBS-M (previously folded as described in Section 1.1) and incubated overnight at 37°C under stirring. Finally, beads were washed twice with PBS-M.

1.1.3 Assessing StrepApt5 immobilization efficiency on silica microbeads

5 mg of StrepApt5 decorated silica microbeads were resuspended in 100 μL of 10 μM Cy5-labelled cDNA in PBS and incubated for 1 h at 25 °C under stirring. After centrifugation the supernatant was recovered and the beads washed twice with 100 μL of PBS. After each washing step, the solution was centrifuged and the supernatant recovered. The supernatants were pooled and diluted 1:10 using PBS; 150 μL of the so obtained solution were added to 350 μL of PBS and the light emitted at 659 nm was determined by spectrofluorimetric analysis. The concentration of cDNA after incubation with beads was determined using a calibration curve. The amount of StrepApt5 bound to the beads was assessed subtracting the concentration of cDNA before and after incubation with silica beads.

1.1.4 Streptavidin immobilization on StrepApt5 decorated silica microbeads

5 mg of StrepApt5 decorated silica microbeads were resuspended in 100 μL of 0.1 mg/mL (=10 μg) streptavidin in PBS-M and incubated 1 h at 25°C under stirring. After centrifugation the supernatant was recovered and the beads washed twice with 100 μL of PBS-M. After each washing step, the solution was centrifuged and the supernatant recovered. The supernatants were pooled and streptavidin concentration was measured by Bradford protein

assay. As the negative control the same experimental procedure was repeated on 5 mg of MCP-6 coated silica microbeads.

1.1.5 Streptavidin release on StrepApt5 decorated silica microbeads

5 mg of StrepApt5 decorated silica microbeads were resuspended in 300 μL of 1 mg/mL streptavidin in PBS-M and incubated 1 h at 25°C under stirring. Beads were washed twice with PBS-M and then incubated with 100 μL of 10 μM cDNA in PBS for 1 h at 25°C under stirring. After centrifugation the supernatant was recovered and streptavidin concentration was measured by Bradford protein assay. As negative control the same experimental procedure was repeated on 5 mg of MCP-6 coated silica microbeads.

1.1.6 Synthesis of biotinylated rabbit IgG

To 100 μL of 1 mg/mL solution of polyclonal rabbit IgG in PBS, 3.15 μL of 8.5 mM NHS-PEG_4-biotin (40 equivalents) were added and allowed to react for 30 min at 25°C. Reaction was quenched by adding 10 μL of 1 M Tris-HCl pH 8. After 5 min unreacted biotin linker was removed by centrifugation of Amicon Ultra 100MWCO centrifugal filter (3 × 5 min at 12.000×*g*). After centrifugation, the volume was adjusted to 100 μL with PBS.

1.1.7 Antibody immobilization on StrepApt5 decorated silica microbeads

5 mg of StrepApt5 decorated silica microbeads were resuspended in 300 μL of 1 mg/mL streptavidin in PBS-M and incubated 1 h at 25°C under stirring. Beads were washed twice with PBS-M and then incubated with 40 μL of 0.5 mg/mL (=20 μg) biotinylated rabbit IgG in PBS-M for 1 h at 25°C under stirring. After centrifugation the supernatant was recovered and the beads washed twice with 40 μL of PBS-M. After each washing step, the solution was centrifuged and the supernatant recovered. The supernatants were pooled and antibody concentration was measured by Bradford protein assay. As negative control the same experimental procedure was repeated on 5 mg of StrepApt5 decorated silica microbeads, incubated with native rabbit IgG without biotin modification.

1.2 Results & Discussion

Preliminary experiments of aptamer-mediated antibody immobilization using microarrays have demonstrated that the efficiency of StrepApt5 is strictly related to its density on the surface. In particular, they highlighted the presence of a critical concentration of the aptamer that provides the best immobilization rate for streptavidin. The optimal density is achieved

by spotting the aptamer at 10 µM concentration (see Section 2.2). We expected to see the same behavior is expected to be observed on silica microbeads. Therefore, the concentration of DBCO-modified StrepApt5 to be used for microbeads functionalization had to be finely tuned.

Previous experiments on DNA microarrays, performed using IRIS detection technique, revealed that by spotting ssDNA at a concentration of 10 µM, the density of the oligonucleotide on the surface ranges between 1-2 ng/mm^2 [103]. Knowing the density of DNA produced by incubating silica microbeads with different concentrations of DBCO-modified ssDNA (see Table 6.1), we extrapolated that the optimal amount of StrepApt5 immobilized on the surface could be obtained at 10 µM concentration also for beads functionalization.

In order to confirm this prediction, 5 mg of silica beads were coated using MCP-6 and functionalized with 10 µM StrepApt5 as described in Section 1.1.2. Functionalized beads were incubated with 100 µL of 10 µM Cy5-labeled cDNA, and the residual fluorescence in the supernatant was determined by spectrofluorimetry. The results, summarized in Figure 7.1, indicate that, under these experimental conditions, StrepApt5 is immobilized on the surface of silica microbeads with a density of 1.32 ng/mm^2. This density on the surface was considered to be optimal for further steps.

a)

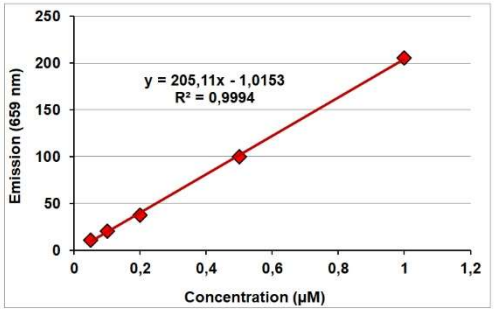

b)

Bound StrepApt5 (pmol)	Molecular Weight (g/mol)	Surface Area* (µm^2)	Surface Density (ng/mm^2)
585.4 ± 8	8452	3,75*10^9	1.32 ± 0.01

***Figure 7.1**. a) Calibration Curve for Cy5-labeled cDNA. b) Amount of StrepApt5 immobilized on beads expressed as pmoles and surface density.*

** All results are referred to 5 mg of silica microbeads.*

First of all, the ability of StrepApt5-functionalized beads to immobilize streptavidin was evaluated. To this scope, 5 mg of aptamer-functionalized beads were incubated with 100 µL of 0.1 mg/mL streptavidin in PBS-M and then washed as described in Section 1.1.5. As the negative control, 5 mg of MCP-6 coated silica microbeads were treated in the same way.
Finally, the supernatant was recollected and streptavidin concentration was assessed by Bradford protein assay. The results are shown in Figure 7.2. As it can be noticed, 145.3 pmoles are effectively captured on beads functionalized with StrepApt5, while only a negligible amount is measured on the negative control. These results confirmed that the aptamer, once immobilized on silica microbeads, retains its ability to effectively and selectively bind streptavidin.

a)

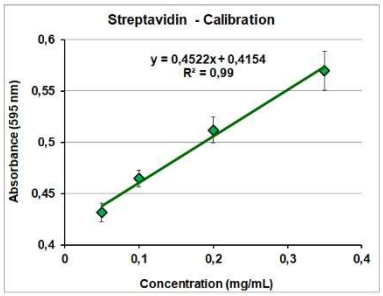

b)

	StrepApt5 functionalized beads	Negative control
Immobilized streptavidin (pmol)	145.3 ± 0.5	6.1 ± 0.8

***Figure 7.2**. Results for streptavidin immobilization on StrepApt5-functionalized silica microbeads. a) Calibration Curve for streptavidin using Bradford protein assay. b) Amount of streptavidin captured on StreptApt5-exposing beads and on the negative control. Results are referred to 5 mg of silica microbeads.*

To know if streptavidin captured on the surface of beads could actually be released upon incubation with cDNA, an additional experiment was performed: 5 mg of StrepApt5-functionalized silica microbeads were incubated with 200 µL of 1 mg/mL streptavidin in PBS-M. After washing, beads were incubated with 100 µL of 10 µM cDNA in PBS. At the end of the incubation, the supernatant was recollected and the concentration of streptavidin was assessed by Bradford protein assay. As a negative control, 5 mg of MCP-6 coated silica microbeads (without StrepApt5) underwent the same experimental protocol.
Results, shown in Figure 7.3, confirm that 126.5 pmoles of streptavidin can actually be released from aptamer-functionalized beads after incubation with cDNA, thus demonstrating the suitability of this system to be used in capture and release experiments. On the contrary, streptavidin could not be captured on the surface of negative control beads, and no traces of this protein were found after cDNA treatment (the negative value probably results from

the fact that streptavidin concentration is below the limit of detection of the Bradford protein assay).

a)

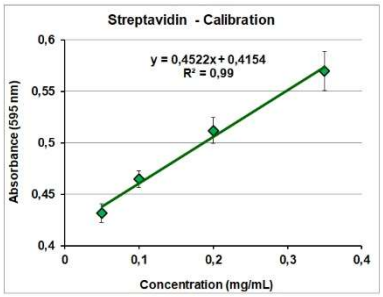

b)

	StrepApt5 functionalized beads	Negative control
Released streptavidin (pmol)	126.5 ± 23.3	< 0

***Figure 7.3**. Results for streptavidin release from StrepApt5-functionalized silica microbeads. a) Calibration Curve for streptavidin using Bradford protein assay. b) Amount of streptavidin released from StreptApt5-exposing beads and from the negative control. Results are referred to 5 mg of silica microbeads.*

Once the feasibility of the aptamer-mediated reversible immobilization of streptavidin has been demonstrated, we investigated the immobilization of biotin-labeled antibodies on the surface of aptamer-bound streptavidin.

To this purpose, polyclonal rabbit IgG was biotinylated according to Section 1.1.6. MCP-6 coated silica microbeads were functionalized with StrepApt5 and streptavidin as described in the Sections 1.1.2 and 1.1.4; 5 mg of these beads were incubated with 40 µL of 0.5 mg/mL biotinylated rabbit IgG in PBS-M. As a negative control, 5 mg of beads were prepared in the same way and were incubated with unmodified rabbit IgG, which, lacking of biotin modification, was not supposed to bind to streptavidin.

After incubation the supernatants were recollected and the antibody concentration was assessed by Bradford protein assay. Subtracting the residual antibody concentration to the initial concentration, it was possible to determine the amount of antibody captured on the surface of beads under these experimental conditions. Results are shown in Figure 7.4 and clearly demonstrate that biotinylated IgGs are effectively captured on aptamer-bound streptavidin. This interaction is driven by the affinity between biotin and streptavidin, the same antibody without biotin modification could not be immobilized on the surface of beads.

a)

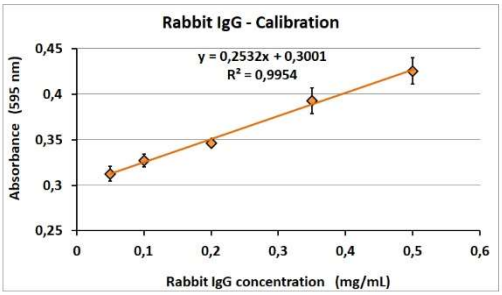

b)

	Biotinylated rabbit IgG	Negative control
Captured antibody (µg)	17.3 ± 0.4	< 0

***Figure 7.4**. Results for antibody immobilization on StrepApt5-functionalized silica microbeads. a) Calibration Curve for rabbit IgG using Bradford protein assay. b) Amount of rabbit IgG captured on beads functionalized with aptamer-bound streptavidin and on the negative control. Results are referred to 5 mg of silica microbeads.*

The results described in this section confirmed the suitability of aptamer-mediated antibody immobilization to generate a platform for capture and release of biotinylated molecules. In the next sessions the approach will be applied to the separation of EVs from complex biological fluids.

2. EVs separation through aptamer-mediated immobilization of antibodies

After initial proof-of-concept experiments and the development of aptamer-mediated immobilization approach on microarrays, the procedure was transferred to silica microbeads. In order to do that, silica beads were coated with MCP-6 copolymer and their ability to bind DBCO-labeled biological probes was demonstrated. Then, also StrepApt5 was successfully immobilized on beads and proved to be effective in capturing streptavidin. Aptamer-bound streptavidin was able to immobilize biotin-labeled antibodies and could be finally released upon incubation with cDNA.

As a final step, the ability of this system to provide EVs separation from complex biological fluids was assessed. AntiCD9 was used to functionalize silica beads via aptamer-mediated immobilization and the functionalized matrix was exploited to provide reversible immuno-precipitation of EVs. Experimental details are outlined in following Sections.

2.1 Materials

Ammonium sulfate ($(NH_4)_2SO_4$), phosphate buffer saline tablets (PBS), Trizma base, 37% chloric acid (HCl), magnesium chloride ($MgCl_2$), NHS-PEG_4-biotin, Amicon Ultra 100MWCO centrifugal filters, streptavidin and polyclonal rabbit IgG were purchased from Sigma Aldrich (St. Louis, MO, USA). Biotinylated mouse antihuman CD9 IgG (clone MEM-61) was a kind gift of Hansa BioMed Life Sciences Ltd (Tallinn, Estonia). Oligonucleotides were synthesized by MWG-Biotech AG (Ebevsberg, Germany): see Section 2.1.1 for oligonucleotide sequences. StrepApt5 was modified with DBCO-linker in 5' position. Oligonucleotides were freeze-dried and resuspended in de-ionized water (DI water) at a final concentration of 100 µM before use. StrepApt5 underwent a folding procedure before immobilization on solid supports: aptamer solutions were heated at 95°C for 8 min, transferred into ice at -20°C for 10 min and finally left at room temperature for 15 min.

Silica microbeads were purchased from Bangs Laboratories Inc. (Fishers, IN, USA). Nanoparticle Tracking Analysis was performed with NanoSight NS300 using 3.2 Dev Build 3.2.16 software (Malvern Instruments Ltd, Malvern, UK).

2.1.1 Oligonucleotide sequences

- *StrepApt5*: 5'-GGGAACGCACCGATCGCAGGTTTCCC-3'
- *cDNA*: 5'-ACCTGCGATCGGTGCGTTCCC-3'

2.1.2 Functionalization of silica microbeads with antiCD9 through aptamer-mediated immobilization

5 mg of silica microbeads were coated with MCP-6 as described in Section 3.1.3. StrepApt5 was immobilized on beads as reported in Section 1.1.2. Beads were incubated with 300 µL of 1 mg/mL streptavidin in PBS-M for 1 h at 25°C under stirring. Beads were washed twice with 1 mL of PBS-M and recovered by centrifugation. Beads were then incubated with 40 µL of 0.5 mg/mL biotinylated antiCD9 in PBS-M for 1 h at 25°C under stirring. Beads were finally washed twice with 1 mL of PBS-M and recovered by centrifugation. For the negative controls, a different set of beads was prepared using the same experimental protocol, but using biotinylated rabbit IgG (synthesized as reported in Section 1.1.6) instead of antiCD9.

2.1.3 EVs separation from HEK-293 cell culture supernatant using aptamer-mediated immobilization

2.1.3.1 Separation of EVs from HEK-293 cell culture medium by ultracentrifugation. HEK-293 cells were seeded on 150 mm dishes in DMEM culture medium supplemented with 10% EV-depleted FCS (obtained by recovering the supernatant after ultracentrifugation of the FCS at 150.000 x g for 17 h), 2 mM L-Glutamine, 100 U/mL penicillin and 100 µg/mL streptomycin-sulphate. After 72 h incubation, the culture medium was collected and centrifuged at 450 x g for 25 min to remove cell debris. The obtained supernatant was filtered through 0.22 µm filter and then ultracentrifuged at 150.000 x g for 2 hours at 4°C (Beckman Coulter). The EV-containing pellet was finally resuspended in PBS.

2.1.3.2 EVs characterization by *Nanoparticle Tracking Analysis*. All samples were analyzed using Nanosight NS300 (Malvern Panalytical, Malvern, UK) configured with 532 nm laser. Videos were analyzed by the in-build NanoSight Software NTA 3.2 Dev Build 3.2.16. The Camera type, Camera level, and Detect Threshold were sCMOS, 14 and 4, respectively. A syringe pump with constant flow injection was used. The number of completed tracks in NTA measurements was 5 (a 60 seconds movie was registered for each measurement). Sample was diluted in PBS to a final volume of 1 mL. The ideal concentration was assessed by pre-testing the optimal particle per frame value (20-100 particles per frame).

2.1.3.3 EVs separation using aptamer-mediated immobilization of antiCD9. 5 mg of silica microbeads were functionalized with antiCD9 using aptamer-mediated immobilization as described in Section 2.1.2. Beads were then incubated with 150 µL of EVs separated from HEK-293 cell culture supernatant by ultracentrifugation and diluted in PBS-M to a final concentration of $1.95*10^{11}$ particles/mL. After 2.5 h of incubation at 25°C under stirring, supernatants were removed and beads washed twice with 1 mL of PBS-M and recovered by centrifugation. Beads were finally incubated with 100 µL of 10 µM cDNA in PBS for 1 h at 37°C under stirring. After incubation the supernatant was recovered and analyzed by Nanoparticle Tracking Analysis. As the negative control, 5 mg of beads were functionalized with rabbit IgG instead of antiCD9 and underwent the same experimental protocol.

2.1.4 EVs separation from human blood plasma using aptamer-mediated immobilization

2.1.4.1 Plasma collection: Blood samples were obtained from healthy blood donors in non-fasting conditions at the Department of Clinical Immunology at Aalborg University Hospital. Blood samples were collected in a bag system LQT6283LE (Macopharma, France) using CPDA as anticoagulant and centrifuged at 4800 x g for 10 min to separate plasma. The plasma was removed, aliquoted, and stored at -40°C. Before analysis, plasma was centrifuged at 10.000 x g for 10 min, and then filtered through 0.45 µm syringe filters (Corning, NY, USA). Finally, to 3.136 µL of plasma 64 µL of 100 mM $MgCl_2$ were added (final concentration 2 mM) to ensure StrepApt5 correct folding during EVs capture step.

2.1.4.2 EVs separation using aptamer-mediated immobilization of antiCD9. Two aliquots of 10 mg silica microbeads were functionalized with antiCD9 using aptamer-mediated immobilization as described in Section 2.1.2. Each aliquot then incubated with 800 µL of human blood plasma collected and processed as described in Section 2.1.4.1. After 2.5 h of incubation at 25°C under stirring, supernatants were removed and beads washed twice with 1 mL of PBS-M and recovered by centrifugation. Beads were finally incubated with 200 µL of 10 µM cDNA in PBS for 1 h at 37°C under stirring. After incubation the supernatant was recovered, pooled and analyzed by Nanoparticle Tracking Analysis. As the negative control, two aliquots of 10 mg beads were functionalized with rabbit IgG instead of antiCD9 and underwent the same experimental protocol.

2.2 Results & Discussion

The novel aptamer-mediated immobilization of antibodies had been developed and described in the previous sections. In this last part of the work, we demonstrated EVs separation through this antibody immobilization approach. For this purpose, silica microbeads were coated using MCP-6 and functionalized with StrepApt5.

Aptamer decorated beads were then used to sequentially immobilize streptavidin and biotinylated antibodies. In particular, to perform EVs separation an antibody against CD9 was chosen. CD9 is a member of tetraspanins family and is commonly found on the surface on different EVs subpopulations. Alongside, a different set of beads was functionalized with biotinylated rabbit IgG in order to be used as the negative control.

In order to determine whether the herein proposed approach for immuno-affinity precipitation works for EVs separation or not, its performance was evaluated on two different samples of increasing complexity.

First, we assessed the yield of the process by performing the separation of EVs from a sample purified from HEK-293 cell culture supernatant by ultracentrifugation. Two sets of silica microbeads, one functionalized with antiCD9 and on with rabbit IgG through aptamer-mediated immobilization, were separately incubated with EVs diluted in PBS-M at a final concentration of $1.95*10^{11}$ particles/mL for 2.5 h at room temperature. After washing, beads were incubated with 10 µM cDNA in PBS to release complexes composed by streptavidin, antibodies and EVs. The beads were separated and supernatant recollected and analyzed by Nanoparticle Tracking Analysis.

Results, shown in Figure 7.5, indicate that the buffer (i.e. 10 µM cDNA in PBS, blue curve) displays only a small number of particles without a specific size distribution. The sample released from the beads functionalized with rabbit IgG is similar to the release buffer, confirming that using the negative control only a minimal number of particles is captured on the surface. The experiment with antiCD9-functionalized beads instead, show that a high number of particles with the typical size distribution of sEVs, ranging in size from 75 nm to 200 nm, are captured and released. The experiment proves that by using aptamer-mediated immobilization of antibodies for EVs separation, an excellent degree of selectivity can be reached.

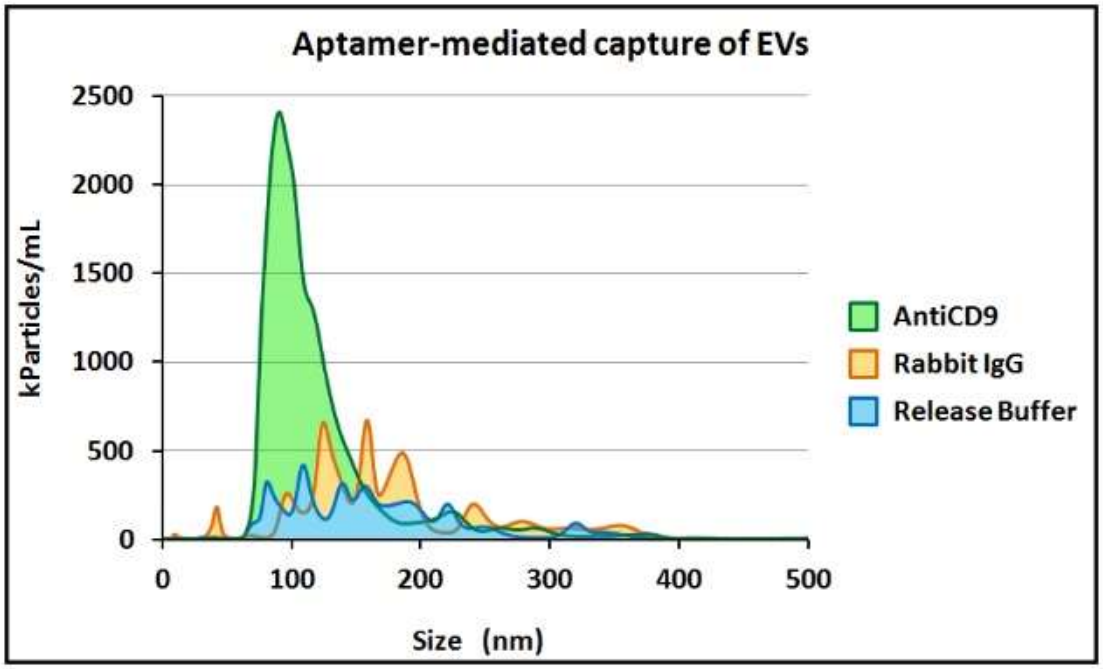

***Figure 7.5**. Nanoparticle Tracking Analysis of samples released from silica beads functionalized with aptamer-mediated immobilization of antiCD9 (green) and rabbit IgG (orange) after incubation with EVs separated from HEK-293 cell culture supernatant. Also the release buffer alone (i.e. 10 µM cDNA in PBS) was analyzed (blue).*

Encouraged by these results, we repeated the same experimental procedure on human blood plasma. Plasma was collected from healthy subjects, filtered over 450 µm membrane to remove larger particles, and added with 2 mM $MgCl_2$. Then plasma was used to incubate beads functionalized either with antiCD9 or rabbit IgG by aptamer-mediated immobilization to provide immuno-affinity capture of EVs. Finally, beads were incubated with cDNA solution to release captured particles and the supernatant was analyzed by NTA (see Figure 7.6).
The green curve represents the size distribution of the particles released from beads functionalized using antiCD9; it confirms the ability to separate particles with the typical size distribution of a sEV subpopulation. This result is significant since it demonstrates the possibility to apply aptamer-mediated immobilization of antibodies to separate EVs from complex biological fluids. Also in this experiment, using the negative control (i.e. beads functionalized with rabbit IgG via aptamer-mediated immobilization) a lower number of particles was released from beads, thus confirming the selectivity of the approach, also in complex media.

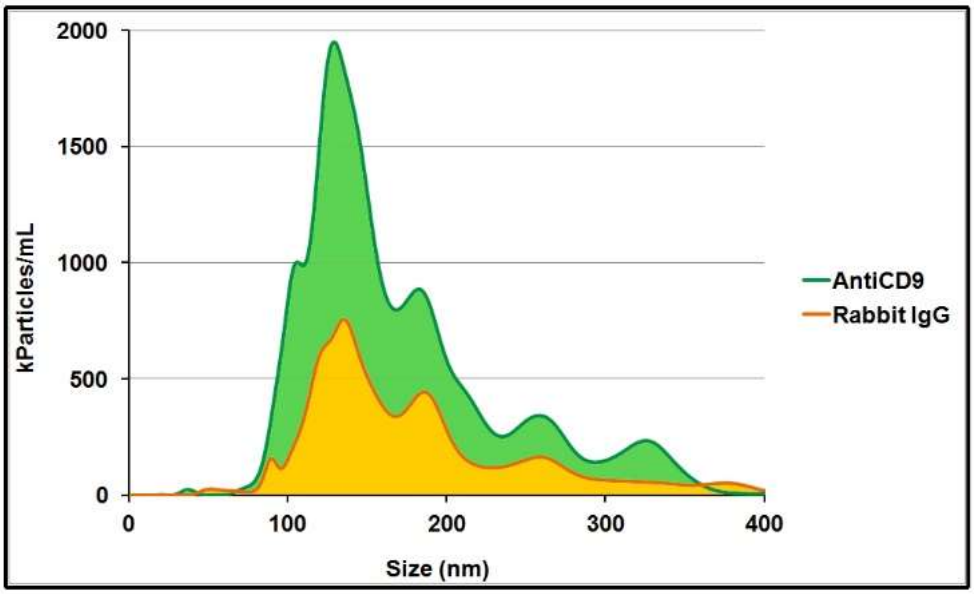

***Figure 7.6**. Nanoparticle Tracking Analysis of samples released from silica beads functionalized with aptamer-mediated immobilization of antiCD9 (green) and rabbit IgG (orange) after incubation with human blood plasma.*

CHAPTER 8

INDEX PROJECT

1. Project overview

Methods for advanced characterization of molecular signatures associated with each subset of EVs are rapidly emerging. When this thesis work started, a deep analysis of the state-of-the-art revealed two primary unmet needs: lack of i) efficient technologies for high purity separation of EVs and ii) methods to detect, quantify and characterize EVs simultaneously. The most popular separation methods mainly involved ultracentrifugation and were very lengthy, complex, and unreliable. Different approaches had already been developed but were far from being ready to enter a routine clinical environment. To-date, several on-the-chip devices for EV based protein detection rely on immunoaffinity isolation coupled to EV detection trough either sandwich immunoassay, or label free sensor technology. Despite conspicuous financing received after high ranked publications, all have failed to reach the scaling up and robust performance needed for a beta testing phase and implementation in diagnostic grade assays. Some encouraging experimental results have also been reported using commercially available immunoassay platforms, such as SIMOA (Quanterix) and photonic devices, including high resolution cytometry (nFCM Nanoanalyzer or Amnys/ Luminex), microscopy (dSTORM or STED)) and Plasmonic technologies (SPR, SERS). All Photonic/imaging techniques today available are bulky, expensive, time-consuming and require highly skilled operators. However, the most complex node to be solved for implementation of biosensing platforms for Liquid Biopsy is the high selectivity/specificity and sensitivity that would enable the detection of vanishingly small amounts of cancer molecules. The detection of EVs is made difficult by their intrinsic characteristics (small size, low refractive index) that prevent the use of optical microscopy and conventional flow cytometry. A few years ago, EVs were mainly detected using TEM while their phenotype was analyzed by Western Blot. Both techniques are time-consuming, costly and low throughput. More recently, two detection technologies were introduced (i.e. Nanoparticle Tracking Analysis and Tunable Resistive Pulse Sensing) to facilitate EV detection and quantitation. However, appropriate phenotyping approaches are still lacking.

To fill these gaps and facilitate the translation of EVs from research to clinics, the Chemistry and Technology for Bioscience group of SCITEC-CNR has coordinated a FET-OPEN project entitled “Integrated Nanoparticle Isolation and Detection System for Complete On-Chip Analysis of Exosomes” (INDEX). This project started in 2018 with the ambitious goal of developing an integrated platform for inline separation of EVs from complex biological fluids and downstream EV number, size and phenotyping characterization. The project aimed to deliver a robust, quantitative, high-throughput, and low-cost technology suitable to be integrated into clinical workflow that potentially replaces expensive and bulky equipment, trained personnel and extensive protocols with a simple lab-on-chip system. An analytical platform that fulfills these requirements, certainly represents a breakthrough in the diagnostics field and paves the way toward the actual implementation of EV-based liquid biopsies in clinical settings. The following sections provide an overview of the project technology and illustrate the role of the innovation brought about by this thesis work in enabling the different analytical steps of the platform.

2. INDEX Project overall concept

The project workflow is divided in different stages (see Figure 8.1), each involving the development of novel technologies. The overall project goal is their integration into a single instrument.

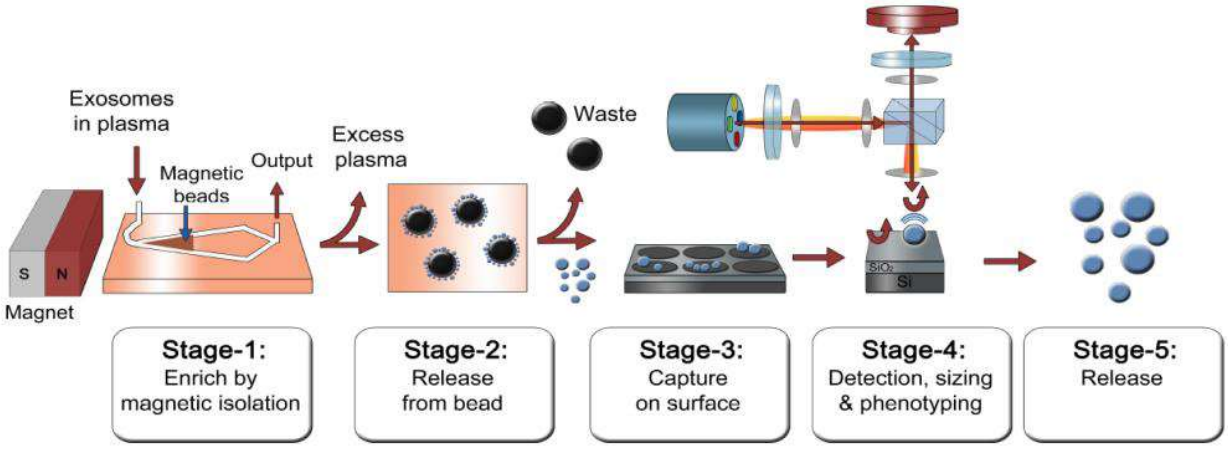

***Figure 8.1**. INDEX project overall concept.*

Briefly, the device is composed of a separation module (stages 1-2) and a detection module (stages 3-4). In the separation module antibody-functionalized magnetic beads are

recirculated in a microfluidic chamber to perform immuno-affinity capture of EVs starting from complex biological fluids, such as blood plasma. During Stage-2, captured EVs are released as intact vesicles and enter the detection module. They are immobilized on a microarray chip functionalized with antibodies to provide EVs phenotyping and detected and sized using an optical sensor. As an optional step, in Stage-5, EVs can be potentially released a second time to analyze their cargo.

The overall performance of this system is meant to be tested and clinically validated using blood plasma samples from lung cancer patients and healthy individuals. Biological samples are collected by a partner in Aalborg University.

The novel technologies involved in this concept are the microfluidic device, the chemistry of reversible immuno-affinity capture of EVs, and the optical sensor for their detection and characterization.

The development of the microfluidic chamber was carried out by the Curie Institute in Paris, which pioneered an innovative platform for the recirculation of magnetic beads (Figure 8.2)[104].

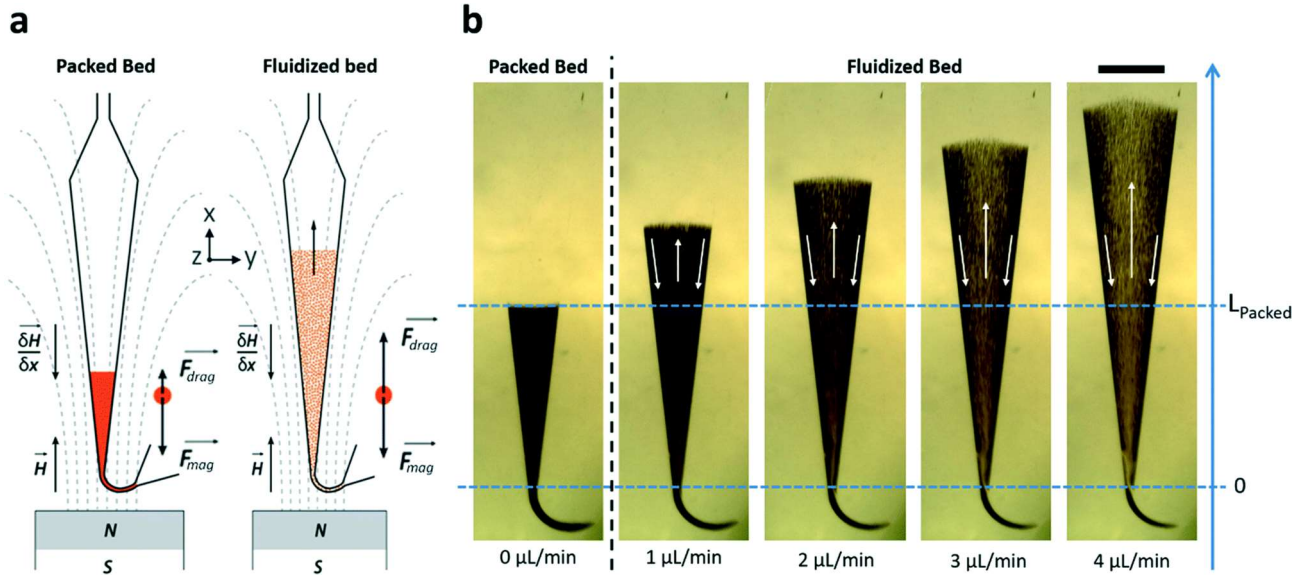

***Figure 8.2**. a) Schematic representation of microfluidic fluidized bed chip geometry. b) real picture of the chip filled with magnetic beads. Increasing the flow rate the bed height increases and recirculation of beads occurs.*[104]

This emerging technology, called *microfluidic fluidized bed*, combines magnetic beads with a microfluidic device with fast diffusion, high loading capacity, high surface to volume ratio, and enables high capture efficiency from molecules to cell. It's potentially applicable to EVs. The device's design comprises an external permanent magnet to generate a strong

magnetic field parallel to the main chamber axis. The magnetic field induces a force, F_{mag}, on magnetic beads that compact into a dense and static bed called plug. When a solution is flown inside the chamber at a given flow rate, the liquid exerts a hydrodynamic force, F_{drag}, that counterbalances the magnetic force. As a consequence, the confinement effect on the beads is reduced, and the plug inches up until an equilibrium state where F_{mag} equals F_{drag}. Under this condition, a recirculation flow is spontaneously generated, causing a net particle income in the center of the channel and backflows close to channel walls, thus favoring the interaction between magnetic beads and biological target to be captured by overcoming mass-transfer or reaction kinetics limitations.

Regarding the optical sensor, the detection of individual biological nanoparticles as EVs presents unique challenges due to polydispersity, small size, and low refractive index.

Even if optical microscopy is an indispensable tool for studying biological entities, conventional light scattering microscopy cannot resolve objects that are smaller than the wavelength of illumination. Although this diffraction limit can be overcome by utilizing non-linear phenomena in fluorescence microscopy as described in studies that led to 2014 Nobel Prize in Chemistry, these optical nanoscopy techniques require labeling with fluorescent molecules. However fluorescent labels do not represent the optimal choice due to instability of the signal at the detector coming from particle over time.

Conventional imaging based on light scattering contrast is more advantageous in these terms than fluorescent methods. Still, unfortunately the elastically scattered light intensity induced by the illumination of the nanoparticles, scales with the sixth power of the particle size. Thus, the contrast produced by biological nanoparticles is extremely small and difficult to detect over the background scattering. That is why many emerging optical techniques rely on image contrast enhancement using different methods as background reduction as in dark-field microscopy, plasmonic resonance, and interferometry.

The optical sensor for biological nanoparticles developed within INDEX is based on an innovative technology developed by Boston University called *Interferometric Reflectance Imaging Sensor* (IRIS)[105] and was previously applied for the detection of viruses, which are nanoparticles that share the same size of smaller EVs (but characterized by a higher refractive index)[106].

Further development of the IRIS technique, the Single Particle IRIS (SP-IRIS), is based on the enhanced contrast in the scattering signal from particles captured on a layered sensor surface. More in detail, to detect and size individual nanoparticles, SP-IRIS shines light from visible LED sources onto the sensor surface composed of a silicon dioxide layer on top of a

silicon substrate (i.e. an antibody microarray chip). When an extracellular vesicle is bound to the sensor, it modifies the interference of light reflected from the surface, thus producing a distinct signal that correlates with the size of the particle as shown in Figure 8.3 (the bigger the particle, the higher the contrast).

By using this setup is possible to digitally detect, count and size individual biological nanoparticles from 50 nm to 200 nm in diameter (see Figure 8.4). Additionally, using an antibody microarray as sensor surface, EVs can be phenotyped based on their surface composition[107].

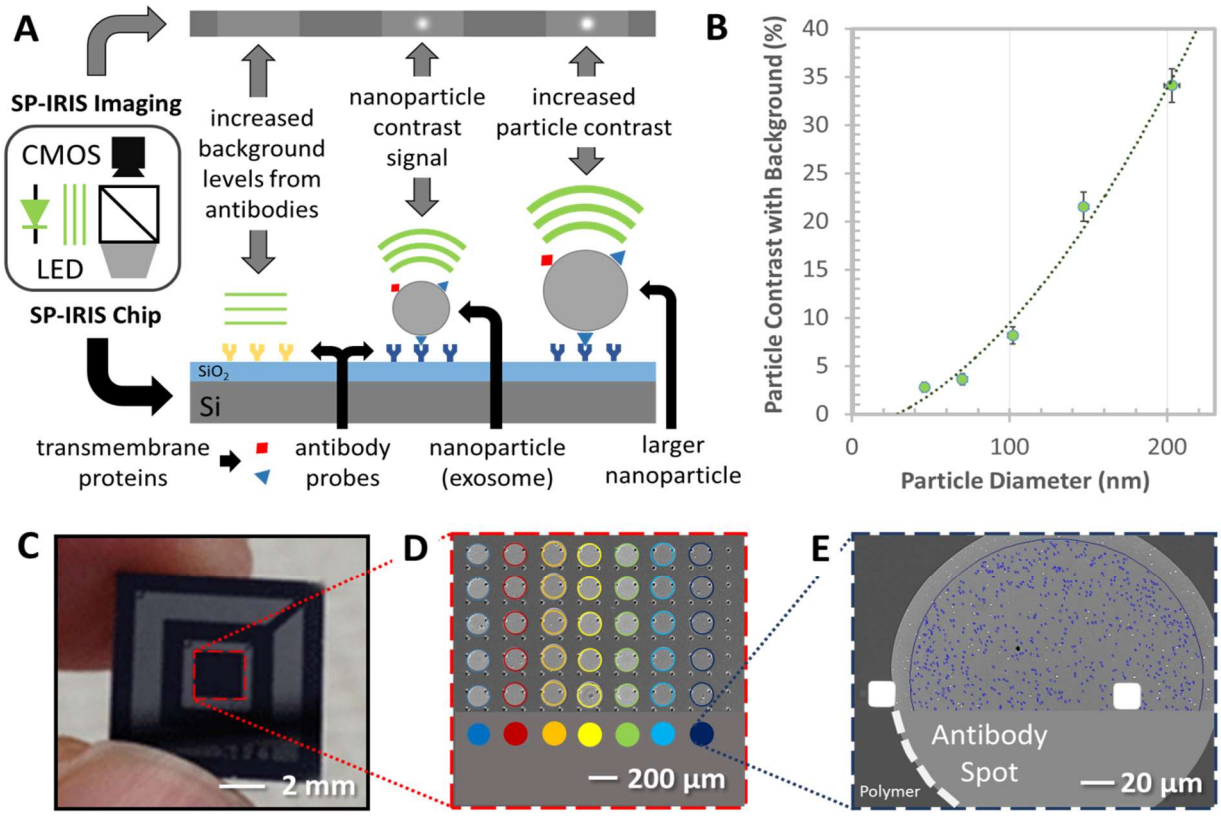

***Figure 8.3**. A) Scheme for operation setup of SP-IRIS device. B) Correlation between size of nanoparticle and contrast produce in the image. C) Picture of a SP-IRIS microarray chip with enlargements showing the array of antibodies and a single spot where single EVs are highlighted as blue dots (D and E, respectively).*

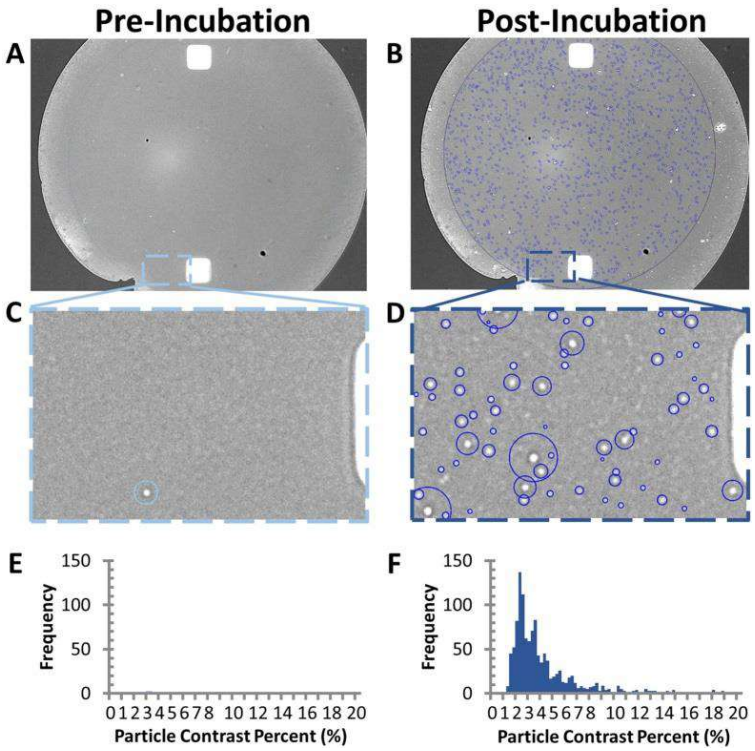

***Figure 8.4**. Picture of a single antibody spot, its enlargement and size distribution of captured EVs before (A, C and E) and after (B, D, F) an incubation.*

Separation and detection modules are meant to be integrated in a single instrument within INDEX project to go directly from the injection of a complex biological fluid into the microfluidic chamber to the digital detection and characterization of EVs contained in the sample.

Besides the hardware, what enables the integration of the separation and detection modules is the reversible immuno-affinity capture of extracellular vesicles on magnetic beads by a chemical approach allowing to release of intact EVs. The integrity of the vesicles is essential for downstream analysis on the optical biosensor.

Thus, the key to success in the INDEX project is the choice of an appropriate strategy for immuno-affinity-based separation of EVs from complex biological fluids. The ideal approach foresees i) an antibody immobilization technique that allows the capture of EVs with high yield and selectivity and ii) a subsequent effective release of EVs under mild conditions preserving their integrity as to be compatible with SP-IRIS downstream detection.

Focusing on these goals, the immobilization strategy selected was the *DNA-directed immobilization of antibodies* (DDI). DDI suits well to INDEX requirements since dsDNA has been demonstrated to be an excellent linker for antibodies on solid surfaces since it enhances the availability of antibody binding sites for biological nanoparticles capture by decreasing the steric hindrance surrounding the protein[60]. This characteristic has already

been confirmed in work by Seymour et al.[61] where DDI of antibodies was used to capture viruses on microarray substrates. In addition, in this work viruses were detected using the SP-IRIS technique, further confirming how DDI represents an excellent choice to achieve INDEX project goals.

3. INDEX Project outcomes

Simultaneously with optimizing the DDI-based approach for EVs separation, INDEX project partners developed microfluidic separation and interferometric detection modules. Once the two modules were ready, their integration was carried out at CNR in Milan, collaborating with Curie Institute in Paris and Fluigent (Paris) partners. After the technical validation was completed demonstrating the actual capability of the system to provide in-line separation and detection of EVs, the integrated platform was supposed to be transferred to Aalborg University partners for the clinical validation of EVs diagnostic potential in lung cancer. Unfortunately, just before sending all the components to Denmark, COVID-19 outbreak in Italy and shortly after in the rest of the world, forcing the partners to adopt a different strategy. The physical integration of the instrument would have required traveling to assemble the prototype and train the partners on its use. Unfortunately, the partners were experiencing lockdowns and were not allowed to enter their research facilities. Therefore, separation and detection of EVs from plasma were carried out separately. Specifically, separation of EVs from plasma was carried out in Paris and Aalborg, EV-containing samples were sent to Boston for interferometric detection. Finally, the statistical analysis of data was performed at Aalborg University. In the meantime, as part of this thesis work, at CNR we synthetized DACs that were shipped to Paris and Aalborg. Microarray chips for interferometric detection were prepared and sent to Boston University.
Details regarding the development of separation and detection modules, as well as a description of technical and clinical validation outcomes are reported in following sections.

3.1 Development of microfluidic separation module

The development of the separation module, and its validation, were carried out at Curie Institute in Paris. Starting from microfluidic device developed and described in [104], a second-generation fluidized bed was developed in order to accommodate higher flow rates, thus enabling the processing of larger volumes. Basically, the volume of the chamber was

increased but then additional measures were required to maintain the instrument overall performance. Specifically, two options were selected: adding vibration at the entrance of the device as well as tuning the composition of the beads (two different sizes of beads have been selected and co-injected in the microfluidic chamber to prevent aggregation phenomena)[108].

The second generation microfluidic fluidized bed (see Figure 8.5), was tested for the separation of EVs from plasma.

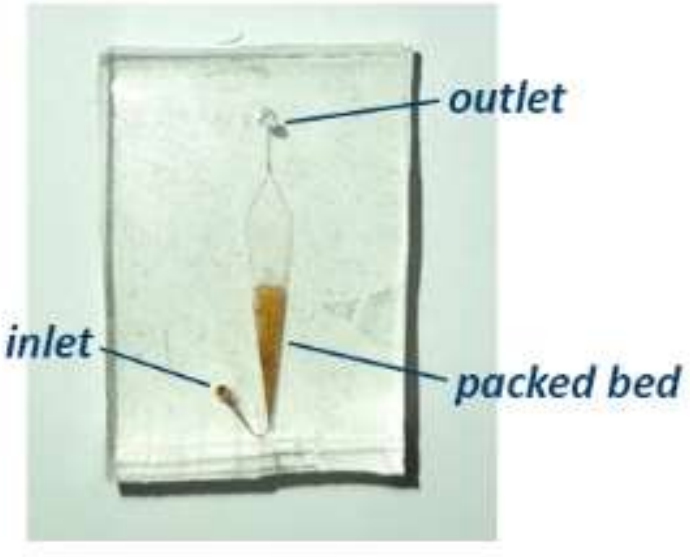

***Figure 8.5**. Example of a PDMS chip incorporating the second generation microfluidic fluidized bed.*

Human blood plasma samples were obtained from healthy donors and made available by Aalborg University Hospital. The plasma was centrifuged at 10,000 x *g* for 10 min and then filtered through 0.22 µm syringe filter. The capture of EVs was carried out on streptavidin-coated magnetic beads functionalized as described in Section 2.1.6.2 and loaded in the second-generation fluidized bed. Two sets of beads were prepared, either functionalized with antiCD63 or antiCD9 antibody, both immobilized through DDI. After loading the functionalized beads into the chip, the human plasma (125 µL) was injected at a flow rate of 0.5 µL/min (total incubation time: 4h 10 min). During the capture, a vibration motor (2.5V and 0.04 A) was positioned on the inlet tubing of the chamber to improve the beads mixing. The temperature was set at 25°C and controlled through a temperature controller installed on the platform through a thermocouple placed inside the PDMS chip. Following capturing on the fluidized bed, the chip was rinsed with PBS at 5µL/min for 15 min before the release

step. For release, a solution of DNase I (250 mKunitz/µL) was injected inside the chip at a flow rate of 0.5 µL/min during 1h 40min at 37°C to collect 50 µL of EVs-containing sample. This procedure was repeated twice, once using antiCD63 functionalized beads, while the second time, antiCD9 was used as a capture agent.
Eluted samples were analyzed by NTA and results are shown in Figure 8.6.

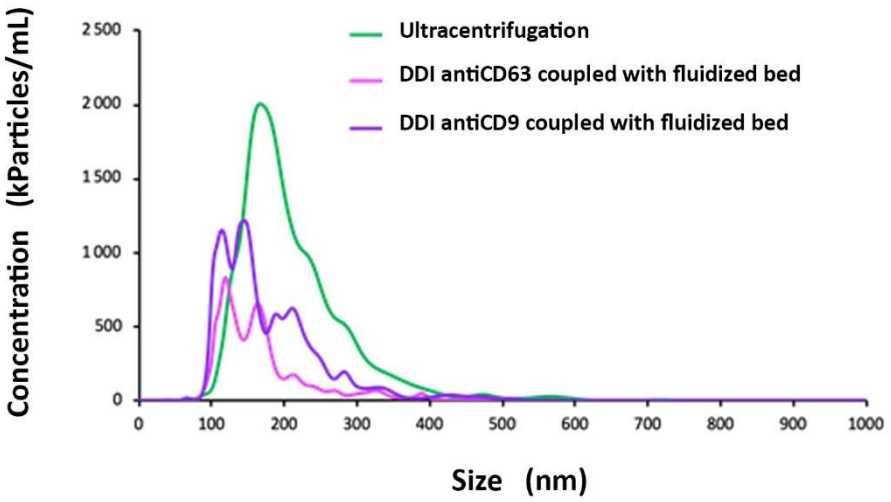

***Figure 8.6**. NTA profiles of EVs separated from human blood plasma using ultracentrifugation and DDI-based approach. DDI approach was repeated twice functionalizing magnetic beads with different antibodies, namely antiCD63 and antiCD9.*

Samples recovered using the DDI-based approach presented a $5.1*10^{10}$ particles/mL and $2.3*10^{10}$ particles/mL concentration for antiCD9 and antiCD63 antibodies, respectively. Both samples showed a higher concentration in particles ranging from 100 to 200 nm. Interestingly, a subpopulation of particles ranging from 200 to 300 nm is selectively separated using DNA-directed antiCD9. Separating EVs from the same plasma sample using ultracentrifugation, a higher number of particles is obtained. It is probably due to the separation of the whole population of EVs (not only CD63+ or CD9+ vesicles) or to the presence of contaminants (e.g. lipoproteins). Moreover, the NTA profile showed the presence of bigger particles in the sample obtained by ultracentrifugation (up to 400 nm), which may result from aggregation of smaller vesicles induced by high centrifugal forces.
Encouraged by the results of these experiments, a more compact and portable fluidized bed prototype was developed by Institute Curie in collaboration with Fluigent partners. The instrument (see Figure 8.7) was equipped with different fluidic modules (valves, manifold, FB chip holder, camera, pumps) and monitored by dedicated software to allow an automated EVs extraction and release.

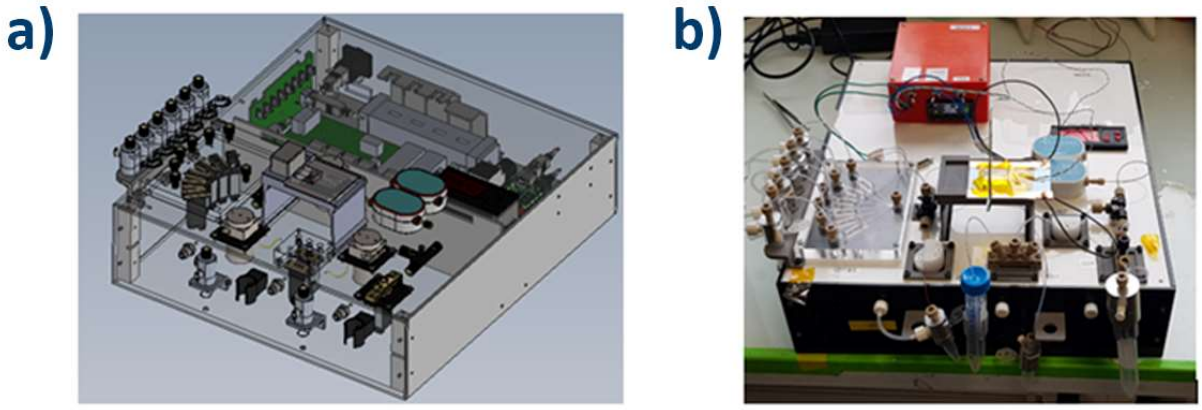

***Figure 8.7**. Design of the automated Microfluidic Fluidized Bed prototype. Computer rendering (a) and real picture of the bench instrument (b).*

The prototype was then tested against the conventional approach for magnetic separation, which uses magnetic beads inside an Eppendorf tube to perform the immuno-affinity capture, and a magnetic stand to separate magnetic beads and supernatant. For this purpose, a sample of human blood plasma, obtained from a healthy donor, was centrifuged at 10.000 x g for 10 min and then filtered over 0.22 µm syringe filter. Then, processed plasma was divided into two aliquots, and EVs were extracted using either conventional tube experiment or microfluidic fluidized bed, following protocols described previously. In both experiments, magnetic beads were functionalized with antiCD9 via DNA-directed immobilization. Obtained samples were then analyzed by NTA and SP-IRIS experiments and the results compared.

Nanoparticle Tracking Analysis results are shown in Figure 8.8. DDI-based separation could extract EVs from plasma using both tube and microfluidic platform setup. In both experiments, the particle concentration was higher than the negative control (i.e. the DNase I-containing release buffer) with a size distribution compatible with an EV population.

Most importantly, despite the size distribution of particles separated using the two experiments is quite similar (as expected, since the two methods selectively separate the same subpopulation of EVs), the concentration obtained applying DDI-based approach in combination with the microfluidic fluidized bed is higher, confirming that the automated platform can improve the binding capacity of magnetic beads leading to a better performance. Sample recovered from fluidized bed also show a lower number of particles larger than 200 nm, suggesting that continuous recirculation of beads in the microfluidic device prevents EVs aggregation.

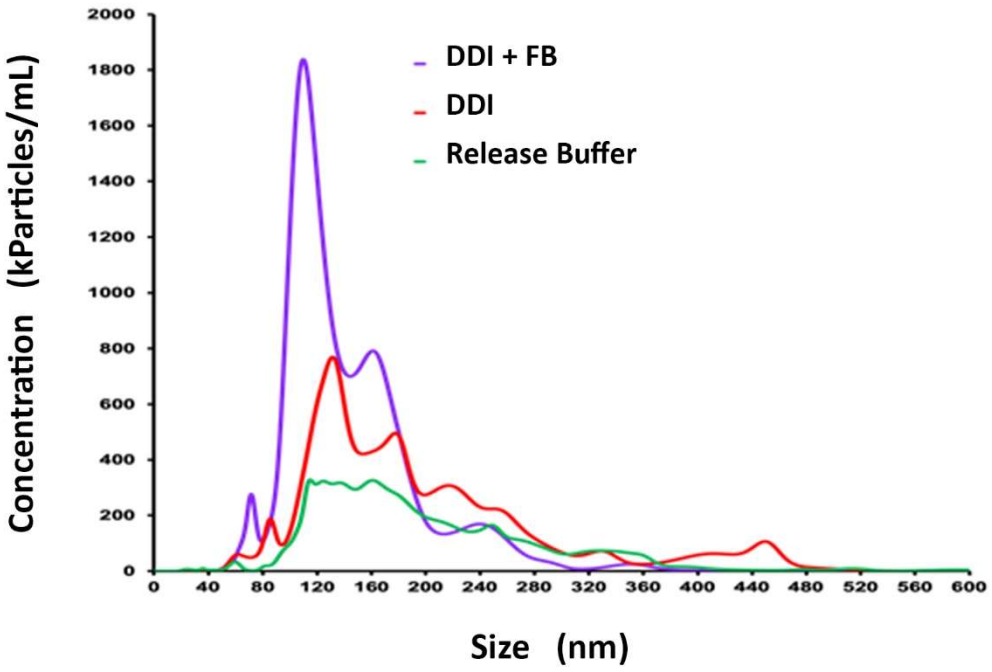

***Figure 8.8**. Nanoparticle Tracking Analysis of EVs separated from human blood plasma using DDI approach on Eppendorf tube (DDI) and microfluidic fluidized bed platform (DDI + FB). As the negative control, DNase I-containing release buffer was also analyzed.*

Results obtained by NTA were also confirmed using the SP-IRIS technique. Silicon chips were functionalized with EV-binding peptides as described in [109] and analyzed using ExoView R100 instrument. These EV-binding peptides are based on a short amino acid sequence (RPPGFSPFR, BK) derived from bradykinin which binds highly curved lipid nanovesicles, including EVs. In particular, three different peptidic baits were immobilized on silicon chips, which are the linear (BP), branched (BPb), and tandem (BPt) derivatives of BK. As the negative control, BPn was also deposited on a microarray chip. BPn is the BP derivative with opposite charges (negative instead of positive charges). Silicon chips were incubated with EVs extracted using DDI approaches, analyzed, and results are shown in Figure 8.9.

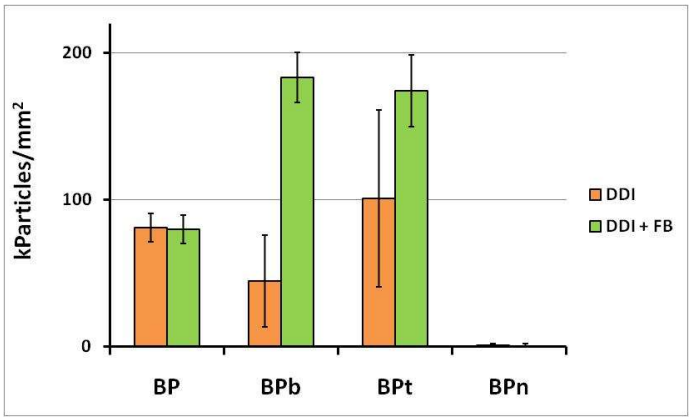

***Figure 8.9**. SP-IRIS analysis of EVs separated from human blood plasma using DDI approach on Eppendorf tube (DDI) and microfluidic fluidized bed platform (DDI + FB).EVs were recaptured on silicon microarray chips functionalized with membrane binding peptides. BPn was used as the negative control.*

No signal was detected on BPn, while high signals were registered on EV-binding peptides, confirming the effective separation of EVs from human blood plasma using DDI based approach. The SP-IRIS experiment also confirmed NTA results since higher signals (corresponding to higher concentration of EVs) were measured on sample recovered combining DDI approach and microfluidic fluidized bed technology.

In conclusion, after this set of experiments the technological advantage provided by the use of microfluidic fluidized bed platform in the separation of extracellular vesicles from biological samples. Despite the potential of this ground-breaking technology, there were still different limitations to overcome. As an example, a total time of almost 6 h (4h 10 min are required for the capture step and 1h 40 min for the release) was required to process 125 µL of plasma, a time definitely too long for clinical settings. Together with the colleagues of Curie Institute we performed an extensive optimization of the working parameters. We used for the optimization the same DNA-directed antiCD63 that was used in Eppendorf tubes. Additionally, it was decided to increase the volume of processed plasma from 125 to 250 µL.

Fine tuning of flow rates of capture and release solutions was carried out. Initially, experiments were performed using a flow rate of 0.5 µL/min for both phases, resulting in an operating time of 6 h. To reduce experimental time the flow rate during capture step was increased to 1.66 µL/min, so that the capture of EVs from 250 µL of plasma could be completed in 2h 30 min, while the flow rate for release was maintained to 0.5 µL/min. In another combination the flow rate for both capture and release was increased to 1.66 µL/min.

The results obtained using different flow rates were analyzed using NTA and TEM and are shown in Figure 8.10.

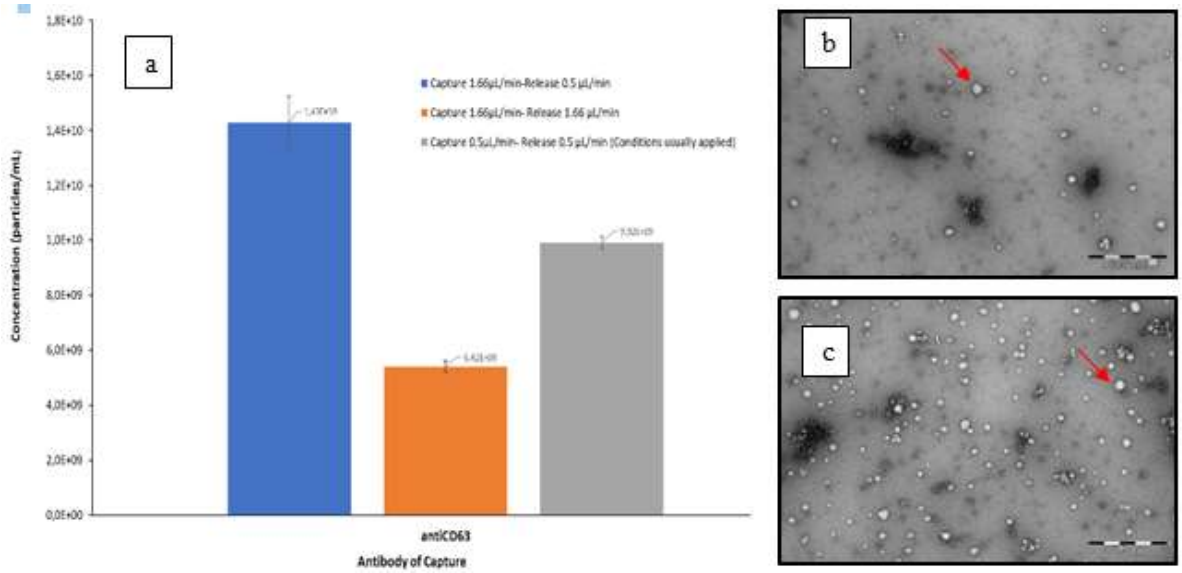

***Figure 8.10**. Effect of flow rate on the concentration of EVs purified from human plasma by using DDI of antiCD63 antibody in combination with microfluidic fluidized bed (a). TEM images of released EVs: b) Capture 0.5 µL/min, Release 0.5 µL/min and c) Capture 1.66 µL/min, Release 0.5 µL/min.*

As shown in Figure 8.10a, increasing only the flow rate during the capture step (blue bar) produces the extraction of a higher number of EVs in comparison with previous experimental conditions (grey bar), probably as a results of the larger amount of plasma processed. Contrarily, increasing the flow rate also in release step (orange bar) negatively affected EVs concentration. This may be due to the insufficient time given to DNase I to catalyze the cleavage of the linker.

EVs separated in optimized conditions (250 µL of plasma processed, 1.66 µL/min for capture, 0.5 µL/min for release) were compared to those obtained with previous experimental conditions by Transmission Electron Microscopy. After optimization, TEM detected a higher number of intact vesicles (Figure 8.10c). The separation experiment using the new parameters required 4h 10 min.

Optimized parameters were also applied in subsequent experiments aimed at providing further characterization of EVs separated using DDI-based approach. Thanks to this optimization of flow rate, it was possible to carry out a Cryo-EM analysis, a high-resolution technique to analyze small structures likes EVs that needs a higher quantity of material. Cryo-EM not only confirmed that small EVs with a perfectly rounded shape were successfully detached from magnetic beads, but also that vesicles were fully surrounded by

an intact lipid bilayer (around 4 nm in thickness). Proteins were detected inside EVs, confirming that they still retained their cargo after the separation (see Figure 8.11).

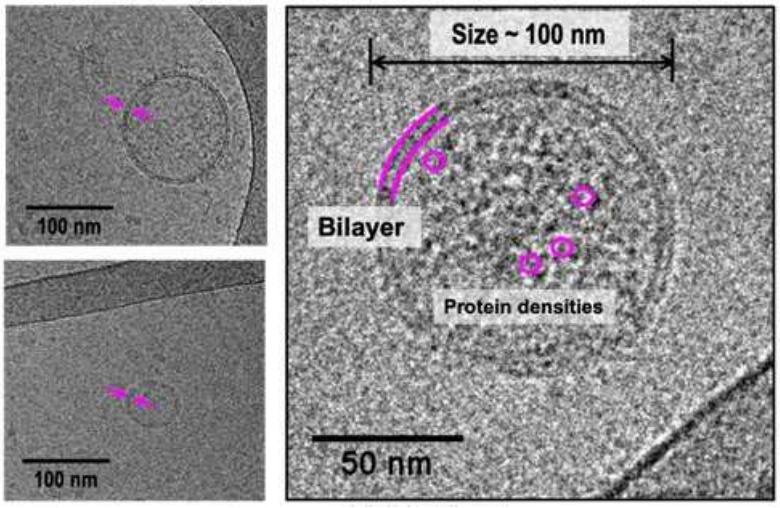

***Figure 8.11**. Cryo-EM images of extracellular vesicles separated from human plasma by using DDI of antiCD63 in combination with microfluidic fluidized bed.*

Complementary to imaging techniques, a novel technique for EVs characterization was applied, namely Capillary Electrophoresis coupled with Laser-Induced Fluorescence (CE-LIF). This technique has been recently developed and allows to detect and characterize EVs based on their electrophoretic mobility[110]. EVs needs to be labeled with fluorescent probes to be detected using this technique. They were stained using CFSE (already described in Section 2 for Nanoscale Flow Cytometry experiment) and analyzed. The results shown in Figure 8.12 confirmed the presence of intact nanoparticles since three peaks were observed (corresponding to three different CD63+ EV subpopulations). Contrarily the presence of EV-derived fragments would have been identified by the presence of spikes in the electropherogram.

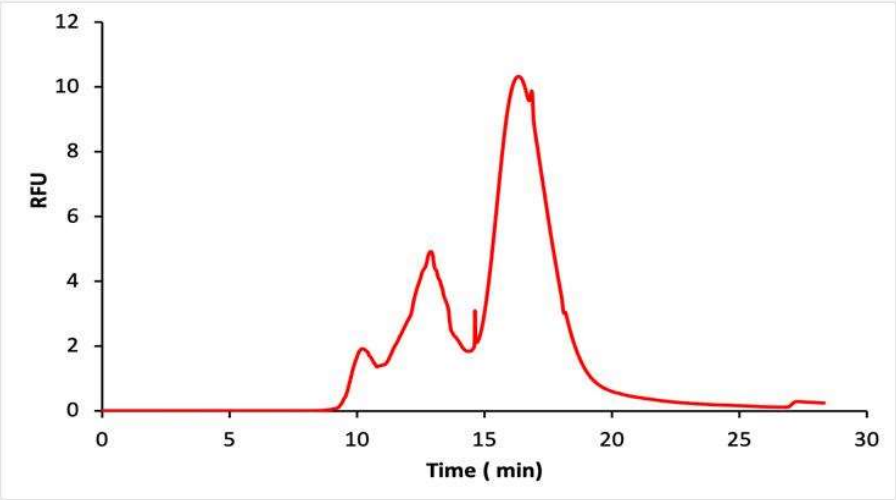

***Figure 8.12**. CE-LIF electropherogram of fluorescently-labeled EVs separated from human plasma by using DDI of antiCD63 antibody in combination with microfluidic fluidized bed. Three peaks, corresponding to three subpopulations of CD63+ EVs, were detected.*

To further shorten the analysis time, a new combination of flow rates was tested, namely 3.4 µL/min for capture step and 1.0 µL/min for release, and the performance compared with that obtained with previously optimized combination (1.66 µL/min for capture, 0.5 µL/min for release).

The separation experiments were repeated with three different sets of beads, each functionalized with a different antibody immobilized via DDI. The three antibodies were antiCD63, antiCD9 and rabbit IgG (used as the negative control). We performed magnetic separations of EVs from human blood plasma on the microfluidic fluidized bed using both the flow rate combinations described in the previous paragraph. The sample solutions recovered from the chips were analyzed by NTA (see Figure 8.13a). NTA data show that EVs concentration using the two different combinations of flow rates are the same. Even though the increased flow rates did not provide a further increase in EVs concentrations (under optimized conditions this parameter is probably limited by the saturation level of beads) it still represented an analytical advantage since the separation could be performed in a shorter time (about 2 h) without losing separation efficiency. Additionally this experiment further demonstrated the selectivity of the DDI-based separation protocol, since only negligible signals were detected for the negative control (data confirmed by sample protein concentration, see Figure 8.13c).

CE-LIF also confirmed the presence of three different subpopulations both in CD9+ and CD63+ vesicles. Three peaks were registered also for the negative control and may be due to EVs non-specifically captured on rabbit IgG. However, the intensity of the peaks for rabbit

IgG in sensibly lower than that registered for samples separated using DDI antiCD9 and antiCD63 (Figure 8.13b).

a)

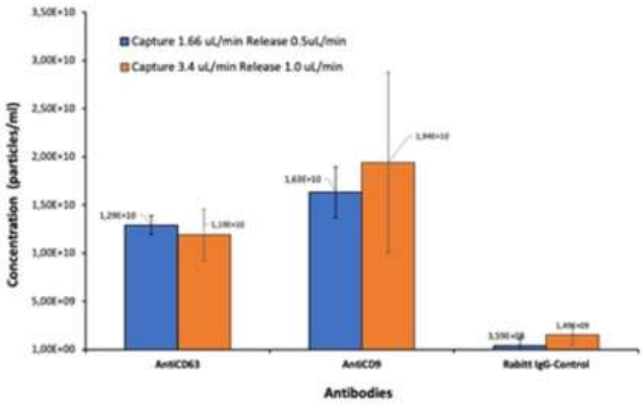

b)

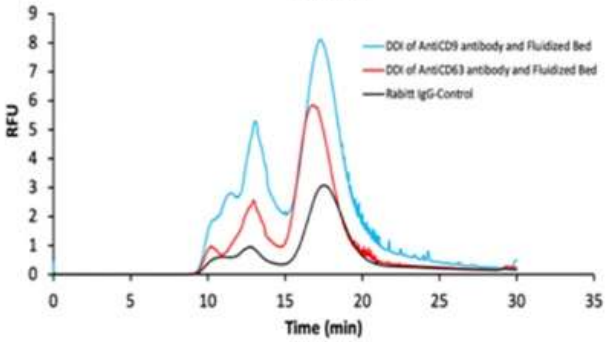

c)

Antibody	Protein Concentration (µg/mL)
antiCD63	155
antiCD9	187
rabbit IgG	16

***Figure 8.13**. Effect of flow rate on the concentration of EVs, measured by Nanoparticle Tracking Analysis (a). CE-LIF electropherograms of fluorescently-labeled EVs separated from human blood plasma using DDI antiCD63, antiCD9 or rabbit IgG (b). Protein concentration EVs-containing samples obtained from human blood plasma using DDI antiCD63, antiCD9 or rabbit IgG (c).*

The separation of intact EVs from complex biological fluids was demonstrated using optimized flow rates (3.4 µL/min for capture and 1.0 µL/min for release) and plasma volumes of 250 µL. These conditions were used in the clinical validation phase.

3.2 Development of detection module

The detection module was developed by the group of Prof. Selim Unlu at Boston University. It exploits the SP-IRIS technique and is easily integrable with the separation module. The SP-IRIS technology works by enhancing the visibility of biological nanoparticles through interferometry. Under this condition, the contrast of the particles with respect to their background depends on their refractive index and their size. Thus knowing or assuming the refractive index of the material that composes the particles it is possible to precisely quantify their size.

The final design of the EVs detection prototype is depicted in Figure 8.14. In particular a horizontal setup was chosen, with the purpose of increasing the stability of the instrument and reduce the propagation of vibration which can be detrimental and act as a source of noise while imaging EVs.

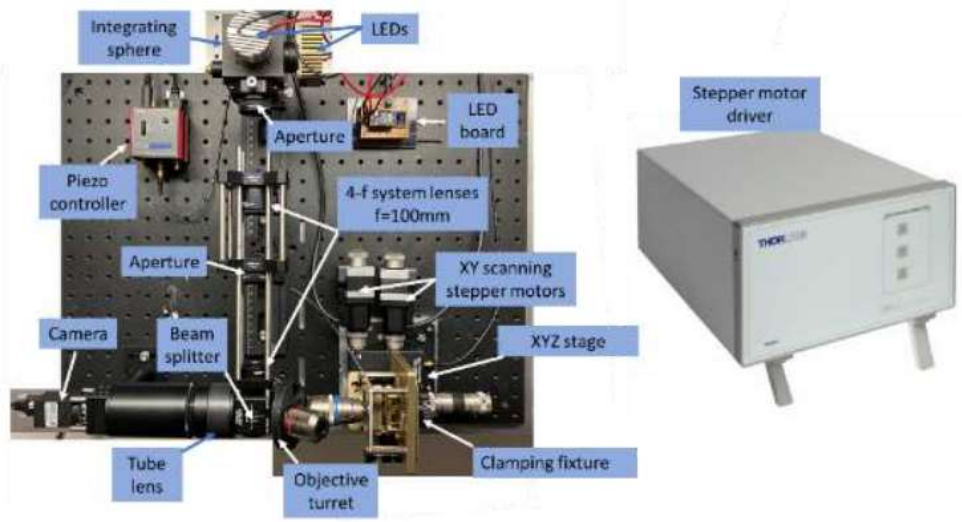

Figure 8.14. *Final design of nanoparticles detection prototype based on SP-IRIS technique.*

Two high-power single color blue light emitting diodes (LEDs) with a wavelength of 457 nm were chosen for illumination and mounted on an integrating sphere to generate a uniform output beam. The aperture is set and imaged in order to enhance the visibility of biological nanoparticles. Two microscope objectives (5X and 60X) are mounted on a revolving turret that allows to easily switch between the objectives. This feature is particularly important to navigate on the recapture microarray chip. In fact, using 5X objective (that possesses a 12-fold larger field of view) different spots can be easily found. Once the spot of interest is placed in the center of the field of view, it is possible to increase its magnification just by

swinging the revolving turret to 60X objective position. Images are captured by a 7.1 MP monocolor CMOS camera with a global shutter.

A chip cartridge is placed in the chip fixture that is connected with fluidic system. The cartridge is composed by a sensor chip with inlet and outlet holes for fluidics, and a flow channel is formed by attaching a cover glass (0.7 mm in thickness) to the sensor using a patterned silicone spacer layer in between (50 µm in thickness). Cartridge design is shown in Figure 8.15.

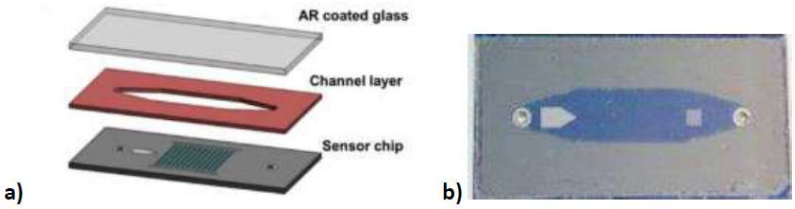

***Figure 8.15**. Sensor chip/cartridge assembly. a) CAD scheme and b) a picture of the assembled cartridge.*

The chip fixture is mounted on a XYZ Nanomax stage that provides a 4 mm travel range in all three directions to provide easy access to the different locations on the chip surface. Two stepper motors are used for scanning in XY axis and are controlled through the stepper motor driver. The movement along the Z axis is controlled through a manual actuator for coarse focusing and a piezoelectric controller for fine adjustment (20 µm travel range).

The movement of the stages and camera acquisition are controlled by a custom-made software. A python code integrates the functionalities of all the single elements that compose the prototype and provides an intuitive user interface allowing for easy control of the instrument.

In order to assess the sensor performance in terms of counting and sizing nanoparticles, the instrument was calibrated choosing polystyrene beads of 100 nm in diameter to define the analysis parameters which would then be used for the extracellular vesicles measurements. Polystyrene beads were spin-coated on top of an IRIS chip that was previously treated with oxygen plasma. Then, images of immobilized beads were acquired on the IRIS setup and system parameters (e.g. the optimal size of the background ring to be selected around the particle to provide accurate contrast measurement) were selected

Polystyrene beads have a much higher refractive index (RI = 1.6) than EVs. Due to their heterogeneous composition, EVs do not possess a well-defined refractive INDEX, but a range of values varying between 1.37 and 1.39 [111]. The upper limit RI = 1.39 was assumed for further experiments.

EVs were purified from human blood plasma through size exclusion chromatography using IZON qEV 70 nm column. Fraction F7 was used to incubate microarray chips (functionalized with antiCD81 antibody spots) inside the microfluidic chamber, mimicking a real integrated experiment. After incubation, chips were washed with PBS and dried by flowing nitrogen. Images of single spots on the chip were acquired before and after the incubation with EVs and the system proved to be effective in counting and sizing EVs.

3.3 Clinical validation

The separation and detection modules were clinically validated in the liquid biopsy of lung cancer patients. Our role in this task was to synthesize the chemicals used in the sensing platform, including: DNA-tagged antibodies and polymers for coating the surface. For EVs phenotyping silicon microarray chips were used. We used custom polymers to prepare coated chips spotted with the oligonucleotides complementary to the DNA tags. Separation of EVs from plasma samples was carried out at Institute Curie and in Aalborg University Hospital. Samples containing EVs were collected and sent to Boston University for their analysis using the SP-IRIS device. Finally, data collected in Boston were sent to Aalborg University Hospital for statistical analysis.

3.3.1 EVs separation from human blood plasma

The plasma of patients with lung cancer was collected with EDTA as anticoagulant. After centrifugation at 1800g for 6 min, the isolated plasma was aliquoted and stored at – 80 °C. For this demonstration 12 samples from patients with adenocarcinoma stage IV was selected together with 14 samples from healthy controls. The separation of EVs from plasma samples was carried out in two modalities. Half of the samples were separated at Curie Institute using the automated microfluidic platform and the optimized protocol (250 µL of plasma, capture flow rate = 3.4 µL/min, release flow rate 1.0 µL/min). The remaining samples were separated using a conventional tube experiment in Aalborg University Hospital following the procedure developed by CNR in Milan. EVs-containing samples were stored at 4°C soon after separation and shipped within 2 days to Boston, always keeping a temperature of 4°C.

3.3.2 EVs characterization using SP-IRIS device

3.3.2.1 EVs' antigen selection for microarray fabrication: A set of 6 antibodies was chosen to provide phenotyping of EVs:

- CD9: is a member of tetraspanin 4 superfamily that organize membrane microdomains by forming clusters and interacting with a large variety of transmembrane and cytosolic signaling proteins. EVs are highly enriched in tetraspanins and CD9 have a broad tissue distribution[112].
  The CD9 was chosen to be implemented in the validation as the only general EV marker.
- EpCAM: Epithelial Cell Adhesion Molecule is a transmembrane glycoprotein that mediates cell-cell adhesion in epithelia. It is also involved in cell signaling, migration, proliferation and differentiation. EpCAM possesses an oncogenic potential and can be used as diagnostic marker for various cancer. It has been demonstrated that epithelial tumor cells secrete EpCAM-presenting EVs[113].
- EGFR: Epidermal Growth Factor Receptor is a transmembrane receptor tyrosine kinase protein. Its overexpression or mutation has been reported to be implicated in the pathogenesis of many human malignancies and has been associated to various lung cancers including Non-Small Cells Lung Cancer (NSCLC)[114].
- CD151: a surface glycoprotein that plays a role in the regulation of cell development, growth and motility. In cancer cells it promotes cell motility, invasion and metastasis, as well as neo-angiogenesis[115].
- Tspan8: is a member of the tetraspanin family that is overexpressed in tumor tissues where it induces angiogenesis. Its expression correlates with higher tumor grade. Different studies have highlighted Tspan8 as a potential biomarker in various types of lung cancer[116].

3.3.2.2 Microarray chips fabrication: Silicon chips were pre-treated with oxygen plasma for 15 min: the oxygen pressure was set to 1.2 bars with a power of 29.6 W. To coat the chips, MCP-2 copolymer was dissolved in DI water to a final concentration of 2% w/v and then diluted 1:1 with a solution of ammonium sulphate 1.6 M. The chips were immersed into each solution for 30 min, then rinsed with bidistilled water, dried, and finally cured at 80 °C for 15 min.

Antibodies, dissolved at 2 mg/mL concentration in PBS containing 50 mM trehalose, were spotted in triplicate on the chips using a noncontact microarray spotter (sciFLEXARRAYER S12, Scienion, Berlin) equipped with an 80 µm nozzle.

Four hundred pL drops of spotting solution were deposited at room temperature and 65% humidity. Immediately after spotting, the chips were stored overnight in a sealed chamber

filled at the bottom with sodium chloride saturated water (40 g/100 mL H_2O). After incubation, the chips were treated with a blocking solution of ethanolamine (50 mM in 0.1 M Tris/HCl buffer pH 9) at room temperature for 1 h. Then chips were rinsed with bidistilled water and dried.

Following this protocol, chips were functionalized with 5 antibodies directed against EVs' antigens described in Section 3.3.4.1 plus polyclonal rabbit IgG as the negative control. Each antibody was printed on the chip in triplicate, and the distance between each antibody spot was set to 300 µm.

3.3.2.3 SP-IRIS detection of extracellular vesicles: Microarray chips, prepared as described in Section 3.3.4.2, were mounted into the microfluidic chamber of the optical device and incubated with EV-containing samples obtained as described in Section 3.3.2. Incubation was carried out with 5X-diluted samples (dilution with PBS) for 2 h at a flow rate of 2 µL/min. After incubation, chips were briefly rinsed with bidistilled water and gently dried using a nitrogen stream. Antibody spots were imaged on the SP-IRIS system before and after incubation with the samples. Images were then analyzed to digitally count and size individual nanovesicles captured on antibody spots using of a custom MATLAB dedicated software.

3.3.3 Data analysis

Data analysis was performed using Excel 365 (Microsoft), GraphPad Prism 8 (GraphPad Software, LLD), and the R-based software MetaboAnalyst 5.0. ROC curves were elaborated. The ROC curve is a fundamental tool for diagnostic test evaluation. It provides a complete and easily visualized sensitivity/specificity report visualization. In a ROC curve, the true positive rate (sensitivity) is plotted in function of the false positive rate (specificity) for different cut-off points of a given parameter. Each point on the ROC curve represents a sensitivity/specificity pair corresponding to a particular decision threshold. A test with perfect discrimination (no overlap in the two distributions) has a ROC curve that passes through the upper left corner (100% sensitivity, 100% specificity). Therefore the closer the ROC curve is to the upper left corner, the higher the overall test's accuracy. The closer the ROC curve to the diagonal line, the poorer the diagnostic power of the test. The area under the ROC curve measures of how well a parameter can distinguish between two diagnostic groups, in this case, healthy donors and lung cancer patients.

3.3.4 Results & Discussion

EVs separated from the plasma of 26 patients (14 healthy donors and 12 lung cancer patients) were analyzed in the detection module using the SP-IRIS setup. Each sample was used to incubate a single microarray chip, and results in terms of particles counted on the surface of antibody spots were measured before and after the incubation. A non-parametric t-test was run, revealing a significant difference ($p<0.0001$) between particles counted before and after the incubation.

We tested the diagnostic potential of the INDEX system to distinguish samples from healthy individuals and from lung cancer patients. The average of post-incubation counts subtracted from pre-incubation counts was used to measure the number of particles bound to antibody spots during the incubation. Firstly single markers were analyzed, but non-parametric t-test revealed no significant differences between the two groups.

The Calculation was repeated, normalizing data to CD9 counts for each individual (chosen as a parameter to describe to a total concentration of EVs in the sample, which may vary in different individuals), but it gave the same result.

Then, ratios between two markers were considered, as they may carry more information than the two corresponding markers alone. A log transformation of the data set was performed in order to include the internal ratios of the 5 markers. Using ratios in the diagnostic calculation revealed a more significant potential than using single markers. A statistically significant result was obtained with the ratio between counts on EpCAM and EGFR spots (see Figure 8.16). Generating the ROC curve and setting a cut-off value of 0.763, an AUC of 0.806 was found, and the test demonstrated a specificity of 0.82 (CI 0.54-1.0) and sensitivity of 0.80 (CI 0.6-0.93). Ratios between the two groups (healthy and lung cancer patients) were found to be significantly different ($p = 0.012$).

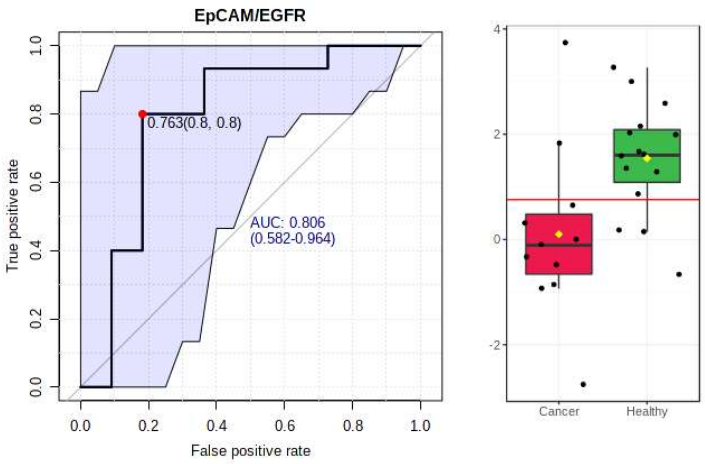

Figure 8.16. Receiver Operating Curve (ROC) obtained with the ratio between EVs counts on EpCAM and EGFR spots. An area under curve (AUC) of 0.806 was obtained and the counts between the groups were found to be significantly different (p-value 0.012).

These results demonstrated an actual diagnostic potential of the INDEX setup for liquid biopsy of lung cancer.

Encouraged by this relevant finding, a multivariate analysis including all markers was performed. ROC curves were generated by Monte-Carlo cross-validation (MCCV) using balanced sub-sampling. In each MCCV, two thirds (2/3) of the samples are used to evaluate the feature importance. The top 2, 3, 5, 10 important features are then used to build classification models which are validated on the 1/3 the samples that were left out. The procedure was repeated multiple times to calculate the performance and confidence interval of each model.

The multivariate validations were performed using the three models: Support Vector Machines (SVM), Partial least squared regression (PLS) and RandomForest. The best result (AUC = 0.762) were obtained using SVM and the three markers EGFR, EpCAM and CD151 (Figure 8.17). The confusion matrix obtained from cross-validation gives the power of the diagnostic tool, which showed a sensitivity of 0.81 and a specificity of 0.6.

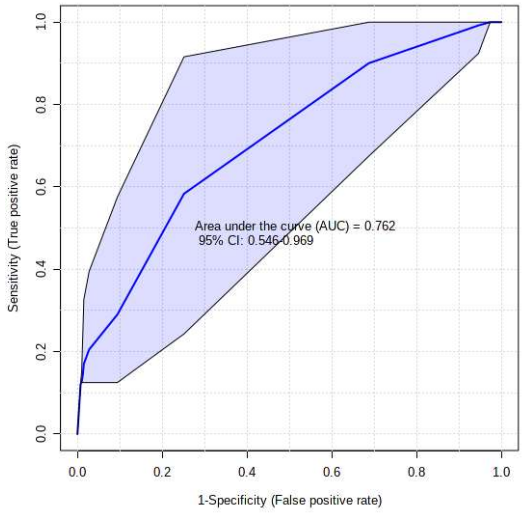

Confusion Matrix
(Cross-Validation)

	0	1
0	9	5
1	2	10

***Figure 8.17**. ROC obtained with the three markers EGFR, EpCAM and CD151. AUC of 0.762 (CI 0.546-0.969). The confusion matrix from the cross-validation shows the outcome of the samples.*

CONCLUSIONS

Despite the existence of extracellular vesicles was demonstrated in 1967, their importance in biological systems has been clarified only recently. The small size and heterogeneity of EVs hamper the analysis of their biological role and obstacle their potential application in diagnostics.

To facilitate the translation of EVs from research to clinics, an effective separation strategy that allows their enrichment with good yield and purity, is of primary importance. To date, most separation strategies rely on physical properties of extracellular vesicles and often result in samples contaminated by lipoproteins, soluble proteins, and protein aggregates. Additionally, these techniques are not able to discriminate different EV subpopulations.

A promising alternative is the separation of EVs through immuno-affinity precipitation. Using this strategy, EVs are captured by specific antibodies immobilized on solid surfaces. Immuno-affinity precipitation offers unmatched results in terms of purity and selectivity, but unfortunately, its application is still limited. In fact, releasing EVs from an antibody requires harsh conditions that damage them and impair downstream analysis.

To overcome this limitation, a different approach for immuno-affinity separation has been proposed within this Ph.D. project. Different strategies for reversible antibody immobilization have been developed.

The first strategy was *DNA-directed immobilization* (DDI), an approach where antibodies are anchored on the sensor's surface through a dsDNA linker.

This linker improves the exposure, and reduces steric hindrance surrounding the antibody, thus enhancing EV binding capacity. By exploiting this feature, we provided an optimized protocol to fabricate antibody microarray platforms for detecting EVs, based on DDI. This approach exploits the peculiar advantages of DNA microarrays (ease of fabrication, lower costs, and more extended stability), providing a microarray substrate that can be turned into a customized antibody microarray. The analytical performance of antibodies immobilized by DDI is similar to, or even better than that of covalently immobilized antibodies.

In addition, the dsDNA linker can be cleaved by exploiting the catalytic activity of DNase I. DDI and DNase I-mediated release used in combination on magnetic beads, allowed the reversible immobilization of antibodies directed against EVs' marker CD63, and provided effective immuno-affinity separation of intact EVs from human plasma.

A second approach, called *aptamer-mediated immobilization*, foresees the use of StrepApt5, a streptavidin-binding aptamer able to capture streptavidin. Steptavidin, anchored to the aptamer, maintains its ability to bind biomolecules labeled with biotin. Finally, streptavidin and biotinylated antibodies were released from the solid surface upon incubation with a sequence of DNA complementary to StrepApt5. Microarray tests revealed that antiCD9 immobilized through the aptamer captures EVs with improved efficiency compared to the same antibody immobilized covalently.

We then transferred the protocol to magnetic particles to separate EVs from complex media. To this purpose, we developed a novel approach for particle functionalization. Silica microbeads were coated with a copolymer that exposes azido groups. DBCO-labeled StrepApt5, immobilized on the surface of microbeads, captured streptavidin first, and then biotinylated antibodies. Finally, silica microbeads functionalized with antiCD9 through aptamer-mediated immobilization were used to separate EVs from human blood plasma.

The work of this thesis was part of the European FET-OPEN project INDEX, aimed at developing an integrated platform for the in-line separation and characterization of EVs. The INDEX prototype is composed by two distinct modules: a microfluidic separation device, based on microfluidic fluidized bed technology, and a detection module that exploits Single Particle Interferometric Reflectance Imaging Sensor (SP-IRIS) technology. In the workflow, EVs are separated by immuno-affinity precipitation in the microfluidic module and detected by SP-IRIS instrument.

The key point to enable the integration of the two modules was the choice of an appropriate strategy for the reversible capture of EVs. To this purpose, we used DNA-directed immobilization of antibodies in combination with DNAse I-mediated enzymatic release.

The two modules were optimized, and technical validation proved that the integration could be successfully achieved. Clinical validation for the liquid biopsy of lung cancer was also performed: plasma samples of healthy individuals and lung cancer patients were collected, and EVs were separated using DDI-based approach. EVs were then captured on a microarray surface, and detected by the SP-IRIS instrument.

INDEX prototype was able to discriminate between healthy individuals and lung cancer patients with good specificity and sensitivity, proving that its use could be ground-breaking in the EV-related diagnostic field.

CREDITS

This work was supported by European Union Horizon 2020 under Grant 766466: INDEX, Integrated Nanoparticle isolation and Detection system for complete on-chip analysis of Exosomes.

I thank all INDEX partners for the great collaboration and support that led to successful outcomes. A special thank goes to Dr. Diogo Fortunato and Dr. Mattia Criscuoli (Exosomics Siena), for the support with nanoFCM experiments.

I am also grateful to Dr. Riccardo Vago (Urological Research Institute, Division of Experimental Oncology, IRCCS San Raffaele Scientific Institute, Milan, Italy) for providing HEK-derived EV samples.

I want to thank Prof. Daniela Maggioni and Dr. Marco Minneci (University of Milan) who performed Zeta-Potential measurements.

REFERENCES

1. Doyle, L. M. & Wang, M. Z. Overview of Extracellular Vesicles, Their Origin, Composition, Purpose, and Methods for Exosome Isolation and Analysis. *Cells* **8**, 727 (2019).
2. van Niel, G. & Raposo, G. Shedding light on the cell biology of extracellular vesicles. *Nat. Publ. Gr.* **19**, (2018).
3. Théry, C. *et al.* Journal of Extracellular Vesicles Minimal information for studies of extracellular vesicles 2018 (MISEV2018): a position statement of the International Society for Extracellular Vesicles and update of the MISEV2014 guidelines.
4. Wolf, P. The Nature and Significance of Platelet Products in Human Plasma. *Br. J. Haematol.* **13**, 269–288 (1967).
5. Jaiswal, R. & Sedger, L. M. Intercellular Vesicular Transfer by Exosomes, Microparticles and Oncosomes - Implications for Cancer Biology and Treatments. *Front. Oncol.* **0**, 125 (2019).
6. Zaborowski, M. P., Balaj, L., Breakefield, X. O. & Lai, C. P. Extracellular Vesicles: Composition, Biological Relevance, and Methods of Study. *Bioscience* **65**, (2015).
7. Borges, F. T., Reis, L. A. & Schor, N. Extracellular vesicles: structure, function, and potential clinical uses in renal diseases. *Brazilian J. Med. Biol. Res.* **46**, 824–830 (2013).
8. Bobrie, A., Colombo, M., Raposo, G. & Théry, C. Exosome Secretion: Molecular Mechanisms and Roles in Immune Responses. *Traffic* **12**, 1659–1668 (2011).
9. Palmisano, G. *et al.* Characterization of Membrane-shed Microvesicles from Cytokine-stimulated β-Cells Using Proteomics Strategies. *Mol. Cell. Proteomics* **11**, 230 (2012).
10. Di Vizio, D. *et al.* Large Oncosomes in Human Prostate Cancer Tissues and in the Circulation of Mice with Metastatic Disease. *Am. J. Pathol.* **181**, 1573–1584 (2012).
11. Cohen, J. D. *et al.* Detection and localization of surgically resectable cancers with a multi-analyte blood test. *Science* **359**, 926 (2018).
12. Palmirotta, R. *et al.* Liquid biopsy of cancer: a multimodal diagnostic tool in clinical oncology: *https://doi.org/10.1177/1758835918794630* **10**, (2018).
13. Gold, B., Cankovic, M., Furtado, L. V., Meier, F. & Gocke, C. D. Do Circulating

Tumor Cells, Exosomes, and Circulating Tumor Nucleic Acids Have Clinical Utility?: A Report of the Association for Molecular Pathology. *J. Mol. Diagnostics* **17**, 209–224 (2015).

14. Huang, X. *et al.* Characterization of human plasma-derived exosomal RNAs by deep sequencing. *BMC Genomics 2013 141* **14**, 1–14 (2013).
15. Bergsmedh, A. *et al.* Horizontal transfer of oncogenes by uptake of apoptotic bodies. *Proc. Natl. Acad. Sci.* **98**, 6407–6411 (2001).
16. Valenti, R. *et al.* Human Tumor-Released Microvesicles Promote the Differentiation of Myeloid Cells with Transforming Growth Factor-β–Mediated Suppressive Activity on T Lymphocytes. *Cancer Res.* **66**, 9290–9298 (2006).
17. Ciravolo, V. *et al.* Potential role of HER2-overexpressing exosomes in countering trastuzumab-based therapy. *J. Cell. Physiol.* **227**, 658–667 (2012).
18. Taylor, D. D. & Gercel-Taylor, C. MicroRNA signatures of tumor-derived exosomes as diagnostic biomarkers of ovarian cancer. *Gynecol. Oncol.* **110**, 13–21 (2008).
19. Y, M. *et al.* Quantification of plasma exosome is a potential prognostic marker for esophageal squamous cell carcinoma. *Oncol. Rep.* **36**, 2535–2543 (2016).
20. Liu, Q. *et al.* Plasma exosome levels in non-small-cell lung cancer: Correlation with clinicopathological features and prognostic implications. *Cancer Biomarkers* **22**, 267–274 (2018).
21. Shen, M. *et al.* Progress in exosome associated tumor markers and their detection methods. *Mol. Biomed. 2020 11* **1**, 1–25 (2020).
22. Skotland, T. *et al.* Molecular lipid species in urinary exosomes as potential prostate cancer biomarkers. *Eur. J. Cancer* **70**, 122–132 (2017).
23. Zhou, W. *et al.* Cancer-Secreted miR-105 Destroys Vascular Endothelial Barriers to Promote Metastasis. *Cancer Cell* **25**, 501–515 (2014).
24. KR, J. *et al.* Exosomal proteins as potential diagnostic markers in advanced non-small cell lung carcinoma. *J. Extracell. Vesicles* **4**, 26659–26659 (2015).
25. H, F. *et al.* Exosomal TRIM3 is a novel marker and therapy target for gastric cancer. *J. Exp. Clin. Cancer Res.* **37**, 162–162 (2018).
26. SM, van D. *et al.* Cetuximab treatment alters the content of extracellular vesicles released from tumor cells. *Nanomedicine (Lond).* **11**, 881–890 (2016).
27. Liangsupree, T., Multia, E. & Riekkola, M. L. Modern isolation and separation techniques for extracellular vesicles. *J. Chromatogr. A* **1636**, 461773 (2021).
28. Konoshenko, M. Y., Lekchnov, E. A., Vlassov, A. V. & Laktionov, P. P. Isolation of

Extracellular Vesicles: General Methodologies and Latest Trends. *Biomed Res. Int.* **2018**, (2018).

29. Pariset, E., Agache, V. & Millet, A. Extracellular Vesicles: Isolation Methods. *Adv. Biosyst.* **1**, 1700040 (2017).
30. Cheruvanky, A. *et al.* Rapid isolation of urinary exosomal biomarkers using a nanomembrane ultrafiltration concentrator. *Am J Physiol Ren. Physiol* **292**, 1657–1661 (2007).
31. Musante, L. *et al.* A Simplified Method to Recover Urinary Vesicles for Clinical Applications and Sample Banking. *Sci. Reports 2014 41* **4**, 1–11 (2014).
32. Taylor, D. D. & Shah, S. Methods of isolating extracellular vesicles impact down-stream analyses of their cargoes. *Methods* **87**, 3–10 (2015).
33. Askeland, A. *et al.* Mass-Spectrometry Based Proteome Comparison of Extracellular Vesicle Isolation Methods: Comparison of ME-kit, Size-Exclusion Chromatography, and High-Speed Centrifugation. *Biomed. 2020, Vol. 8, Page 246* **8**, 246 (2020).
34. Van Deun, J. *et al.* The impact of disparate isolation methods for extracellular vesicles on downstream RNA profiling. *J. Extracell. Vesicles* **3**, (2014).
35. Deregibus, M. C. *et al.* Charge-based precipitation of extracellular vesicles. *Int. J. Mol. Med.* **38**, 1359–1366 (2016).
36. Brownlee, Z., Lynn, K. D., Thorpe, P. E. & Schroit, A. J. A novel “salting-out” procedure for the isolation of tumor-derived exosomes. *J. Immunol. Methods* **407**, 120–126 (2014).
37. Notarangelo, M. *et al.* Ultrasensitive detection of cancer biomarkers by nickel-based isolation of polydisperse extracellular vesicles from blood. *EBioMedicine* **43**, 114–126 (2019).
38. Lakhin, A. V., Tarantul, V. Z. & Gening, L. V. Aptamers: Problems, solutions and prospects. *Acta Naturae* vol. 5 34–43 (2013).
39. Zhang, K. *et al.* Rapid Capture and Nondestructive Release of Extracellular Vesicles Using Aptamer-Based Magnetic Isolation. *ACS Sensors* **4**, 1245–1251 (2019).
40. Ghosh, A. *et al.* Rapid Isolation of Extracellular Vesicles from Cell Culture and Biological Fluids Using a Synthetic Peptide with Specific Affinity for Heat Shock Proteins. *PLoS One* **9**, e110443 (2014).
41. Shao, H. *et al.* Protein typing of circulating microvesicles allows real-time monitoring of glioblastoma therapy. *Nat. Med. 2012 1812* **18**, 1835–1840 (2012).
42. He, M., Crow, J., Roth, M., Zeng, Y. & Godwin, A. K. Integrated immunoisolation and

protein analysis of circulating exosomes using microfluidic technology. *Lab Chip* **14**, 3773–3780 (2014).

43. J, P. *et al.* Integrated Kidney Exosome Analysis for the Detection of Kidney Transplant Rejection. *ACS Nano* **11**, 11041–11046 (2017).
44. Dudani, J. S. *et al.* Rapid inertial solution exchange for enrichment and flow cytometric detection of microvesicles. *Biomicrofluidics* **9**, (2015).
45. Sitar, S. *et al.* Size Characterization and Quantification of Exosomes by Asymmetrical-Flow Field-Flow Fractionation. *Anal. Chem.* **87**, 9225–9233 (2015).
46. Wunsch, B. H. *et al.* Nanoscale lateral displacement arrays for the separation of exosomes and colloids down to 20nm. *Nat. Nanotechnol.* **11**, 936–940 (2016).
47. Lee, K., Shao, H., Weissleder, R. & Lee, H. Acoustic Purification of Extracellular Microvesicles. *ACS Nano* **9**, 2321–2327 (2015).
48. Zhao, Z., Wijerathne, H., Godwin, A. K. & Soper, S. A. Isolation and analysis methods of extracellular vesicles (EVs). *Extracell. Vesicles Circ. Nucleic Acids* **2**, 80–103 (2021).
49. Patton, M. C., Zubair, H., Khan, M. A., Singh, S. & Singh, A. P. Hypoxia alters the release and size distribution of extracellular vesicles in pancreatic cancer cells to support their adaptive survival. *J. Cell. Biochem.* **121**, 828–839 (2020).
50. Szatanek, R. *et al.* The Methods of Choice for Extracellular Vesicles (EVs) Characterization. *Int. J. Mol. Sci. 2017, Vol. 18, Page 1153* **18**, 1153 (2017).
51. NanoFCM. https://www.nanofcm.com/.
52. Ridolfi, A. *et al.* AFM-Based High-Throughput Nanomechanical Screening of Single Extracellular Vesicles. *Anal. Chem.* **92**, 10274–10282 (2020).
53. S, Y. *et al.* Quantitative Nanomechanical Analysis of Small Extracellular Vesicles for Tumor Malignancy Indication. *Adv. Sci. (Weinheim, Baden-Wurttemberg, Ger.* 2100825 (2021) doi:10.1002/ADVS.202100825.
54. Daaboul, G. G. *et al.* Digital Detection of Exosomes by Interferometric Imaging. *Sci. Rep.* **6**, 1–10 (2016).
55. Melo, S. A. *et al.* Glypican-1 identifies cancer exosomes and detects early pancreatic cancer. *Nat. 2015 5237559* **523**, 177–182 (2015).
56. Xiao, D. *et al.* Identifying mRNA, MicroRNA and Protein Profiles of Melanoma Exosomes. *PLoS One* **7**, e46874 (2012).
57. Lee, J. H., Kim, J. A., Jeong, S. & Rhee, W. J. Simultaneous and multiplexed detection of exosome microRNAs using molecular beacons. *Biosens. Bioelectron.*

86, 202–210 (2016).

58. Niemeyer, C. M. et al. Oligonucleotide-Directed Self-Assembly Of Proteins: Semisynthetic DNA-Streptavidin Hybrid Molecules As Connectors For The Generation Of Macroscopic Arrays And The Construction Of Supramolecular Bioconjugates. *Nucleic Acids Res.* 22, 5530–5539 (1994).
59. Meyer, R., Giselbrecht, S., Rapp, B. E., Hirtz, M. & Niemeyer, C. M. Advances In DNA-Directed Immobilization. *Current Opinion in Chemical Biology* vol. 18 8–15 (2014).
60. Wacker, R., Niemeyer, C. M. DDI-µFIA-A Readily Configurable Microarray-Fluorescence Immunoassay Based on DNA-Directed Immobilization of Proteins. *ChemBioChem* **5**, 453–459 (2004).
61. Seymour, E. *et al.* DNA-Directed Antibody Immobilization for Enhanced Detection of Single Viral Pathogens. *Anal. Chem.* **87**, 10505–10512 (2015).
62. Nicholas J. Agard, Jennifer A. Prescher, and Bertozzi, C. R. A Strain-Promoted [3 + 2] Azide−Alkyne Cycloaddition for Covalent Modification of Biomolecules in Living Systems. *J. Am. Chem. Soc.* **126**, 46, 15046–15047 (2004).
63. Pirri, G. *et al*. Characterization of A Polymeric Adsorbed Coating for DNA Microarray Glass Slides. *Anal. Chem.* **76**, 5, 1352–1358 (2004).
64. Albisetti, E. *et al.* Conditions for efficient on-chip magnetic bead detection via magnetoresistive sensors. *Biosens. Bioelectron.* **47**, 213–217 (2013).
65. Needham, J. W., Ünlü, N. L., Yurdakul, C. & Ünlü, M. S. Interferometric Reflectance Imaging Sensor (IRIS) for Molecular Kinetics with a Low-Cost, Disposable Fluidic Cartridge. in *Methods in molecular biology* **2027**, 15–28 (2019).
66. Daaboul, G. G. *et al.* LED-based Interferometric Reflectance Imaging Sensor for quantitative dynamic monitoring of biomolecular interactions. *Biosens. Bioelectron.* **26**, 2221–2227 (2011).
67. Sevenler, D. & Selim Ünlü, M. Numerical techniques for high-throughput reflectance interference biosensing. *J. Mod. Opt.* **63**, 1115–1120 (2016).
68. Daaboul, G. G. *et al.* Digital Sensing and Sizing of Vesicular Stomatitis Virus Pseudotypes in Complex Media: A Model for Ebola and Marburg Detection. *ACS Nano* **8**, 6047–6055 (2014).
69. Zilio, C., Sola, L., Damin, F., Faggioni, L. & Chiari, M. Universal hydrophilic coating of thermoplastic polymers currently used in microfluidics. *Biomed. Microdevices* **16**, 107–114 (2014).

70. Dennler, P., Fischer, E. & Schibli, R. Antibody Conjugates: From Heterogeneous Populations to Defined Reagents. *Antibodies* **4**, 197–224 (2015).
71. Ekins, R. P. *Multi-analyte immunoassay*. *Journal of Pharmaceutical & Biomedical Analysis* **7**, 2, 155–168 (1989).
72. Gygi, S. P., Rochon, Y., Franza, B. R. & Aebersold, R. Correlation between Protein and mRNA Abundance in Yeast. *Mol. Cell. Biol.* **19**, 1720–1730 (1999).
73. Sutandy, F. X. R., Qian, J., Chen, C. S. & Zhu, H. Overview of protein microarrays. *Curr. Protoc. Protein Sci.* **72**, 27.1.1-27.1.16 (2013).
74. Gupta, S., Manubhai, K. P., Kulkarni, V. & Srivastava, S. An overview of innovations and industrial solutions in Protein Microarray Technology. *Proteomics* **16**, 1297–1308 (2016).
75. Jonkheijm, P., Weinrich, D., Schröder, H., Niemeyer, C. M. & Waldmann, H. Chemical strategies for generating protein biochips. *Angewandte Chemie - International Edition* **47**, 9618–9647 (2008).
76. Gandor, S. *et al.* A protein-interaction array inside a living cell. *Angew. Chemie - Int. Ed.* **52**, 4790–4794 (2013).
77. Vermesh, U. *et al.* High-density, multiplexed patterning of cells at single-cell resolution for tissue engineering and other applications. *Angew. Chemie - Int. Ed.* **50**, 7378–7380 (2011).
78. Twite, A. A., Hsiao, S. C., Onoe, H., Mathies, R. A. & Francis, M. B. Direct attachment of microbial organisms to material surfaces through sequence-specific DNA hybridization. *Adv. Mater.* **24**, 2380–2385 (2012).
79. Complete Exosome Characterization, ExoView R100. https://www.nanoviewbio.com/exoview-r100.
80. Wang, S. *et al.* Recent advances in single extracellular vesicle detection methods. *Biosensors and Bioelectronics* **154**, 112056 (2020).
81. Sambrook, J. & Russell, D. W. Molecular Cloning : A Laboratory Manual. *Cold Spring Harbor Laboratory Press* (2001).
82. González, M. *et al.* Interaction of Biotin with Streptavidin: Thermostability And Conformational Changes Upon Binding. *J. Biol. Chem.* **272**, 11288–11294 (1997).
83. Zhu, S. *et al.* Light-Scattering Detection below the Level of Single Fluorescent Molecules for High-Resolution Characterization of Functional Nanoparticles. *ACS Nano* **8**, 10, 10998–11006 (2014).
84. Tian, Y. *et al.* Protein Profiling and Sizing of Extracellular Vesicles from Colorectal

Cancer Patients via Flow Cytometry. *ACS Nano* **12**, 671–680 (2018).
85. Tian, Y. *et al.* Quality and efficiency assessment of six extracellular vesicle isolation methods by nano-flow cytometry. *J. Extracell. Vesicles* **9**, 1697028 (2020).
86. Morales-Kastresana, A. *et al.* Labeling extracellular vesicles for nanoscale flow cytometry. *Sci. Rep.* **7**, 1–10 (2017).
87. Konoshenko, M. Y., Lekchnov, E. A., Vlassov, A. V & Laktionov, P. P. Isolation of Extracellular Vesicles: General Methodologies and Latest Trends. *Biomed Res Int.* **2018**, 8545347 (2018).
88. Carnino, J. M., Lee, H. & Jin, Y. Isolation and characterization of extracellular vesicles from Broncho-alveolar lavage fluid: a review and comparison of different methods. *Respiratory research* **20**, 240 (2019).
89. Wakui, K. *et al.* Rapidly Neutralizable and Highly Anticoagulant Thrombin-Binding DNA Aptamer Discovered by MACE SELEX. *Mol. Ther. - Nucleic Acids* **16**, 348–359 (2019).
90. Lu, Y. *et al.* Aptamer-based electrochemical sensors with aptamer-complementary DNA oligonucleotides as probe. *Anal. Chem.* **80**, 1883–1890 (2008).
91. Ruigrok, V. J. B. *et al.* Kinetic and Stoichiometric Characterisation of Streptavidin-Binding Aptamers. *ChemBioChem* **13**, 829–836 (2012).
92. Zhang, Y., Lai, B. S. & Juhas, M. Recent advances in aptamer discovery and applications. *Molecules* **24**, 941 (2019).
93. Lin, Y. *et al.* DNA-mediated reversible capture and release of circulating tumor cells with a multivalent dual-specific aptamer coating network. *Chem. Commun.* **55**, 5387–5390 (2019).
94. Gori, A. *et al.* Membrane-binding peptides for extracellular vesicles on-chip analysis. *J. Extracell. Vesicles* **9**, 1751428 (2020).
95. Sola, L., Damin, F., Gagni, P., Consonni, R. & Chiari, M. Synthesis of clickable coating polymers by postpolymerization modification: Applications in microarray technology. *Langmuir* **32**, 10284–10295 (2016).
96. Brambilla, D. *et al.* EV Separation: Release of Intact Extracellular Vesicles Immunocaptured on Magnetic Particles. *Anal. Chem.* **93**, 5476–5483 (2021).
97. Gao, Y. & Kyratzis, I. Covalent Immobilization of Proteins on Carbon Nanotubes Using the Cross-Linker 1-Ethyl-3-(3-dimethylaminopropyl)carbodiimide—a Critical Assessment. *Bioconjug. Chem.* **19**, 1945–1950 (2008).
98. Carl, P., Ramos, I. I., Segundo, M. A. & Schneider, R. J. Antibody conjugation to

carboxyl-modified microspheres through N-hydroxysuccinimide chemistry for automated immunoassay applications: A general procedure. *PLoS One* **14**, e0218686 (2019).

99. Sola, L., Damin, F., Gagni, P., Consonni, R. & Chiari, M. Synthesis of clickable coating polymers by postpolymerization modification: Applications in microarray technology. *Langmuir* **32**, 10284–10295 (2016).
100. Sola, L. & Chiari, M. Modulation of electroosmotic flow in capillary electrophoresis using functional polymer coatings. *J. Chromatogr. A* **1270**, 324–329 (2012).
101. Meissner, J., Prause, A., Bharti, B. & Findenegg, G. H. Characterization of protein adsorption onto silica nanoparticles: influence of pH and ionic strength. *Colloid Polym. Sci. 2015 29311* **293**, 3381–3391 (2015).
102. Parida, S. K., Dash, S., Patel, S. & Mishra, B. K. Adsorption of organic molecules on silica surface. *Adv. Colloid Interface Sci.* **121**, 77–110 (2006).
103. Chiodi, E. *et al.* A Reliable, Label Free Quality Control Method for the Production of DNA Microarrays with Clinical Applications. *Polym. 2021, Vol. 13, Page 340* **13**, 340 (2021).
104. Pereiro, I. *et al.* Magnetic fluidized bed for solid phase extraction in microfluidic systems. *Lab Chip* **17**, 1603–1615 (2017).
105. Avci, O. et al. Interferometric Reflectance Imaging Sensor (IRIS)--A Platform Technology for Multiplexed Diagnostics and Digital Detection. *Sensors* **15**, 17649–17665 (2015).
106. Daaboul, G. G. *et al.* Enhanced light microscopy visualization of virus particles from Zika virus to filamentous ebolaviruses. *PLoS One* **12**, e0179728 (2017).
107. Daaboul, G. G. *et al.* Digital Detection of Exosomes by Interferometric Imaging. *Sci. Rep.* **6**, 1–10 (2016).
108. Alexandre, L. Développement (et compréhension) de lits fluidisés magnétiques en microfluidique : applications à la détection ultrasensible en bio-analyse. *http://www.theses.fr* (2018).
109. Gori, A. *et al.* Membrane-binding peptides for extracellular vesicles on-chip analysis. *J. Extracell. Vesicles* **9**, 1751428 (2020).
110. Morani, M. *et al.* Electrokinetic characterization of extracellular vesicles with capillary electrophoresis: A new tool for their identification and quantification. *Anal. Chim. Acta* **1128**, 42–51 (2020).
111. Gardiner, C. *et al.* Measurement of refractive index by nanoparticle tracking analysis

reveals heterogeneity in extracellular vesicles. *https://doi.org/10.3402/jev.v3.25361* **3**, 25361 (2014).

112. Andreu, Z. & Yáñez-Mó, M. Tetraspanins in Extracellular Vesicle Formation and Function. *Front. Immunol.* **0**, 442 (2014).
113. Kahlert, C. & Kalluri, R. Exosomes in tumor microenvironment influence cancer progression and metastasis. *J. Mol. Med.* **91**, 431–437 (2013).
114. Sorensen, B. S. *et al.* Monitoring of epidermal growth factor receptor tyrosine kinase inhibitor-sensitizing and resistance mutations in the plasma DNA of patients with advanced non–small cell lung cancer during treatment with erlotinib. *Cancer* **120**, 3896–3901 (2014).
115. Tokuhara, T. *et al.* Clinical Significance of CD151 Gene Expression in Non-Small Cell Lung Cancer. *Clin. Cancer Res.* **7**, 4109–4114 (2001).
116. Sandfeld-Paulsen, B. *et al.* Exosomal proteins as prognostic biomarkers in non-small cell lung cancer. *Mol. Oncol.* **0**, 7170–7185 (2016).